Assessment of the effect of SPM variations on the phytoplankton dynamics in the Bohai Sea

Dissertation with the aim of achieving a doctoral degree
at the Faculty of Mathematics, Informatics and Natural Sciences
Department of Earth Sciences
of Universität Hamburg

submitted by

Feifei Liu
2016 in Hamburg

Day of oral defense: 13.04.2016
The following evaluators recommend the admission of the dissertation:
PD Dr. Thomas Pohlmann
Dr. Andreas Moll

0.1 Summary

In this thesis, the Bohai Sea phytoplankton dynamics is studied by satellite data analysis and model simulation. The Bohai Sea is characterized with high suspended particulate matter (SPM) concentration. Because of the complex physical forcing, the SPM concentration has high variabilities both spatially and temporally. The variability can influence the phytoplankton dynamics by affecting the underwater light availability. The presented work examines in detail the effect of the SPM variations on the phytoplankton dynamics in the Bohai Sea. This study consists of three main parts:

In the first part, the role of the SPM variations on the summer-autumn bloom dynamics was analyzed. Daily Medium Resolution Imaging Spectrometer (MERIS) satellite scenes of chlorophyll (Chl-a) concentration, SPM concentration and light attenuation coefficient (K_{min}) as well as the QuikSCAT-derived wind mixing from 2003 to 2009 were used in the analysis. Three biological variables were used to characterize the bloom: the bloom onset time (denoted as bloom onset), the bloom magnitude and the Chl-a increase rate during the bloom period. Onshore-offshore gradients were observed predominantly in the spatial patterns of the three biological variables. Delayed bloom onset, depressed Chl-a increase rate and elevated bloom magnitude were observed in the onshore areas. Thesis spatial variations were independent of bathymetry. The spatial pattern of the bloom onset was in accordance with that of the bloom-period wind mixing, whereas the Chl-a increase rate and bloom magnitude exhibited high spatial correlations with the bloom-period SPM concentration and K_{min}. Furthermore, the interannual variabilities of the three biological variables were examined by the empirical orthogonal function (EOF) analysis. The major mode of the three biological variables exhibited large spatial incoherency. The temporal patterns of the bloom onset and the Chl-a increase rate resembled that of the SPM concentration and K_{min}, indicating that the interannual variability of the summer-autumn bloom in terms of bloom timing and biomass increase rate can be explained, in large part, by the interannual variability of the underwater light availability caused by the SPM variations. The interannual variability of the bloom magnitude exhibited similar pattern with the bloom-period wind mixing. In summary, the study of this part suggested that light was a crucial limiting factor for the summer-autumn phytoplankton dynamics. SPM variation was an important source of the spatial and interannual variabilities of the summer-autumn bloom by modulating the light attenuation. Wind influenced Chl-a dynamics in several ways and at various scales. Spatially, weak wind mixing prior to bloom events provided favorable light conditions for the bloom development. Enhanced wind mixing supplied the upper layer of the water column with nutrients and thus promoted an intensified bloom magnitude.

In the second part, the ecosystem model (ECOHAM) operating on one well-mixed water column representing the Bohai Sea condition was proposed to test the response patterns of the phytoplankton spring bloom to the SPM variations. In this model, the underwater light attenuation coefficient was directly related to the SPM concentration. Model results demonstrated that simulations using constant, instead of time-varying, SPM concentration led to significant deviations in the estimation of the phytoplankton spring bloom. The neap-spring cycle of SPM concentration modulated the bloom development by creating sub-fluctuations of the phytoplankton biomass on a fortnight scale. The model results also indicated that the tidally-driven SPM variation interfering with the diel light cycle was insufficient to cause deviated predictions if the daily averaged SPM concentration was identical. The SPM settlement during wind slacks had more profound effect on the bloom development then the wind-induced SPM resuspension. In order to have an accurate description of the phytoplankton spring bloom development, the cutoff temporal resolution of the SPM time series should be about daily.

In the third part, a three-dimensional hydrodynamic-ecosystem model HAMSOM-ECOHAM was adopted in the Bohai Sea to simulate the annual cycle and spatial distribution of phytoplankton and nutrients. This work allowed to extend the investigation in the second part to a full three-dimensional manner. The model was integrated for 2006 and the results were compared with the observations. The time series of the simulated surface Chl-a concentration exhibited reasonable agreements with the observations during the development phase of the spring bloom and the post-bloom period in late autumn. The model overestimated the Chl-a concentration from late spring to early autumn and consequently failed to reproduce the decay of the spring bloom. The simulated annual cycle of surface nutrients were within the range of in situ observations. Monthly spatial patterns of simulated Chl-a concentration agreed well with the observations in 1982/193 and in 1992/1993, which were characterized with high concentration in the three bays while low concentration in the Central Bohai Sea. Underestimations were found at the top of the three bays in summer, possibly because only the Yellow River input was considered in the simulation, while the inputs of the other rivers were ignored. Similar conditions were found in the nutrients simulations. The general simulated patterns agreed with the observations. Discrepancies were found caused by the ignorance of the other river inputs as well as the highly inter-annual variability, which can be seen from the comparison of the observations between 1982/1983 and 1992/1993. The phytoplankton succession was simulated by considering two phytoplankton groups. Model results showed that the spring bloom was predominated by diatoms while in summer-autumn period, there was a coexisting of diatoms and the other species which were mainly flagellates. With the three-dimensional model simulation, the effect of the SPM variations on the spatial patterns of the spring bloom was investigated. The model results showed that the absence of SPM seasonal variation resulted in significant discrepancies of the spatial patterns of the bloom onset and peak time. The neap-spring cycle of SPM led to an alternation of the bloom peak time. The spatial pattern of the bloom intensity was unaffected by the additional high-frequency variations of the SPM in the scenario simulations.

Thus, the combination of satellite data and model simulation provides a comprehensive approach to investigate the mechanisms of the phytoplankton dynamics that is influenced by the SPM variations. The next step would be to merge more knowledge of the SPM observations and short-term variations to constrain the forcing of underwater light in future Bohai Sea models.

0.2 Zusammenfassung

In dieser Arbeit wird die Phytoplanktondynamik in der Bohaisee mit Hilfe von Satellitendaten und Modellsimulationen untersucht. Das Charakteristikum der Bohaisee ist eine hohe Schwebstoffkonzentration (SPM – suspended particulate matter) im Wasser. Aufgrund der komplexen physikalischen Rahmenbedingungen in der flachen Bohaisee, zeigt sich eine große räumliche Variabilität und zeitliche Änderungen in den Schwebstoffkonzentration. Diese beeinflussen maßgeblich die Unterwasserlichtverhältnisse. Die dadurch hervorgerufene Variabilität im Unterwasserlicht wiederum zeigt sich in einer ausgeprägten Dynamik vom Phytoplankton mit Blüten im Frühjahr und in den Sommermonaten. Mit Hilfe von Satellitendatenauswertung und Modellsimulationen werden mögliche Steuerungsmechanismen aus den Lichtverhältnissen und anderen physikalischen Effekten auf die Phytoplanktonblüten betrachtet. Insbesondere konzentriert sich die vorliegende Arbeit im Detail auf die Auswirkungen der SPM-Variationen und damit Lichtveränderungen auf die Phytoplanktondynamik. Die Studie besteht aus folgenden drei Teilen:

Im ersten Teil wird der Einfluss von SPM auf die Sommer- und Herbstblüten im Phytoplankton analysiert. Dazu wurden tägliche Satellitendaten von MERIS – dem Medium Resolution Imaging Spectrometer für Chlorophyll (Chl-a), SPM und die Lichtattenuation (K_{min}) sowie Winddaten von QuikSCAT für die Jahre 2003-2009 verwendet. Drei biologische Variablen wurden definiert, um die Phytoplanktonblüten näher zu charakterisieren: der Blütenbeginn, das Blütenmaximum und die Chl-Anstiegsrate während der Blütezeit. Die Auswertung der Satellitendaten zeigt erstens die immensen räumlichen Unterschiede dieser Bestimmungsparameter. Dann wurden die zeitlichen Blütenabfolgen anhand der Lichtabschattung durch SPM zu großen Teilen aus den verfügbaren Daten bestimmt. Die Unterschiede in den Blütenstärken der verschiedenen Jahre konnten mit der unterschiedlichen windbedingten Vermischung erklärt werden, sie korrelieren gut. Die Schlussfolgerung aus diesem Teil lautet, der kritische Parameter für die Phytoplanktonblüten im Sommer und im Herbst stellt das Unterwasserlicht durch die SPM Unterschiede dar. Die Windvermischung wirkt auf die Blüten auf verschiedene Weise und vor allem auf verschiedenen Zeitskalen ein. Perioden mit schwachem Wind bestimmen bei günstigen Lichtverhältnissen den Ausbruch der Blüte und deren weitere Entwicklung. Kurzfristige Windvermischungsereignisse versorgen die obere Schicht, die Deckschicht in der Wassersäule mit Nährstoffen und bringen starke Blütenereignisse hervor; dies bestimmt somit das Blütenmaximum.

Im zweiten Teil wird ein Ökosystemmodell (das Modellsystem ECOHAM Ecosystem Model, Hamburg) verwendet, um die Lichtverhältnisse zu vorgegebenen SPM Konzentrationen und Reaktionsmuster des Phytoplankton in den Frühjahrsblüten zu testen. In diesem Modell wird das Unterwasserlicht direkt mit der SPM-Konzentration und dem Chlorophyll im Wasser berechnet. Es werden verschiedene Szenarien für die SPM Konzentrationen im Wasser vorgegeben. Die Modellergebnisse zeigen, dass Simulationen mit konstantem, anstelle von zeitlich variierendem SPM zu erheblichen Unterschieden bei der simulierten Phytoplankton-Frühjahrsblüte führen. Der gezeitenbedingte Spring-Nipp-Zyklus in der SPM-Konzentration moduliert die Blütenentwicklung im vierzehn-Tage Rhythmus. Die Modellergebnisse zum Gezeiteneinfluss zeigten keine einheitlichen Ergebnisse in den Phytoplanktonblüten auf. Dann wurde noch der Einfluss von SPM-Resuspension vom Sediment als Effekt diskutiert. Alles in allem ergeben die verschiedenen Szenarien folgende Schlussfolgerung: Um eine genaue Beschreibung der Phytoplankton-Frühjahrsblüte zu erhalten, muss das Modell mit zeitlich variablem SPM betrieben werden; und die zeitliche Auflösung vom SPM sollte zwischen einem Tag und dem Spring-Nipp-Zyklus sein.

Im dritten Teil wird das räumlich dreidimensionale gekoppelten hydrodynamische Ökosystemmodell (mit dem hydrodynamischen Modellsystem HAMSOM – Hamburg Shelf Ocean Model) verwendet, um den Jahresgang und die räumliche Verteilung von Phytoplankton und Nährstoffen zu simulieren. In diesem Teil wird die Untersuchung vom zweiten Teil auf eine vollständig drei-dimensionale Weise für die Bohaisee erweitert. Das Modell wurde für das Jahr 2006 integriert und die Ergebnisse wurden zuerst mit den Beobachtungen verglichen. Die Zeitreihe der simulierten Oberflächen Chl-a-Konzentration zeigte eine angemessene Übereinstimmung mit den Beobachtungen während der Entwicklungsphase der Frühjahrsblüte und der post-Blütenperioden im Spätherbst. Das Modell überschätzt die Chl-a-Konzentration im Frühjahr und insbesondere im Sommer. Die simulierten Jahresgänge der Nährstoffe waren im Bereich der In-situ-Beobachtungen. Dann wurde ein Vergleich der Beobachtungen aus zwei Meßkampagnen von 1982/1983 und 1992/1993 verwendet und die horizontalen Strukturen verglichen. Damit war die Validation des Modells abgeschlossen. Eine Besonderheit im ECOHAM Modellsystem ist die Berücksichtigung zweier Phytoplankton-Gruppen. Die Modellergebnisse zeigen, dass im Frühjahr Kieselalgen (Diatomeen)

überwiegen, während in der Sommer-Herbst-Periode es eine Koexistenz von Kieselalgen und insbesondere anderen Arten, hauptsächlich Flagellaten, simuliert werden konnten. Und mit dieser vollständig drei-dimensionalen Modellversion wurde der Effekt der SPM Variationen auf die Blüten untersucht. Die Modellergebnisse zeigen erstens, dass erst saisonale SPM Schwankungen zu erheblichen Abweichungen der räumlichen Muster im Blütebeginn und dem Blütenmaxium führen. Zweitens, der Spring-Nipp-Zyklus von SPM führte zu einer Veränderung beim Eintreten des Blütenmaximums. Und sowohl das räumliche Muster der Blüte als auch deren Intensität bleiben in Szenarien mit höher frequenten SPM-Variationen unverändert.

Wir fassen zusammen: die Kombination von Satellitendaten und Modellsimlutionen ist ein erfolgreicher Ansatz um die Rolle von Schwebstoff (SPM) auf die Phytoplanktondynamik in der Bohaisee zu analysieren. Mit Hilfe der Untersuchungsmethoden konnte der Einfluss der Schwebstoffe auf die Phytoplanktonblüten unter bestimmten Hypothesen (Szenarien) bestimmt werden. Als nächster Schritt zur besseren und quantitativen Bestimmung ist es notwendig die Datenbasis der Schwebstoff-Messungen so zu verbessern um daraus realistische und spezifische Antriebsdaten als Steuerungsmechanismus im gekoppelten physikalisch-biologischen Modellsystem zu integrieren.

Contents

Appendices

Chapter 1

Introduction

1.1 Coastal ecosystems and phytoplankton dynamics

Coastal waters are ecological hot sports because they receive large influence from the connectivity to land (e.g., Chen et al., 1997; Carstensen and Conley, 2004). In the recent decades, coastal waters have been faced with challenges caused by anthropogenic disturbance and climate change (Cloern, 1996). As a critical indicator of the coastal ecosystem, phytoplankton act as the major primary producers in the ocean that form the base of the food chains and support production at higher trophic levels including those we harvest for food (Cloern et al., 2014). Phytoplankton blooms, prominent features of phytoplankton dynamics which are defined as episodes of rapid phytoplankton biomass increase, have been treated as an important focus because: (a) varied primary production during blooms alters the population dynamics of consumer organisms including pelagic and benthic grazers as well as bacteria (e.g., Lancelot and Billen, 1984; Platt et al., 2003); (b) the biogeochemical structures are shifted in response to blooms, including the chemical elements such as O, C, N, P, Si, S, Al (e.g., Peterson et al., 1985; Moran and Moore, 1988); and (c) occurrence of harmful algae blooms results in mortality of commercial fish populations or degraded water quality which in turn lead to severe economic loss (Kocum et al., 2002; Carstensen et al., 2007; Liu et al., 2013). Therefore, investigating the phytoplankton dynamics provides useful insights to better understand the coastal ecosystems and is the basis for the ecosystem management.

Phytoplankton are defined as photosynthesizing microscopic organisms that transform inorganic nutrients and carbon dioxide into organic compounds, convert light energy into biochemical energy and release oxygen (Falkowski and Raven, 2013). Phytoplankton dynamics reflects a tight balance between phytoplankton growth (primary production) and losses (respiration, grazing of zooplankton, mortality and physical transports). Blooms occur when the primary production exceeds the losses and the population grows rapidly. Since the phytoplankton community varies with physical-chemical environments, the bloom events are dominated by different groups of species during different seasons. A common annual cycle of the phytoplankton in mid-latitude regions is characterized with strong winter-spring diatom blooms and summer-autumn blooms of small flagellates, dinoflagellates and diatoms (Cloern, 1996). The two important factors that regulate phytoplankton growth are widely considered as light and nutrient, which provide energy and building blocks for the photosynthesis, respectively (Walsh, 1988; Smetacek et al., 1991). These two factors will be described in the following sections.

1.1.1 The underwater light climate

When light propagates in the water column, the intensity exponentially decreases with depth owing to the joint action of absorption and scattering conducted by the water constituents. The light intensity in the water column is approximated by the Lamber-Beer law (Lorenzen, 1972) which is expressed as Eq. 1.1 and illustrated in Fig. 1.1.

$$I_z = I_0 \cdot e^{-K \cdot z} \tag{1.1}$$

where I_z and I_0 are photosynthetically active radiation (PAR) at the depth z and at the water surface respectively. K is the vertical light attenuation coefficient, which is considered as a combination effect of the water constituents: the water itself, phytoplankton, nonliving particulate matter (suspended particulate matter, SPM) and dissolved material (colored dissolved organic matter, CDOM) (Branco and Kremer, 2005). When the light reaches the depth where the light intensity is 1% of the surface, photosynthesis equals to the phytoplankton respiration. This depth is called euphotic depth, only above which the net phytoplankton growth can happen (Pennock, 1985; Moll and Radach, 1991).

1.1.2 The nutrient condition

Three major nutrients (nitrogen, phosphorus and silicon) are often considered as the limiting nutrient for phytoplankton growth (Walsh, 1988). Nitrogen is an essential component of the light-sensitive pigments like chlorophyll a. In aquatic systems nitrogen is available as ammonium, nitrite and nitrate. Compared with

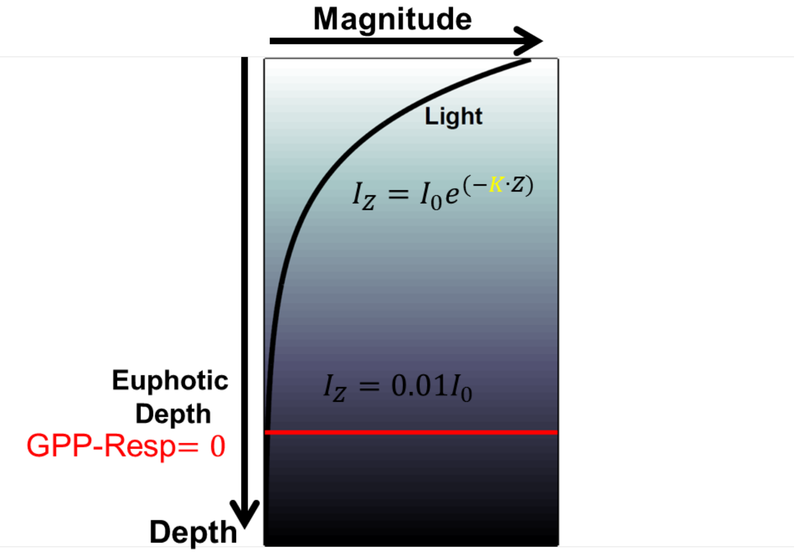

Figure 1.1: Diagram describing the underwater light attenuation. GPP is gross primary production, Resp is phytoplankton respiration.

nitrogen, phosphorus is less sensitive to phytoplankton cells. Silicon is essential to only one phytoplankton group, diatoms, and is available as dissolved silicate.

Nutrient enrichment (eutrophication) becomes a societal issue due to the increased inputs into the coastal zone (Cloern, 1999; Andersen et al., 2006; Howarth and Marino, 2006). The main sources of the coastal eutrophication are the use of fertilizers in agriculture, the presence of livestock, wastewater, urban runoff and the load of the river flow. The coastal ecosystem stores and cycles the nutrients.

1.1.3 The light-nutrient limitation in mid-latitude regions

It is thought that phytoplankton growth is primarily controlled by light during spring and by nutrient availability during summer (Yin et al., 1997; Gomes et al., 2000; Colijn and Cadée, 2003; Hatcher, 2006; Rousseaux et al., 2012). In summer and autumn, nutrient in the upper layer is generally depleted by intense spring blooms, and strong stratification may inhibit the supply of nutrient from deeper waters or the sea floor (Yin et al., 1997; Kim et al., 2007; Chen, 2009). However, summer-autumn nutrient limitation may weaken in eutrophic coastal waters. On one hand, the coastal waters are heavily affected by nutrient-enriched anthropogenic inputs and exhibit a strong water-sediment exchange (Liu et al., 2011), which can alleviate the nutrient limitation. On the other hand, light is attenuated sharply due to the high turbidity caused by large riverine input, sediment resuspension and tidal/wind stirring, which confines the photosynthesis within a narrow photic zone. Thus, in turbid, nutrient-rich waters, light availability could play an important role in limiting phytoplankton growth. Due to the high turbidity, phytoplankton growth can be suppressed by light episodically (e.g., Fisher et al., 1982; Kocum et al., 2002) or even consistently throughout the whole year (e.g., Irigoien and Castel, 1997). The spatial variation of the underwater light availability can result in a heterogeneous distribution of phytoplankton biomass. However, compared with the nutrient limitation, the light limitation received far inadequate attenuation (Branco and Kremer, 2005; Domingues et al., 2011).

1.1.4 Suspended particulate matter (SPM)

SPM is tiny particulate matter that is suspended in water column and is in a state of exchange with the bed sediment reservoir and the river plume (De Jonge, 1994; De Jorge and Van Beusekom, 1995; Guinder et al., 2009). It comprises an inorganic fraction (silt and clay) and an organic fraction (detritus and algae) (Dekker et al., 2001). The origin can be attributed to internal and external sources (De Jonge, 2000). The former include algae growth, erosion and resuspension of the sediment (Jiang et al., 2004). The later consist of river runoff, water mass intrusion through horizontal transportation (Postma, 1967; Velegrakis et al., 1997). In shallow waters, the SPM variation has a complex pattern because of the combination of various physical drivings such as wind stirring and tidal mixing (De Jonge, 1994; De Jorge and Van Beusekom, 1995).

In most near-shore coastal waters, which are classified as Case 2 waters based on their optical characteristics (Moore et al., 1999; Van Der Woerd and Pasterkamp, 2008), SPM is the main determinant of water turbidity because of its capacity to absorb and scatter visible light. The water turbidity, thus the light attenuation ability in some coastal waters, can be estimated from observed SPM concentrations. For instance, Devlin et al. (2008) derived a statistically significant linear relationship between SPM concentration and light attenuation coefficient in the UK marine waters; Lin et al. (2009) found that SPM plays an important role in determining the light attenuation in the Yellow Sea.

Here it is worthwhile to note that generally SPM can be also referred as total suspended matter (TSM) or total suspended solids (TSS) in remote sensing studies (Ouillon et al., 2008; Nechad et al., 2010) because of the identical definitions in field measurements and in bio-optical models. In both, SPM concentration is considered as seston dry weight which is left after the water samples are filtered through cellulose acetate filters with the pore size traditionally 0.45 μm and nowadays 0.2 μm.

1.2 SPM variations in the Bohai Sea

The Bohai Sea, as part of the China Sea (Fig. 1.2), is characterized by relatively high SPM levels compared with the adjacent areas (Fig. 1.3). The high SPM concentration and the shallow depth provide the Bohai Sea a distinct light regime, which may strengthen the light limitation for the phytoplankton growth.

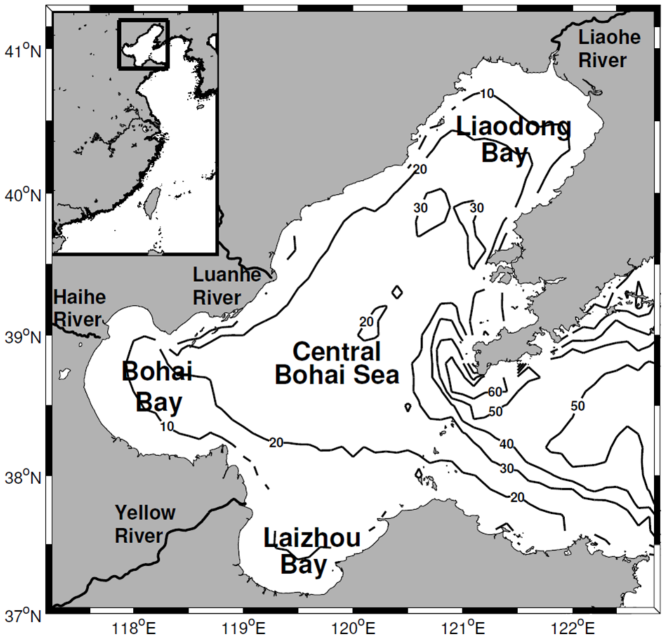

Figure 1.2: Study area with bathymetric contours (m). The Bohai Sea is divided into 4 parts: the Liaodong Bay, the Bohai Bay, the Laizhou Bay and the Central Bohai Sea. The inlet figure in the upper-left shows the location of the Bohai Sea within the China Seas.

Inside the Bohai Sea, the levels of the SPM concentration vary with topography and the influence of the river loads. Fig. 1.4 shows that the Bohai Sea is characterized by an increase in SPM concentration from the coastal onshore regions towards the central. Because of the sediment inputs from the Yellow River, the highest SPM concentration appears near the river mouth. The spatial gradient indicates that the Bohai Sea is subject to different light regimes, which in turn results in spatially resolved seasonal cycles of underwater light climate. The differences are reflected by the annual cycles of water transparency in different regions (Fig. 1.5). All the regions, except for the Bohai Bay, exhibit quite similar

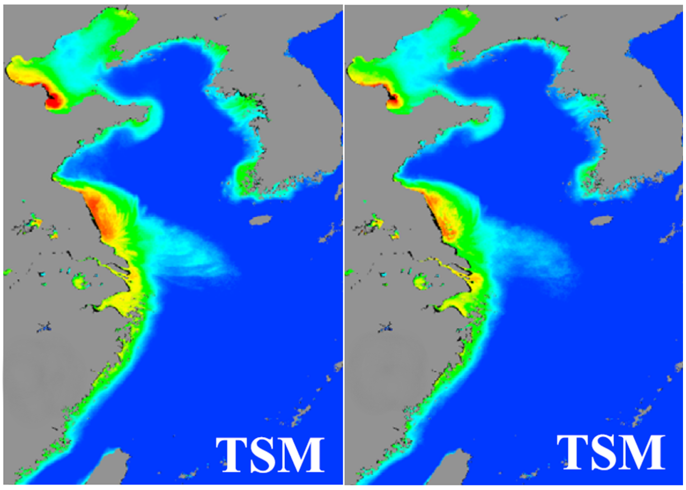

Figure 1.3: Climatology images of TSM at spring tides (left) and neap tides (right). This figure is taken from Shi et al. (2011), Fig. 5.

seasonality of the transparency, indicating high turbidity in winter and released conditions in summer. The Bohai Bay is dominated by low transparency all the year round, as a result of the huge sediment input from the Yellow River.

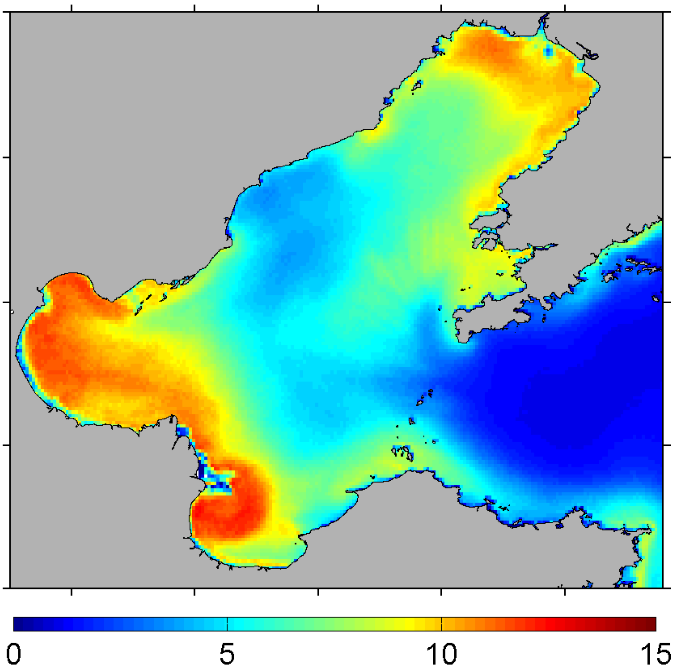

Figure 1.4: Climatic distribution of SPM (g m^{-3}) in the Bohai Sea based on the Medium Resolution Imaging Spectrometer (MERIS) data from 2003 to 2009.

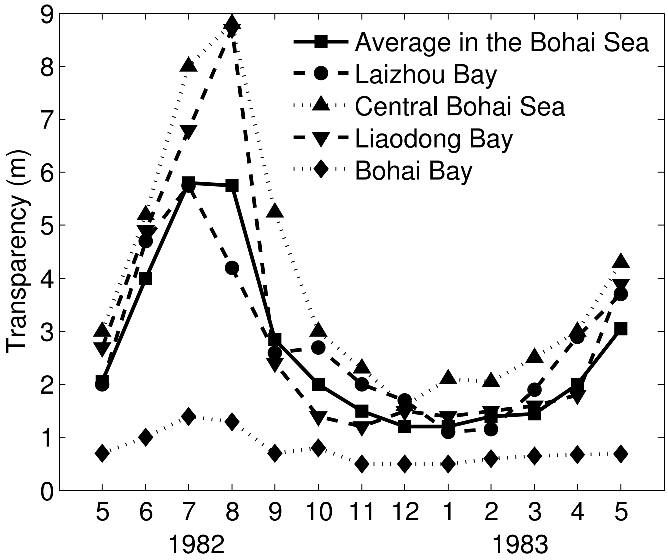

Figure 1.5: Observed water transparency by Secchi disk in different regions of the Bohai Sea from 1982 to 1983. This figure is taken from Fei (1986), Fig.3.

The Bohai Sea is subject to SPM variations with time scales ranging from hours to months (Fig. 1.6). Based on the continuous measurements at an anchor station for 1 day, large variation of SPM concentration with high-frequency was captured in the Bohai Sea (Fig. 1.6 (a)), which shows a tidally resolved cycle. The good correlation between the fluctuations of the SPM concentration and the bottom current speed implies a high dependency of the SPM resuspension on the tidal currents (Jiang et al., 2000). From the satellite data, a bi-weekly cycle of daily SPM concentration was found in the semi-diurnal tidal regime. The fortnight cycle coincides with peaks at spring tides and troughs at neap tides (Fig. 1.6 (b)). Shi et al. (2011) also emphasized the spring-neap tidally-driven resuspension as one of the important hydrodynamic processes to drive the changes of the water column SPM concentration, given that the estimated magnitude of the spring-neap tidal effect on the variations of the SPM was the same order as the seasonal variation in the coastal regions, especially in the Bohai Sea. Jiang et al. (2000) pointed that the seasonal wind variation explained the majority of the SPM seasonality based on the cruise data analysis, with the statement that stronger winds in winter and spring caused more erosion of the sediment fine fraction and the stronger vertical mixing could result in higher SPM concentrations. The seasonal coincidence of the wind speed and the SPM concentration is illustrated in (Fig. 1.6 (c)). From the satellite data, an episodic fluctuation of the SPM concentration was captured during a wind storm (Fig. 1.6 (d)). The elevated SPM concentration lasted for about 10 days and then dropped to the normal level.

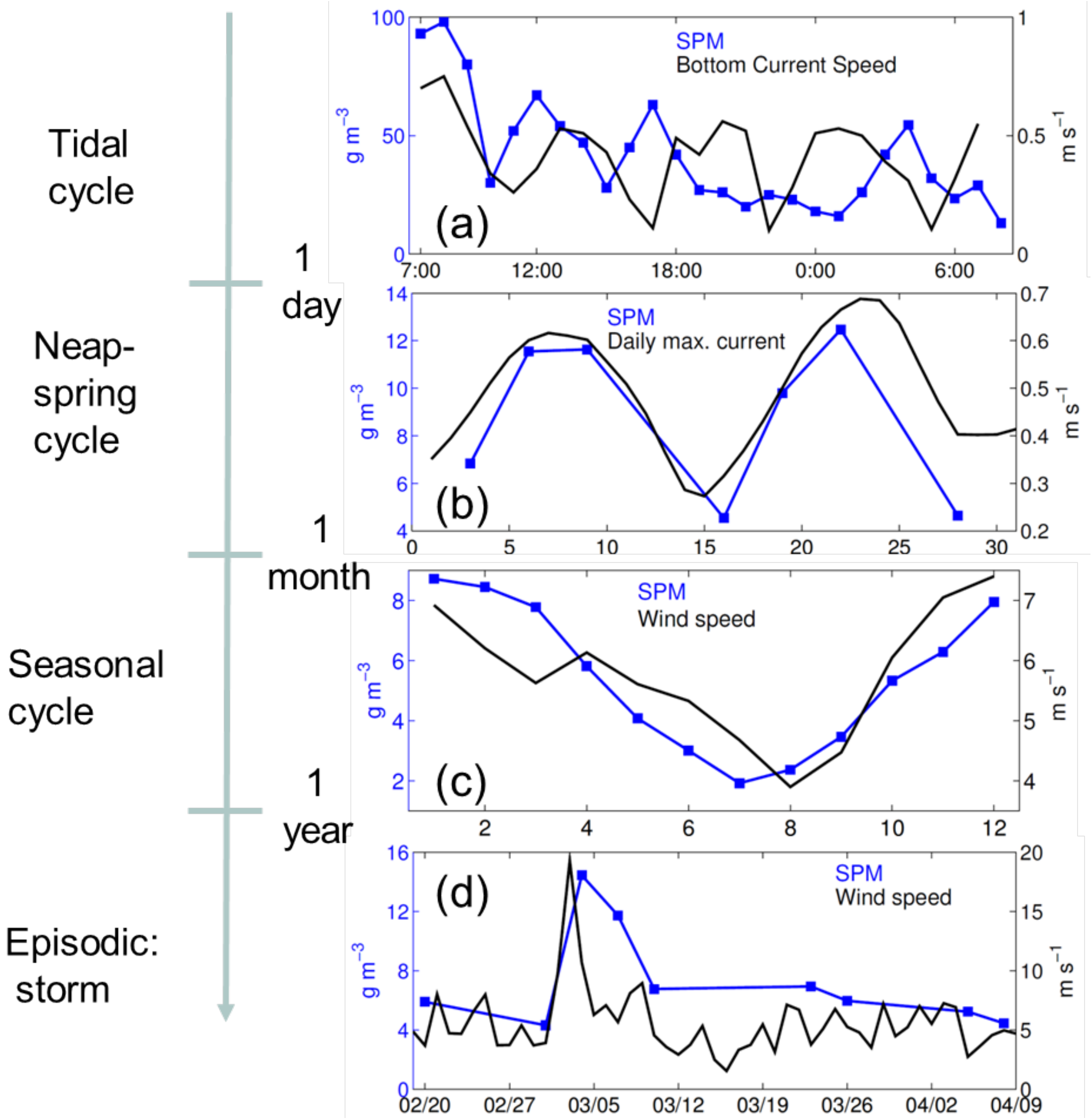

Figure 1.6: Time series of SPM concentration subjected to different variations. Blue lines stand for the time series of SPM concentration. Black lines are the correspondingly possible governing factors. (a) The hourly surface SPM concentration and bottom current speed measured at the anchor station A shown in Fig. 3.1 from 7:00 AM 5th, May 1999 to 7:00 AM 6th, May 1999. (b) The neap-spring cycle of the SPM concentration derived from the MERIS products from 15th January to 15th February 2006 at the Station B shown in Fig. 3.1. The daily maximum current is calculated based on the HAMSOM simulation. (c) The seasonal climatology of SPM concentration over the whole Bohai Sea, which is calculated from 2003 to 2009 based on the MERIS-derived SPM data. Here the SPM concentration is represented in monthly mean. The corresponding wind speed is derived from the NCEP2 database. (d) The MERIS-derived episodic fluctuation of the SPM concentration during a storm event (also derived from the NECP2 database) at Station C shown in Fig. 3.1.

1.3 The phytoplankton dynamics in the Bohai Sea

The Bohai Sea is a productive region which is characterized with high net primary production (112 g C $m^{-2}a^{-1}$ in 1982, Fei, 1991) and high species diversity (Gao et al., 1998). During the last four decades, there have been a few comprehensive investigations implemented in the Bohai Sea. During May 1982 to May 1983, a comprehensive investigation "Investigations of Bohai Sea environmental ecosystem and biological resources" was carried out with a monthly observation frequency, and was continued in 1992 with a seasonal observation frequency in February, May, August and October (Tang and Meng, 1997). In 1998/1999, a joint German-Chinese project was carried out and investigated both the hydrographic and ecological factors including nutrient fluxes and phytoplankton dynamics in the Bohai Sea (Sündermann and Feng, 2004).

The understanding of the Bohai Sea phytoplankton dynamics was supported by model simulations. Several model simulations were established based on the observations and reproduced the temporal evolutions and the heterogeneously horizontal distributions of nutrients, phytoplankton biomass and the primary production (Gao et al., 1998; Wei et al., 2004b; Liu and Yin, 2007b). These models were also used to understand the effect of the factors that may regulate the phytoplankton dynamics in the Bohai Sea (Gao et al., 2001; Zhao and Wei, 2005).

Under the combination of observations and model simulations, the main features of the spatio-temporal dynamics of the phytoplankton were identified. The annual cycle of the phytoplankton biomass is characterized by two blooms appearing in spring and summer-autumn separately (Fei, 1991). The Laizhou Bay has the maximum annual mean biomass and primary production, while the Liaodong Bay has the lowest values (Fei, 1991; Wei et al., 2004b). However, the annual mean biomass in the Bohai Bay and the Central Bohai Sea exhibit higher interannual variability (Fei, 1991; Wei et al., 2004b). Both the observation and model study gained the same conclusion that light played the most important role in initializing the spring bloom (Gao et al., 2001; Liu and Yin, 2007b). However, the role of the underwater light conditions on the summer-autumn blooms has gained less attention. The linkage between the SPM variations and the phytoplankton dynamics has also not been well understood.

1.4 Research gaps and the contribution of this study

Due to the climate change and the proliferation of industries, agriculture, aquaculture and domestic sewage input, nutrient supply has been significantly changed in the Bohai Sea. By comparing the water samples collected in August 2002 with the previous data of corresponding period, Wang et al. (2009) pinpointed out a remarkable increasing of the nitrogen concentration over the last four decades. This tendency intensified the eutrophication in the Bohai Sea. As a consequence, the light limitation should not be ignored over the year. In order to investigate the phytoplankton dynamics under the environmental conditions, it is particularly crucial to understand the influence of the SPM variations on the phytoplankton dynamics.

The interaction between rapid light fluctuations and the seasonal cycle of phytoplankton biomass was overlooked in the past. Currently, this study benefits a lot from remote sensing ocean color images because of the improved temporal and spatial coverage (Chen et al., 2010). The integration of temporally and/or spatially resolved SPM fields with ecosystem modeling enables the recalibration of the depth integrated light availability (Lacroix et al., 2007). Therefore, in this study, I have taken advantage of both the satellite data and the ecosystem model to systemically investigate the potential response of the phytoplankton dynamics to the SPM variations.

Medium Resolution Imaging Spectrometer (MERIS) has a big advantage in capturing features of Case 2 waters in summer because of its increased spectral resolution and more elaborate (neural network) algorithms (Doerffer and Schiller, 2007). Therefore, the effect of the SPM variations on the summer-autumn bloom in the Bohai Sea was assessed by using MERIS images in Chapter 2. The main content of this chapter has already been published (Liu et al., 2014). However, the use of satellite data in winter-spring time is limited because of the high turbidity. Instead, the ecosystem model simulation provides an alternative to extend the investigation to the spring bloom period. In Chapter 3, the possible response of the phytoplankton spring bloom to the SPM variations was studied by experimental simulations with an ecosystem model in a well-mixed water column. In order to further the analysis to the three-dimensional scale, in Chapter 4, a three-dimensional hydrodynamic-ecosystem model HAMSOM-ECOHAM was adopted in the Bohai Sea to simulate the annual cycle and spatial distribution of the phytoplankton and nutrients. The model validation was conducted by comparing the model results with the observations. In Chapter 5, the preliminary investigation of the influence of the SPM variations on the spatial patterns of the phytoplankton spring bloom was presented. A final discussion and conclusion were presented in Chapter 6 and Chapter 7.

Chapter 2

Assessment of the summer-autumn bloom using satellite images to identify the role of the SPM variations

2.1 Abstract

In the Bohai Sea, summer-autumn phytoplankton blooms require thorough investigation because of their large variability in space and time. This variability results primarily from the complex interplay of different governing factors, e.g., nutrient availability, light availability, grazing. SPM is expected to have effects on this variability by modulating the underwater light conditions. In this chapter, the influence of SPM variations on the summer-autumn blooms was investigated by using daily Medium Resolution Imaging Spectrometer (MERIS) satellite scenes from 2003 to 2009. We established a statistical approach to define the biological variables that characterize summer-autumn blooms, i.e., the bloom onset time (denoted as bloom onset), the bloom magnitude, and the rate of chlorophyll (Chl-a) increase during the bloom period (denoted as Chl-a increase rate). Remarkable onshore-offshore gradients in all three biological variables were observed. For example, bloom onsets were delayed in coastal areas compared to deep offshore waters. The bloom onset exhibited a highly spatial correlation with wind mixing rather than SPM, whereas the Chl-a increase rate and bloom magnitude were highly correlated with the distribution of SPM ($R = -0.67$ and $R = 0.68$, respectively). Furthermore, the empirical orthogonal function

(EOF) analysis revealed similar interannual variabilities in the SPM, K_{min}, bloom onset and Chl-a increase rate. Another similar interannual trends were observed in the bloom magnitude and bloom-period wind mixing. The analysis above suggested that light was a crucial limiting factor for summer-autumn phytoplankton dynamics. SPM influenced the spatial and interannual variations of summer-autumn bloom by modulating the light attenuation. Wind influenced Chl-a dynamics in many ways and at various scales. Spatially, weak wind speeds prior to bloom events tended to provide favorable light conditions for the development of blooms. Over the long-term, however, enhanced wind mixing tended to supply the surface layer with nutrients more effectively and thus promoted a higher bloom intensity.

2.2 Introduction

In temperate coastal ecosystems, phytoplankton dynamics reflects a tight balance between nutrient supply and light limitation (Walsh, 1988; Smetacek et al., 1991). It is thought that primary production is primarily controlled by light during spring and by nutrient availability during summer (Yin et al., 1997; Gomes et al., 2000; Colijn and Cadée, 2003; Hatcher, 2006; Rousseaux et al., 2012). In summer and autumn, nutrient concentrations in the water column are generally depleted by intense spring blooms (Yin et al., 1997; Kim et al., 2007; Chen, 2009). However, summer-autumn nutrient limitation may weaken in eutrophic waters because of the climate change and human activities. Therefore, in terms of the elevated nutrients levels, the light availability gains a weighted role in regulating the phytoplankton dynamics in summer-autumn period.

In turbid waters, SPM acts as the main contributor to the water turbidity, which thus directly affects the phytoplankton growth by modifying the light conditions (Colijn, 1982). Because of variations in wind speeds, tidal currents and river flow, SPM concentration varies temporally and spatially, generating variable light exposures which consequently influence the phytoplankton bloom development. In summer-autumn time, phytoplankton seasonality may be tightly controlled by fluctuations in SPM concentrations (Kocum et al., 2002; Adolf et al., 2006).

The summer-autumn phytoplankton bloom dynamics in coastal waters have been poorly investigated in the past, mostly because of the lack of measurements with sufficiently high resolution in space and time (Cloern, 2001). In recent years, a unique means of studying the spatio-temporal distribution of coastal phytoplankton has been provided by high-resolution ocean color sensors (e.g., Tang et al., 2003a; Brickley and Thomas, 2004). Satellite-based studies have clearly identified a strong variability in chlorophyll (Chl-a) concentration over different spatio-temporal scales (Sackmann et al., 2004; Navarro and Ruiz, 2006; Iida and Saitoh, 2007). Although many studies have focused on spring blooms (e.g., Wiltshire et al., 2008; Tian et al., 2009), satellite-based data can also help to quantify variability in summer-autumn blooms and, thereby, start pinpointing the mechanisms behind that variability (Ueyama and Monger, 2005; Kim et al., 2007). Remote sensing data provide simultaneous measurements of Chl-a, SPM and light, thereby enabling the study of the influence of turbidity as a function of SPM concentrations on the phytoplankton summer-autumn blooms.

The Bohai Sea is regarded as an eutrophic area (Wang et al., 2009). On one hand, it experiences low nutrient exchange with the outer open seas because of limited water exchange through the Bohai Strait (Zhao and Shi, 1993). On the other hand, it is heavily affected by nutrient-enriched anthropogenic inputs and exhibits a strong water-sediment exchange (Liu et al., 2011), which can alleviate the nutrient limitation in summer and autumn. The Bohai Sea is dominated by high concentrations of SPM, owing mostly to large SPM loads from the Yellow River (Saito et al., 2001; Jiang et al., 2004). The spatial Chl-a concentration distribution in summer-autumn (May-November), derived from the Medium Resolution Imaging Spectrometer (MERIS) product from 2003 to 2009, exhibits an obvious onshore-offshore gradient (Fig. 2.1 (a)). However, this gradient could not be easily explained by SPM and wind mixing. In this chapter, we investigated the spatio-temporal distribution of three biological variables derived from MERIS data to describe phytoplankton blooms in summer and autumn: the summer-autumn bloom onset time (denoted as bloom onset), the normalized bloom magnitude during the bloom period (denoted as bloom magnitude) and the Chl-a increase rate during the bloom period (denoted as Chl-a increase rate). Further, we investigated the relationships between the bloom dynamics and the SPM variations. We aim to identify the possible underlying mechanisms (i.e., light conditions) behind the observed variabilities in summer-autumn blooms, especially the influence of the SPM variations on the bloom dynamics.

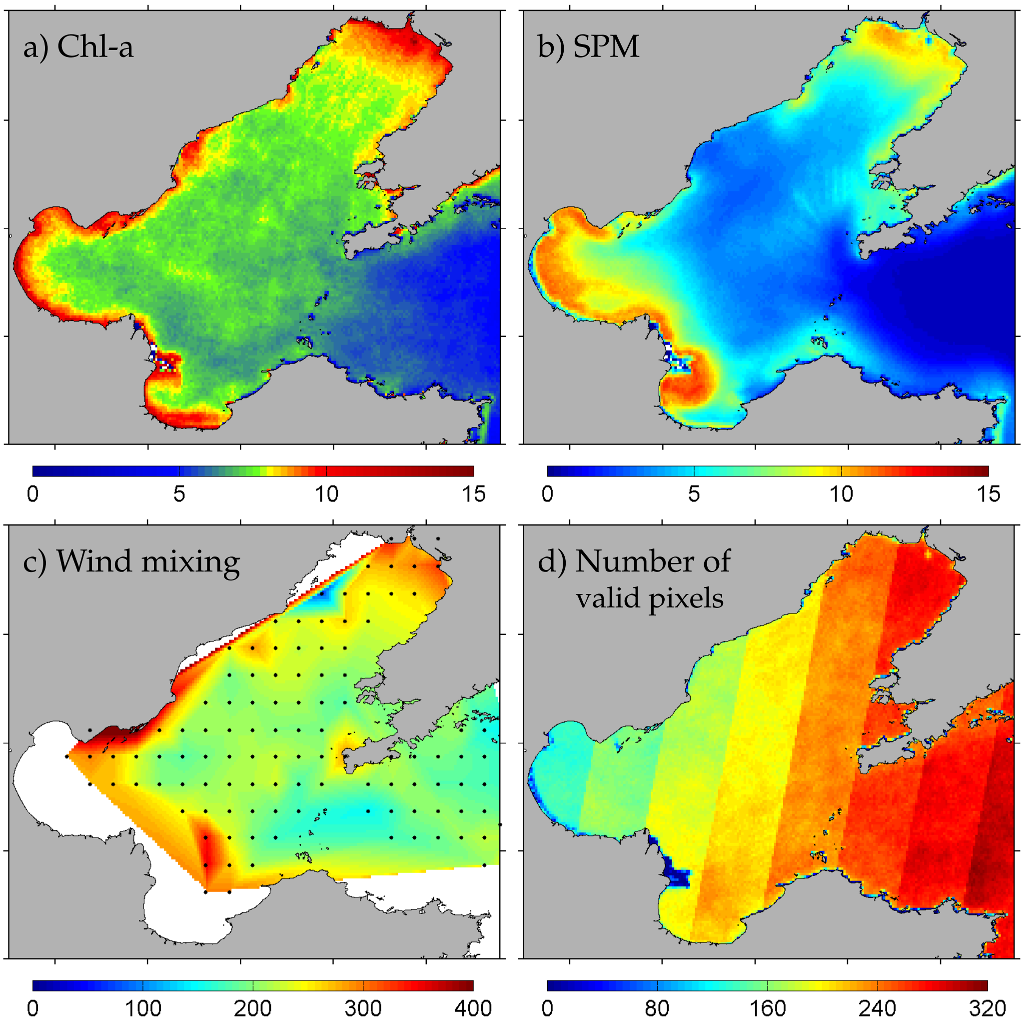

Figure 2.1: Spatial distribution of a) Chl-a concentration (Chl-a, mg m^{-3}), b) SPM concentration (g m^{-3}) averaged over the summer-autumn period (May-November) from 2003 to 2009, c) wind mixing (m^3 s^{-3}). Wind mixing intensity was interpolated to a 0.025° × 0.025° grid from the original 0.25° × 0.25° grid (black dots). d) Number of valid pixels from MERIS gathered for the summer-autumn periods from 2003 to 2009.

2.3 Methods

2.3.1 MERIS Data

MERIS was developed with the aim of analyzing not only the open ocean but also coastal waters (Doerffer et al., 1999). This ability was supported by the European Space Agency (ESA) in supplying special variables for Case-2 waters in standard products. These are, specifically, a Case-2 Chl-a value, a value for TSM, and a measure of absorption due to dissolved and particulate organic matter, called gelbstoff (or colored dissolved organic matter, CDOM). The underlying algorithm for the Case-2 ESA-standard variables was further developed and is also available in several versions as a separate tool, the Case-2 regional processor (Doerffer and Schiller, 2007), including a specific coupled atmospheric correction. Many studies have supported the strength of this concept (e.g., Martinez-Vicente et al., 2004; Ruddick et al., 2008; Cui et al., 2010). MERIS level-1 scenes were processed by the Case-2 regional processor in version 1.4.1 (R. Doerffer, personal communication, May 16, 2011) to retrieve a daily level-2 product. These data were further subsampled over the study area (37-41 °N and 117.5-122.8 °E) at a reduced resolution of $\sim$ 1200 m. Because the analysis in this chapter is focused on summer-autumn phytoplankton bloom dynamics, we selected MERIS data collected from May to November between 2003 and 2009 for the subsequent analysis.

The number of available data for each grid point is weather and trajectory coverage dependent. MERIS collects data every 3 days at the equator and more often at higher latitudes. However, clouds, contrails and sun glint can prevent the observation of the underlying surface. When the satellite passes by, it sometimes captures only part of the Bohai Sea because of the contrail coverage. Therefore, for a large number of days each year, the data were not usable. Fig. 2.1 (d) presents the number of valid retrievals at individual grid point gathered for the summer-autumn period from 2003 to 2009. There is visibly a weak statistical bias towards the western part of the sea.

2.3.2 Statistical approach used to derive biological variables

Bloom period

In shallow coastal waters, a bloom is generally defined as a rapid growth of phytoplankton that leads to a significant increase in biomass (Richardson, 1997). Our definition of the summer-autumn bloom was based on the cumulative variance of Chl-a concentration (Ueyama and Monger, 2005). The succession of phytoplankton bloom in summer-autumn is influenced by many factors (e.g., grazing and nutrient supply), which complicates the story. However, the environmental factors are presumably identical in space and time before the occurrence of the summer-autumn blooms. Therefore, we focused on the first bloom during summer-autumn period as the beginning of the seasonal succession in each year.

We used a least-squares fit curve analysis to determine the bloom period at each

0.025° × 0.025° grid point and for each year (2003-2009). First, we conducted quality control. After filtering extreme values, the data were run through a nine-point spatial median filter. For each year, grid points with more than 10 data points between May and November were then chosen for further analysis. For each grid point, the annual cycle of Chl-a concentration was normalized (hence $\mu = 0$ and $\sigma = 1$) by subtracting the temporal mean and dividing by the standard deviation. Missing values in the time series were filled using linear interpolation (Fig. 2.2, green line). Second, we robustly defined a bloom event as occurring when there was more than one day with a normalized Chl-a concentration higher than 1.5 (Appendix. A). If the time interval between two days with Chl-a concentration (normalized) higher than 1.5 was more than 15 days (Appendix. B), these days were attributed to two different bloom events. For this case, we defined it multiple blooms, otherwise single bloom (Fig. 2.2) so that the first bloom can be separated from the later bloom succession (See the reasoning in Appendix. B). Third, we derived the Chl-a variance time series. For each day, the variance was computed over a 15-day period (analogous to running mean, 7 day window). Fourth, we adjusted the Chl-a variance time series (Fig. 2.2, magenta line). To obtain an ideal “S” curve of the cumulative variance (Fig. 2.2, red line) focused on the first bloom period, the disturbance related to later blooms should be excluded, and the largest Chl-a variance during the first bloom period should be centered in the variance time series (denoted as the central day) with equal time distances forward and backward (Ueyama and Monger, 2005). The time distance was defined as the minimum of the three time intervals, i.e., from 1 May to the central day, from the central day to 30 November and from the central day to the second possible bloom event (for the case of multiple blooms only, otherwise, this time interval was ignored). Fifth, a time series of the cumulative variance was created by generating a cumulative sum of the daily variance corresponding to the new Chl-a variance time series (Fig. 2.2, red line). Sixth, based on this cumulative variance time series, a logistic curve was fitted using a nonlinear least-squares method (Fig. 2.2, black cross). The logistic function

$$f(t) = \frac{C_1}{1.0 + \exp(C_2 - C_3 t)} + C_4 \tag{2.1}$$

contains the time index t and fitted shape constants C_i . Finally, the bloom onset and bloom end time were functionally defined where the slope of the fitted-curve equaled one-tenth of its maximum slope. Typical examples of procedure defining the bloom-period (multiple blooms and single bloom, separately) are illustrated in Fig. 2.2 (a)-(b). At each grid point in the Bohai Sea, this procedure was repeated for each year, from which a 7-year averaged bloom onset was calculated.

a) Multiple blooms

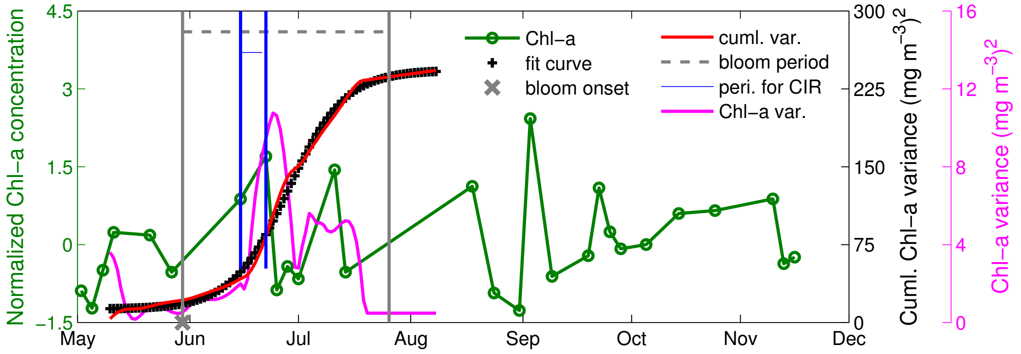

b) Single bloom

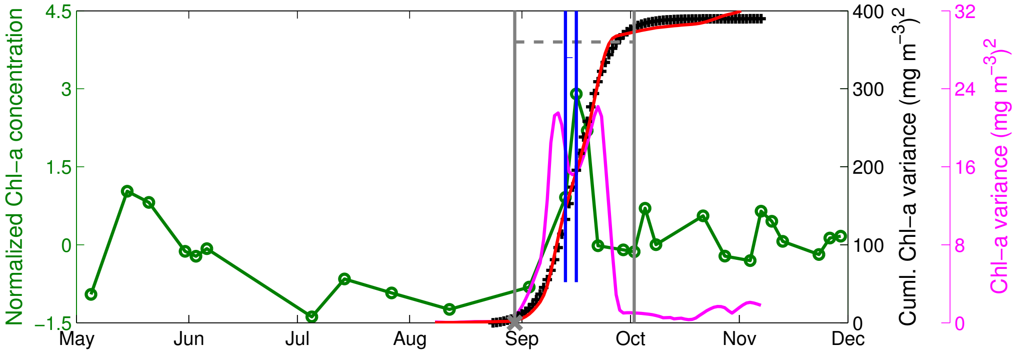

Figure 2.2: Example time series of Chl-a concentration (normalized, green solid line with circle), Chl-a variance (magenta solid line), cumulative variance in Chl-a (solid red line), least-squares fit curve to the cumulative variance (black solid curve with cross), bloom onset (vertical line at X), the bloom period (gray dashed line) and the period used to calculate the Chl-a increase rate during the bloom period (blue solid thin line) during May to November sampled at a) 39.7°N, 120.4°E in 2003 and b) 39.4°N, 119.9°E in 2008, to illustrate the method calculating variables for typical a) multiple blooms and b) a single bloom during the summer-autumn period, respectively. For the condition of multiple blooms a), we derived the variables based on the first bloom.

Bloom magnitude

The magnitude of the summer-autumn bloom was expressed as the index of bloom intensity. We used the normalized index instead of the absolute magnitude so that the relative variation would not be overwhelmed by the large variability in areas of high Chl-a concentration over the whole year. The bloom magnitude was computed by averaging the normalized Chl-a concentration over the bloom period (Fig. 2.2). This procedure was repeated at each grid point for each year, and the averaged bloom magnitude for the 7 years was also calculated.

Chl-a increase rate

During the bloom period, absolute Chl-a concentrations were used to calculate the Chl-a increase rate. For each grid point, as the Chl-a concentration measurements were rather sparse, we selected two measurements between the bloom onset and the peak day of the bloom to calculate the Chl-a concentration difference (Fig. 2.2). Then, the Chl-a increase rate was computed through dividing the difference by the time interval between the two measurements.

Light conditions and SPM during the bloom period

A high correlation between Secchi depth (SD) and diffuse light attenuation coefficient K_d has been found both in the ambient waters of the Bohai Sea, e.g., the Yellow Sea (Son et al., 2005), and other coastal waters that exhibit remarkable similarities in hydrography with the Bohai Sea, e.g., the North Sea (Sündermann and Feng, 2004; Tian et al., 2009). Therefore, we used the MERIS-derived diffuse light attenuation coefficient K_{min} to represent the light conditions. K_{min} is mean of the 3 bands which have minimum attenuation coefficient in all available wavelength-bands of MERIS (Doerffer and Schiller, 2007). We calculated the averaged K_{min} during the bloom period for each grid point for each year. The climatologically averaged K_{min} was computed by averaging the yearly K_{min} during the bloom period over the 7 years. For SPM, we conducted the same treatment to derive the climatological average.

2.3.3 QuikSCAT wind data and wind mixing

QuikSCAT Level 3 daily wind speed data at a $0.25° \times 0.25°$ resolution were obtained from the NASA/DAAC dataset (`ftp://podaac-ftp.jpl.nasa.gov/`) from 2003 to 2009 and further interpolated to a $0.025° \times 0.025°$ grid (Fig. 2.1 (b)). To evaluate wind mixing, we parameterized it as the cube of the surface wind speed and assumed the bulk aerodynamic constant (α in the following equation) to be 1.0. Similar methods have also adopted to study the mixing caused by the surface wind forcing (Brickley and Thomas, 2004; Ueyama and Monger, 2005).

In addition to the bloom-period averaged wind mixing, we obtained the wind mixing preceding and following the bloom to find the lag correlation with the biological variables. Because of missing values, the wind mixing in parts of the Bohai Sea was omitted from the analysis (Fig. 2.1 (b)). The formula is as follows:

$$M_{wind} = \frac{\sum_{n=T_b-i}^{n=T_e-i}(\alpha * \mu_n^3)}{(T_e - T_b)} \tag{2.2}$$

where M_{wind} is wind mixing, T_b and T_e present the bloom onset time and the bloom end time, which are calculated as in Section 2.3.2. α is the bulk aerodynamic constant, which is set to be 1.0 in this study. μ is wind speed derived from the QuikSCAT product. i represents the number of days preceding (positive value) or following (negative value) the bloom when calculating the period-averaged wind mixing.

2.3.4 EOF analysis

Empirical orthogonal function (EOF) analysis was used to examine the spatio-temporal variability of the variables. In this study, the principal components (PCs) represented the interannual variability, whereas the resultant spatial eigenfunctions represented spatial patterns that varied with the corresponding PCs. Data sets were prepared in two steps before applying the EOF analysis. First, the original data were converted to anomaly data by subtracting the temporal mean at each grid point. Second, if a given grid point contained missing data in any year during the 2003-2009 period, the data for that grid point were omitted from the EOF analysis. EOF analyses were performed separately on each variable (the bloom onset, the bloom magnitude, Chl-a increase rate, the wind mixing, K_{min} and SPM during the bloom). Considering that only 7 years of data were available for the analysis, the EOF images were expected to be rather noisy. The temporal and spatial patterns of the second mode and subsequent modes were less coherent and difficult to interpret in terms of possible physical forcing mechanisms. Therefore, we concentrated on the results of the first EOF mode for each variable.

2.4 Results

2.4.1 Long-term averaged spatial pattern

Fig. 2.3 displays a synoptic overview of the 7-year averaged spatial distribution of the biological variables (left panels) and the possible governing factors (right panels). The bloom onset distribution clearly illustrated an onshore-offshore gradient (Fig. 2.3 (a)), i.e., later blooms (after August) always occurred in the nearshore coastal areas, whereas earlier blooms occurred in the offshore Central Bohai Sea. The wind mixing exhibited a significant spatial gradient as well (Fig. 2.3 (b)). Strong wind mixing was observed in the nearshore areas, which corresponded with the areas of late blooms. Across the southwest-northeast direction in the Central Bohai Sea, the water was dominated by weak wind mixing, indicating that weak wind facilitated the enhancement of early summer-autumn blooms. Spatially, the wind mixing distribution was highly correlated with the bloom onset, with a correlation coefficient as high as 0.69 (Table 2.1). However, neither the bloom onset nor the wind mixing displayed a good correlation with bathymetry, with correlation coefficients of -0.26 and -0.33, respectively (Fig. 2.3 (a)-(b)).

Table 2.1: Correlation coefficients between the biological variables and governing factors. The bold numbers highlight the maximum correlation of each biological variable with the governing factors ($p<0.001$).

Correlation coefficient	Bloom onset	Chl-a increase rate (log)	Bloom magnitude
Wind mixing	**0.69**	-0.28	0.45
K_{min}	0.46	-0.65	**0.69**
SPM	0.49	**-0.67**	0.68

The spatial distribution of Chl-a increase rate exhibited a skewed pattern, i.e., the Chl-a increase rate was low in the Laizhou Bay, the Bohai Bay and the northwestern marginal areas of the Central Bohai Sea (Fig. 2.3 (c)), whereas the eastern part of the Central Bohai Sea was characterized by high rates of Chl-a accumulation. For the distribution of SPM (Fig. 2.3 (d)), the spatial variation displayed the opposite pattern. Low SPM values were observed in the Central Bohai Sea, whereas high SPM dominated in the Laizhou Bay and the Bohai Bay, which was consistent with the locations of low Chl-a increase rates. However, the northern Liaodong Bay, characterized by high SPM, did not exhibit the expected low Chl-a increase rate. The spatial correlation coefficient between the Chl-a increase rate and SPM was moderate (Table 2.1, $R = -0.67$). Light attenuation coefficient K_{min} exhibits similar spatial pattern with SPM (Fig. 2.3 (f)). They are highly correlated with a spatial correlation coefficient of 0.94.

The distribution of bloom magnitude also displayed a opposite pattern to that of the Chl-a increase rate (Fig. 2.3 (e)). The three bays were characterized by high bloom magnitude, whereas the southwest of the Liaodong Bay and the Bohai Strait were dominated by low bloom magnitudes. This spatial pattern resembled that of SPM and K_{min}, with a spatial correlation coefficient as high as 0.68 and 0.69, respectively (Table 2.1).

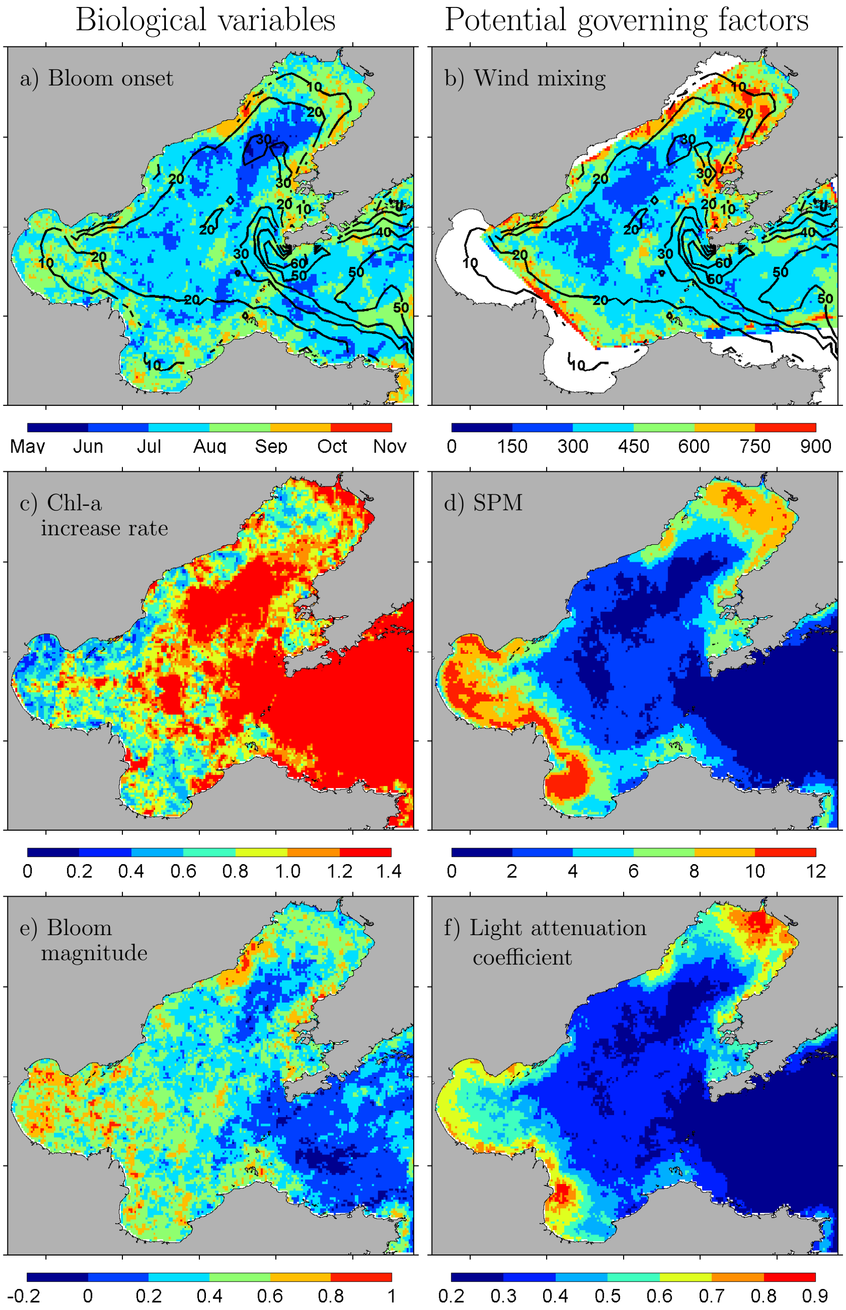

Figure 2.3: Seven year averaged a) bloom onset (month), b) wind mixing during the bloom period (m^3 s^{-3}) superimposed by the bathymetry, c) Chl-a increase rate (mg Chl $m^{-3}d^{-1}$), d) SPM (g m^{-3}), e) bloom magnitude (dimensionless) and f) light attenuation coefficient (K_{min}, m^{-1}) during the bloom period. Spatial correlations were shown in Table 2.1. Here it should be noted that the correlation of SPM and K_{min} is 0.94 ($p<0.001$). The correlation of wind mixing with SPM is 0.62 ($p<0.001$).

2.4.2 Interannual variability

The spatial eigenfunctions of the first EOF mode for the bloom onset illustrated high coherence (Fig. 2.4 (a)). For most parts of the Bohai Sea, the spatial eigenfunctions were positive. The corresponding temporal pattern indicated significant increases in 2003 and 2006 (Fig. 2.5 (a)), implying that in most parts of the Bohai Sea, the summer-autumn blooms were delayed in those years.

For wind mixing, the first EOF mode accounted for approximately 26.5% of the total variance. Significant negative signals occurred in the eastern part of the Bohai Sea and the three bays (Fig. 2.4 (b)), whereas positive signals were observed in the northern and western part of the Central Bohai Sea. For the temporal pattern, there was a strong negative amplitude in 2003 (Fig. 2.5 (b)), implying weak wind mixing in that year.

Spatially, positive eigenfunctions of the Chl-a increase rate were found in the Bohai Bay, the Laizhou Bay and the western Central Bohai Sea for Chl-a increase rate (Fig. 2.4 (c)). In combination with the time temporal pattern (Fig. 2.5 (c)), highest Chl-a increase rate was found in 2006. On the contrary, as illustrated by negative values, the eastern part of the Central Bohai Sea as well as the Bohai Strait were subject to the lowest Chl-a increase rate in 2006.

SPM and K_{min} showed similar spatial and temporal patterns. The most significant interannual variability occurred in the southeastern Central Bohai Sea and the northern Liaodong Bay (Fig. 2.4 (d) and (f)), which were characterized with positive values. The temporal patterns were similar to that of bloom onset and Chl-a increase rate, with positive values in 2003, 2006 and the opposite in 2008 and 2009 (Fig. 2.5 (a) and (c)). Combined with the corresponding spatial patterns, the positive values revealed a high SPM and K_{min} situation in 2003 and 2006. Differences of the interannual patterns were observed in 2004 and 2005. The SPM displayed high positive values while the bloom onset and K_{min} were illustrated as negative years.

The spatial eigenfunction of the bloom magnitude indicated inverse phases between the southeastern Bohai Sea and other areas (Fig. 2.4 (e)). The temporal pattern remarkably resembled that of wind mixing, with a strong negative amplitude in 2003 (Fig. 2.5 (e)) indicating that weaker summer-autumn blooms occurred in the coastal areas of the three bays and the southern part of the Central

Bohai Sea whereas at the same time there were intensified blooms in the other parts of the Bohai Sea (Fig. 2.4 (e)). The positive values in the temporal pattern in combination with the corresponding spatial eigenfunction depicted an inverse distribution of the bloom magnitude in the other years.

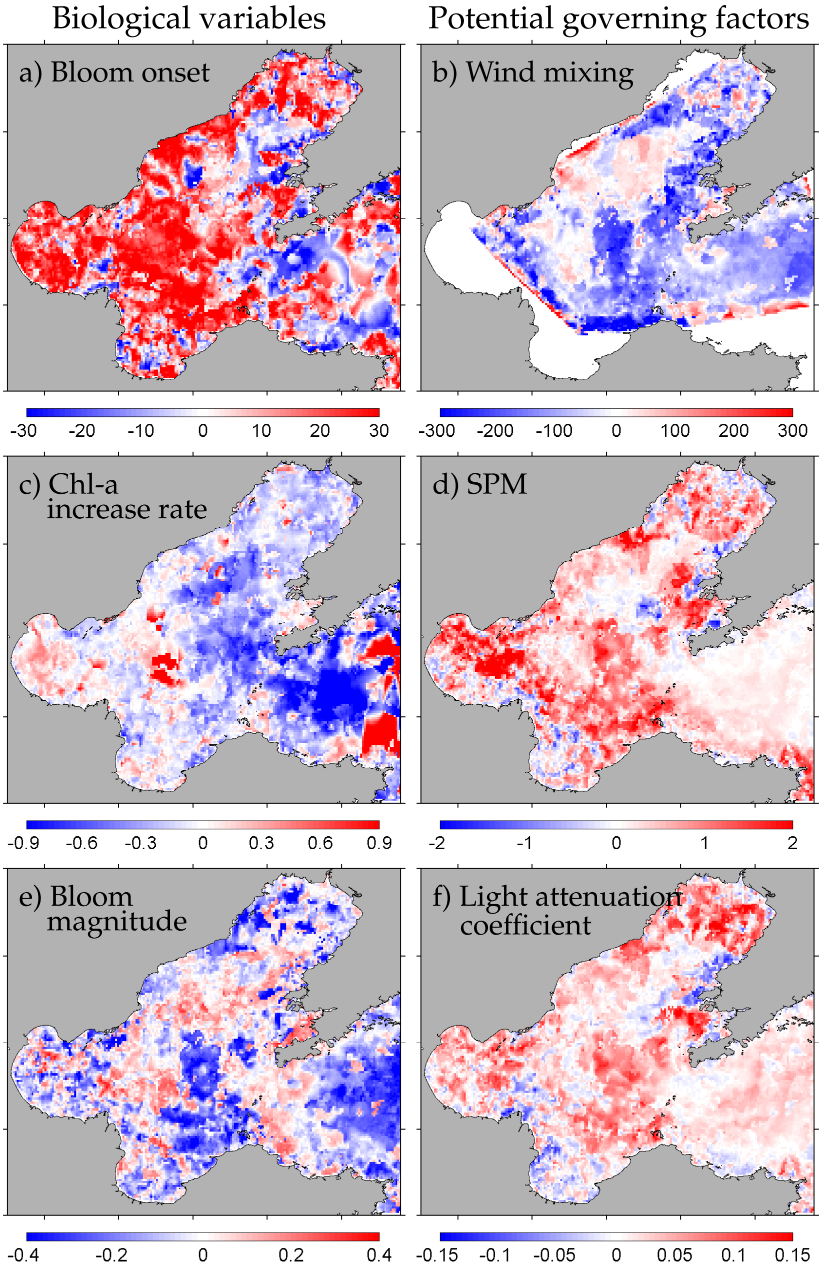

Figure 2.4: Spatial eigenfunctions for the first EOF mode of a) bloom onset, b) wind mixing, c) Chl-a increase rate, d) SPM, e) bloom magnitude, and f) light attenuation coefficient (K_{min}), for the summer-autumn bloom. Each EOF mode accounts for 23.0%, 28.1%, 25.9%, 27.2%, 32.9% and 26.5% of the total variance, respectively.

Based on the analysis above, we can categorize the interannual variabilities into two groups: the bloom onset, Chl-a increase rate, SPM and K_{min} displayed anomaly years in 2003 and 2006, whereas the wind mixing and bloom magnitude were subjected to an anomaly year in 2003. For the former condition, the bloom onset exhibited identical variation as shown by the coincident spatial pattern while the Chl-a increase rate showed an opposite pattern. For the later condition, the wind mixing and bloom magnitude showed a spatial coherence.

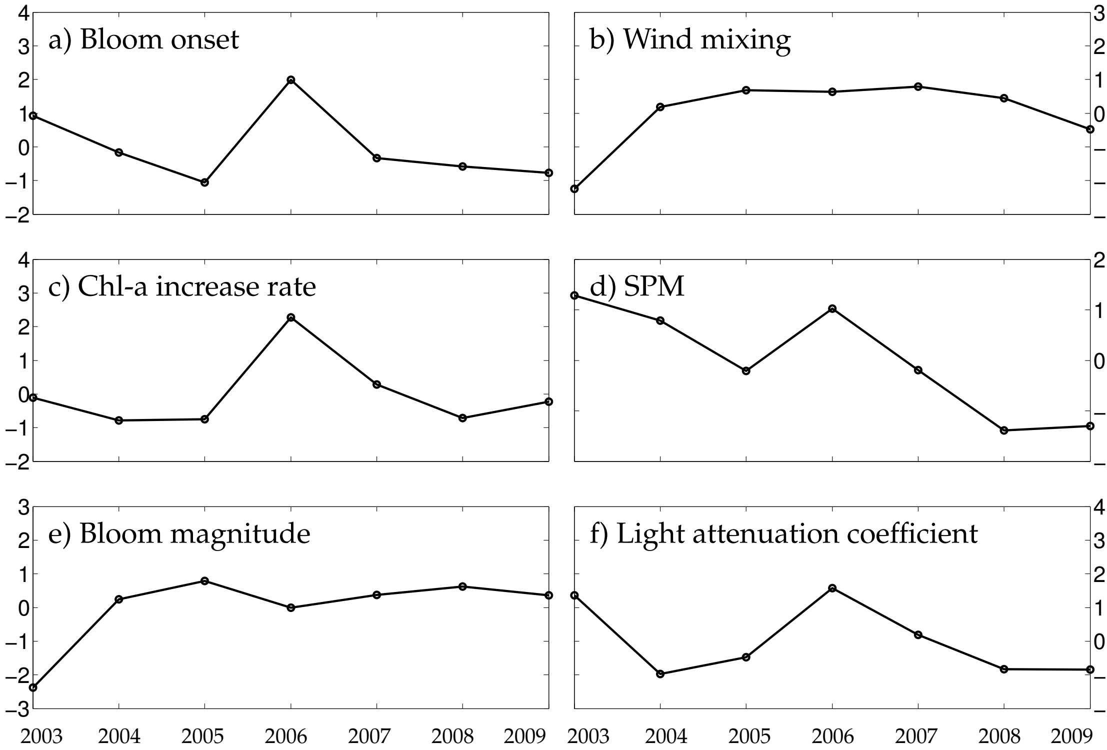

Figure 2.5: Time series for the first EOF mode of a) bloom onset, b) wind mixing, c) Chl-a increase rate, d) SPM, e) bloom magnitude, and f) light attenuation coefficient (K_{min}) during the summer-autumn bloom period.

2.5 Discussion

2.5.1 Light as a limiting factor in summer and autumn

The light attenuation coefficient is a good indicator of light availability for photosynthesis. For the 7-year average, the K_{min} value was higher than 0.2 m^{-1}, implying high turbidity and rather limited light availability in summer-autumn all over the Bohai Sea, which was consistent with the observed conditions in 1982-1983 (Fei, 1986). In our analysis, the Chl-a increase rate and bloom magnitude exhibited strong correlations with K_{min}, revealing that the light condition played an important role in modulating the spatial variability of Chl-a during the bloom period. This conclusion was similar to previous findings for the spring blooms in temperate coastal regions (Yoder et al., 1993; Cloern, 1999; Dore et al., 2002). Guo (1994) also drew the conclusion that the spring bloom in the Bohai Sea occurs when the light input and water temperature increase under calm water conditions. However, the traditional views about the triggers of summer-autumn blooms are concentrated on nutrient replenishment assuming that light availability is sufficient to sustain photosynthesis (Guo, 1994; Wei et al., 2004b; Iida and Saitoh, 2007). To further characterize the role of light limitation in summer-autumn blooms, more in situ measurements concerning water condition and nutrient limitation are required.

2.5.2 The effect of tidal stirring

The timing of a phytoplankton bloom is regulated by the balance between phytoplankton production and losses, which is sensitive to the rate of vertical mixing in the water column (Cloern, 1991). In shallow coastal waters, vertical mixing is manipulated by tidal stresses applied at the bottom and wind stresses on the water surface (Simpson et al., 1991; Cloern, 1996). The tide is strong in the Bohai Sea (Huang et al., 1999), and tidal mixing might have an important influence on phytoplankton dynamics there. However, semi-diurnal and diurnal tides are filtered out in the work because the employed observational data do not resolve the tidal scale explicitly. According to Cloern (1991, 1996), in shallow coastal ecosystems such as the South San Francisco Bay, phytoplankton blooms with short timescale might be regulated by the neap-spring tidal effect, as the phytoplankton biomass increases during periods of weak tidal mixing (neap tides) and declines during spring tides (strong tidal mixing). We selected the year 2008 for a primary analysis (Appendix. C). Fig. C.2 shows that in 2008, summer-autumn blooms developed during both neap and spring tide periods, and the Chl-a increase rate had no obvious correlation with tidal energy. This suggests that the effect of the neap-spring tidal effect might be overwhelmed by other processes.

From another aspect, in this paper, the first bloom in summer-autumn can be referred to as “the seasonal initiation of summer-autumn bloom succession”. To the first order, tides are sub-daily periodic phenomena, we cannot explain the generation of seasonal signals as resulting from the short periodic physical forcing of tides. Therefore, we ignored the influence of tidal stirring and focused our concentration on the influence of wind mixing.

2.5.3 The influence of wind on the summer-autumn bloom

In shallow waters, wind mixing is considered as a critical physical factor for both the SPM variation and biological dynamics. Wind influences bloom development both positively and negatively. Wind-related alterations in vertical mixing, destratification, and upwelling can enhance nutrient supply to the upper layers (Roegner et al., 2002; Tang et al., 2003a; Findlay et al., 2006; Wilkerson et al., 2006). Meanwhile, strengthened vertical mixing can limit depth-averaged light availability by elevating the SPM concentration (Ueyama and Monger, 2005), which can therefore suppress the initiation of blooms in the upper layers. In the Bohai Sea, wind of high variability with different scales leads to complicated local processes and modulates water stability together with tidal mixing, wave mixing and the buoyancy input (Sündermann and Feng, 2004).

The spatial coherence between wind mixing and bloom onset (Fig. 2.3 (a)-(b)) suggests that weak wind over offshore waters stimulates the occurrence of summer-autumn blooms, whereas in coastal areas, strong wind suppresses the blooms. These results differed from previous findings that wind mixing promotes summer-autumn blooms via the nutrient replenishment resulting from vertical-mixing-induced entrainment or the upwelling of nutrient-rich bottom water (Carstensen and Conley, 2004; Ueyama and Monger, 2005; Kim et al., 2007).

Phytoplankton growth is affected by light and nutrient limitation (Bennett et al., 1986). However, Sun et al. (2002) and Liu et al. (2011) reported that, based on observations, in summer-autumn the Bohai Sea is enriched by a high concentration of nutrients from river discharge, sewage discharge, regeneration from sediments, and subsurface groundwater discharge. These observational data imply that in most parts of the Bohai Sea, nutrients might not be the most significant limiting factor in summer-autumn. On the contrary, the analysis of light limitation confirmed that light availability still influences phytoplankton growth in summer-autumn. Wind stirring had a negative effect on the development of summer-autumn blooms by enhancing the sediment resuspension. Concerning the various mechanisms that relate to wind mixing, the time lag between wind mixing and bloom onset varies. The lag correlation analysis (Fig. 2.6 (a)) illustrates a high correlation between wind mixing 0-10 days prior to the bloom and the bloom onset but an independence of the bloom onset from wind mixing after the bloom initiation. The time series data of Chl-a concentration and the corresponding wind mixing at two grid points also indicated weak wind conditions within 10 days before the bloom onset (Fig. 2.6 (b)-(c)). This result confirmed that weak wind conditions preceding blooms created a favorable underwater light environment for bloom initiation. This conclusion implies that wind mixing played the same role in triggering both the spring blooms and the summer-autumn blooms, indicating that in the Bohai Sea, there were similar water conditions in spring and in summer-autumn, which were characterized by high turbidity and relatively rich nutrients. This condition in summer is possibly caused by eutrophication.

2.5.4 Factors driving interannual variability

The large variation in primary productivity is an important characteristic of coastal ecosystem dynamics. Previous observations for the Bohai Sea and adjacent ecosystems indicate that decadal variability in productivity is likely to be modulated by multiple mechanisms (Tang et al., 2003b; Liu et al., 2013). Although it is impossible to derive a reliable correlation between phytoplankton dynamics and climate indices within the limited study period of seven years, the analysis of satellite data can still provide a first explanation of anomalous years such as 2003 and 2006. The resulting hypotheses can then guide the analysis once longer-term time-series data can be introduced.

The multiple ways in which Chl-a variation depends on physical-chemical forcing operate in many ways and at various scales, particularly in a shallow coastal sea. This effect can be observed in the data from 2003, when a negative value appeared in the time series for the first EOF mode of wind mixing and bloom magnitude (Fig. 2.5 (b) and (e)), presenting low wind mixing associated with a small average bloom magnitude. At small spatial scales, wind is here shown to suppress Chl-a accumulation in the Bohai Sea (Table 2.1 and Section 2.5.1). At an annual scale, however, on average reduced wind mixing correlated with a smaller bloom magnitude throughout the summer-autumn period but did not display any correlation with Chl-a increase rate (Fig. 2.5). Given our previous discussion, it can be hypothesized that diminished nutrient availability reduces bloom magnitude in a year with weaker average wind mixing. Although weak winds provided favorable light conditions for a bloom, the wind-mixing-induced nutrient replenishment was low. To conclude, a positive wind influence could be derived at the interannual scale, whereas spatially, bloom development exhibits a negative influence of wind mixing.

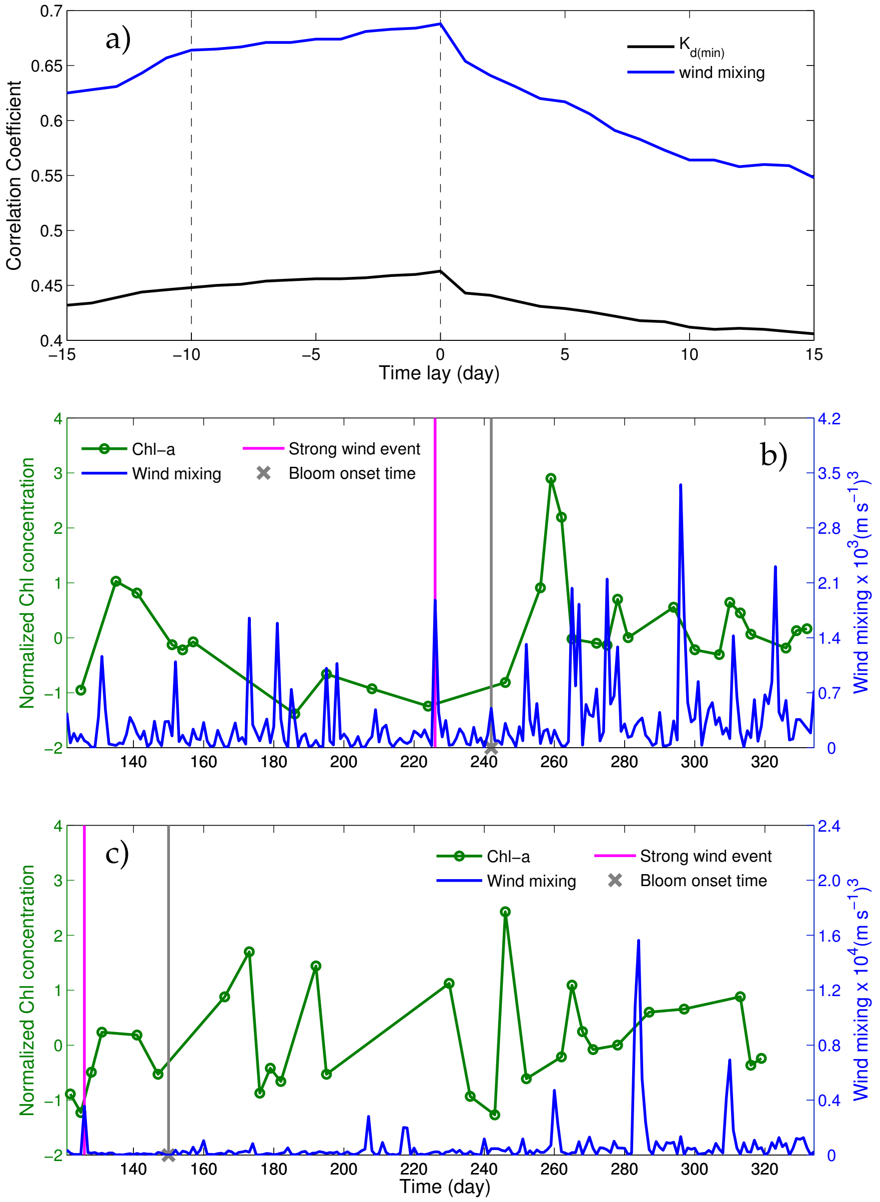

Figure 2.6: The time lag correlation between the spatial distribution of summer-autumn bloom onset and (i) the light attenuation coefficient K_{min} (black line) and (ii) wind mixing (blue line). Positive time lag values indicate co-variation after the bloom onset. The highest correlation appeared between the bloom onset and wind mixing 0-10 days prior to the bloom event (period between the dashed lines). b) and c) display typical time series of Chl-a concentration and the corresponding wind mixing at certain points sampled in Fig. 2.2 to illustrate the relationship between wind mixing and bloom onset.

The year 2006 was also extreme, with a significantly delayed bloom onset but enhanced Chl-a increase rate. This can be explained first by the extreme light conditions. Enhanced light attenuation and reduced light availability would impede bloom initiation but could stimulate photoacclimation if such conditions occur frequently. This extreme year is also related to El Niño/Southern Oscillation (ENSO). Environmental factors in the Bohai Sea are significantly influenced by ENSO. For example, ENSO events resulted in a decrease of approximately 51% in water discharge from the Yellow River to the Bohai Sea (Wang et al., 2006). Because 2006 was an El Niño year (Logan et al., 2008; McPhaden, 2008; Kashino et al., 2009), river discharge during the flood season was relatively low in that year (Fan et al., 2009). Our results may indicate that lower riverine nutrient inputs cause delays in summer-autumn blooms and diminished bloom magnitude but, surprisingly, also increased Chl-a increase rates. The negative correlation between bloom magnitude and Chl-a increase rate might reflect physiological constraints in phytoplankton. Intense short-term variations in Chl-a (Fig. 2.2) very likely reflect effective photoacclimative responses rather than a pure biomass buildup or loss, respectively. Nevertheless, the driving mechanism of summer phytoplankton blooms could be an interplay of water temperature, nutrients, salinity and hydrodynamic conditions (Peng et al., 2012). To elucidate the governing mechanism of interannual variability, a longer time-series of data should be introduced to the analysis system.

2.6 Conclusions

In the Bohai Sea, the spatial and interannual characteristics of summer-autumn blooms were studied using satellite data. In contrast to traditional monthly composite products, in this study, we used daily scenes. A high temporal resolution is a prerequisite for quantifying the statistical relationships between variables that may drive or characterize summer-autumn blooms.

Summer-autumn blooms occurred earlier in the deep offshore waters compared to nearshore areas. The spatial correlation between bloom onset and wind mixing preceding the bloom period were high. Higher Chl-a increase rates with lower bloom magnitudes appeared in the deep offshore waters, which reflected lower SPM concentrations and better light conditions but also the ongoing photoacclimation of phytoplankton cells. Light still represented a key factor modulating bloom intensity and growth during the summer-autumn period in the Bohai Sea, indicating a coexistence of light and nutrient limitation. Interestingly, the triggers of the summer-autumn blooms were similar to those of spring blooms, providing new insight into the ecosystem dynamics of a shallow coastal sea with severe eutrophication.

Interannual variability revealed, in part, different trends from the spatial analysis, which is a further indication of the complexity of the coupling of physical-chemical and biological dynamics. At an annual scale, light attenuation K_{min}, SPM, bloom onset and Chl-a increase rate displayed a clear and positive correlation, which is counterintuitive for K_{min} and the Chl-a increase rate. Also differing from the spatial analysis, annually averaged bloom magnitude and wind mixing exhibited a positive correlation. We found it impossible to apply a single theory to explain the causes of interannual variability in the Bohai Sea ecosystem, as it is likely to be regulated by multiple factors. Hence, we suggest incorporating more MERIS and in situ data in future studies and closely connecting those analyses with integrated and mechanistic modeling.

Chapter 3

Response patterns of the phytoplankton spring bloom to the SPM variations

3.1 Abstract

In this chapter, the ecosystem model (ECOHAM) operating on one well-mixed water column representing the Bohai Sea condition was proposed to test the response patterns of the phytoplankton spring bloom to the SPM variations. In this model, the underwater light attenuation coefficient was directly related to the SPM concentration. Model results demonstrated that simulations using constant, instead of time-varying, SPM concentration led to significant deviations in the estimation of the phytoplankton spring bloom. The neap-spring cycle of SPM concentration modulated the bloom development by creating sub-fluctuations of the phytoplankton biomass on a fortnight scale. The model results also indicated that the tidally-driven SPM variation interfering with the diel light cycle was insufficient to cause deviated predictions if the daily averaged SPM concentration was identical. The SPM settlement during wind slacks had more profound effect on the bloom development then the wind-induced SPM resuspension. In order to have an accurate description of the phytoplankton spring bloom development, the model should be operated with the time resolution of SPM higher than one day.

3.2 Introduction

As the biological engine, phytoplankton production fuels the production at higher trophic levels, and hence, strongly influences the biogeochemical variability (Cloern, 1996). Phytoplankton spring bloom is an important feature in temperate waters since it triggers much of the dynamics in these ecosystems (Edwards and Richardson, 2004; Fuentes-Yaco et al., 2007; Lewandowska et al., 2015). For instance, Platt et al. (2003) found significant correlations between phytoplankton spring bloom timing and the survival of the larval fish on the continental shelf to the east of southern Nova Scotia, Canada. Pörtner and Peck (2010) pointed out that out-of-phase shifts between the seasonal timing of spring blooms of phytoplankton and zooplankton can have consequences for match and mismatch phenomena in food availability for larval and juvenile fishes, possibly leading to regime shifts. Therefore, a thorough understanding and accurate model estimation of the spring bloom is essential.

In eutrophic coastal waters, the underwater light conditions play a critical role in initiating the phytoplankton spring bloom (Cloern, 1999; Colijn and Cadée, 2003). Therefore, it is particularly crucial to investigate with great accuracy the underwater light variability in order to well understand the dynamics of the spring bloom (Tian et al., 2009). In coastal waters, the light extinction properties are largely governed by SPM, which in turn induces a direct effect on the phytoplankton growth and thereby the development of spring blooms. SPM exhibits a high variability on various temporal scales which can be attributed to different physical processes, e.g. the seasonal cycle caused by the wind mixing, the neap-spring cycle and the tidal cycle caused by tidally-driven resuspension, the short-term fluctuation caused by storm events (Grabemann and Krause, 2001). However, the response of phytoplankton spring bloom to the temporal SPM variations in terms of different physical processes has been less investigated in the past, given that the investigation of these processes pertains to scientific disciplines largely evolved independently (Desmit et al., 2005; Tian et al., 2009).

In spite of the lack of a systematic study, we can still find some efforts to demonstrate how the variations of SPM influence the phytoplankton production on various time scales in estuarine/coastal regions. Desmit et al. (2005) demonstrated the importance of the tidal cycle of solids settling and resuspension in estimating phytoplankton productivity, as a significant error occurred when the time-varying light penetration linked to the tidal cycle was neglected. May et al. (2003)

showed that the short-term variation of sediment resuspension, hereafter the turbidity, can significantly enhance the phytoplankton biomass variability. Byun et al. (2007) found that an increase in the PAR (Photosynthetically Active Radiation) attenuation coefficient, taking into account the tidally varying structure of SPM, inhibited phytoplankton blooms. Tian et al. (2009) estimated the importance of SPM dynamics for the phytoplankton spring bloom in the German Bight and emphasized the necessity to involve diurnal cycles or hourly frequent fluctuations of SPM concentration in simulating the initial of the spring bloom. Gohin et al. (2015) postulated that an extension of the storm period in early spring would delay the timing of the spring bloom in the North-West European shelf.

The Bohai Sea (Fig. 3.1) is a typical shallow coastal sea with an average depth of 18 m. This turbid water is subject to SPM variations with time scales ranging from hours to years (Fig. 3.2, detailed explanation can be found in Section 1.2). By far, the linkage of the SPM variations with the phytoplankton spring bloom dynamics is still not well understood. The satellite-derived Chl-a estimates are often perturbed by high turbidity in winter and spring (Su et al., 2015), while the SPM retrieval has an optimal accuracy due to its dominance of the light backscatter (Gohin et al., 2005). As an alternative, the modeling study provides an unique approach, by integrating satellited derived SPM concentrations, to allow the representation of the spring bloom development.

The goal of this chapter is to investigate how the temporal variations of the SPM concentration on different time scales sustain the temporal evolution of the phytoplankton spring blooms. Because of the limited number of cloud-free scenes, the satellite product can not provide SPM data at higher time resolutions than one month. To achieve the goal, several scenario runs were conducted by employing the reconstructed time series of the SPM concentration based on different physical processes.

3.3 Data and methods

3.3.1 MERIS data

The temporally resolved SPM concentration is obtained from the Medium Resolution Imaging Spectrometer (MERIS) satellite products (Rast et al., 1999). It is

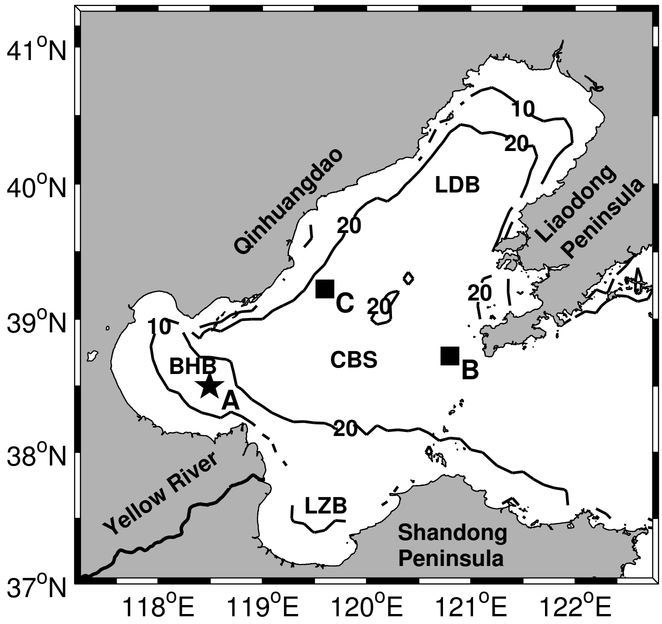

Figure 3.1: Map of the Bohai Sea, with 10m and 20m isobath contours. The four subregions are marked by abbreviations (LDB: the Liaodong Bay; BHB: the Bohai Bay; CBS: the Central Bohai Sea; LZB: the Liaozhou Bay). Station A (marked by black star) is the anchor station where the hourly SPM concentration and bottom current speed were measured from 5th, May 1999 to 6th, May 1999. Station B and C (marked by black squares) are grid sites where the neap-spring cycle and episodic fluctuation of SPM are detected by the remote-sensing data.

one of the standard outputs from MERIS data by the Case 2 Regional Processor developed by Doerffer and Schiller (2007). MERIS collects data every 3 days at the equator and more often at higher latitudes. However, clouds, contrails and sun glint prevent the observation of the underlying surface (Liu et al., 2014), which in turn results in less scenes available. K_{min} is another product of the MERIS data. It is calculated as the mean of those 3 bands which have minimum attenuation coefficient (Doerffer and Schiller, 2007; Tian et al., 2009). The detailed description of the MERIS data can be seen in Section 2.3.1.

3.3.2 Model description

In this study, the ecosystem model ECOHAM (ECOsystem model, HAMburg) was used to simulate the phytoplankton evolution. The detailed model description can be seen in Section 4.3.2. Only the calculation of the light forcing was described in the following section. For the purpose of this study, we concentrated on the water column and not on the effect of advective or diffusive transport on

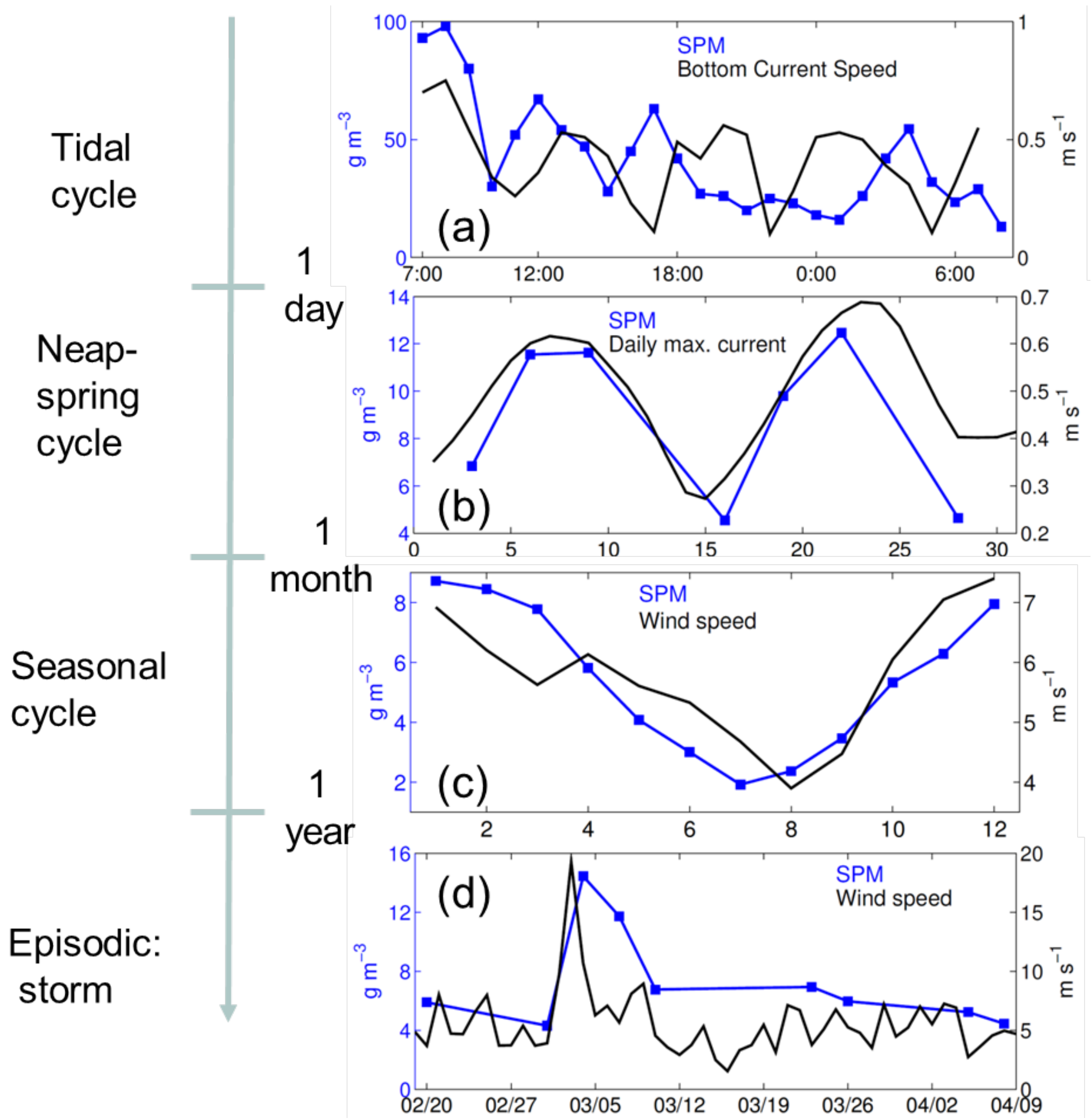

Figure 3.2: Time series of SPM concentration subjected to different variations. Blue lines stand for the time series of SPM concentration. Black lines are the correspondingly possible governing factors. (a) The hourly surface SPM concentration and bottom current speed measured at the anchor station A shown in Fig. 3.1 from 7:00 AM 5th, May 1999 to 7:00 AM 6th, May 1999. (b) The neap-spring cycle of the SPM concentration derived from the MERIS products from 15th January to 15th February 2006 at the Station B shown in Fig. 3.1. The daily maximum current is calculated based on the HAMSOM simulation. (c) The seasonal climatology of SPM concentration over the whole Bohai Sea, which is calculated from 2003 to 2009 based on the MERIS-derived SPM data. Here the SPM concentration is represented in monthly mean. The corresponding wind speed is derived from the NCEP2 database. (d) The MERIS-derived episodic fluctuation of the SPM during a storm event (also derived from the NECP2 database) at Station C shown in Fig. 3.1.

phytoplankton dynamics. Therefore, we applied the model at one single station. The temperature and salinity profiles show that the water column is well mixed during most of the year in the Bohai Sea. Particularly during spring, stratification is unlikely in this shallow system with strong tidal and wind mixing (Jiang et al., 2000). Therefore, the system reduced to zero-dimension (vertically homogeneous) for all constituents (including turbidity), yet to one-dimension considering the vertically attenuation of the PAR. We set a water depth of 16m with 6 vertical layers for the PAR calculation.

The daily physical forcing was provided by the hydrodynamic model (HAMSOM) simulation in 2006. Technically, the simulation started with a 5-year spin-up. A baseline simulation was carried out for the year 2006. Since we were concentrating on the spring bloom, the further analysis was conducted during the first 250 days of the year.

3.3.3 Light forcing

The solar irradiance at the top of the water ($E(\theta, t)$) is given by the ERA-Interim reanalysis data, which is a function of the local latitude θ, time t and the cloudiness. Photosynthetically active radiation (PAR) at the water surface I_0 is calculated as

$$I_0(t) = E(\theta, t) \cdot F_c \tag{3.1}$$

where F_c represents the fraction of total irradiance at PAR wavelength (400-700 nm), here is assigned as 0.43. The time series of I_0 is exhibited in Fig. 3.3.

The underwater light field I_z (z=depth) was calculated according to a simple Beer-Lambert formula (e.g., Lorenzen, 1972):

$$I_z(t) = I_0(t) \cdot e^{-K_d \cdot z} \tag{3.2}$$

where K_d is light attenuation coefficient calculated as a linear combination of various water constituents:

$$K_d = K_b + \varepsilon_{SPM} \cdot SPM + \varepsilon_{Chl} \cdot Chl \tag{3.3}$$

K_b represents the attenuation for background turbidity, which consists of pure seawater and CDOM. ε_{SPM} and ε_{Chl} are diffuse attenuation cross sections of SPM and phytoplankton, respectively. In this study, the monthly SPM concentration derived from the MERIS data were used in the standard run.

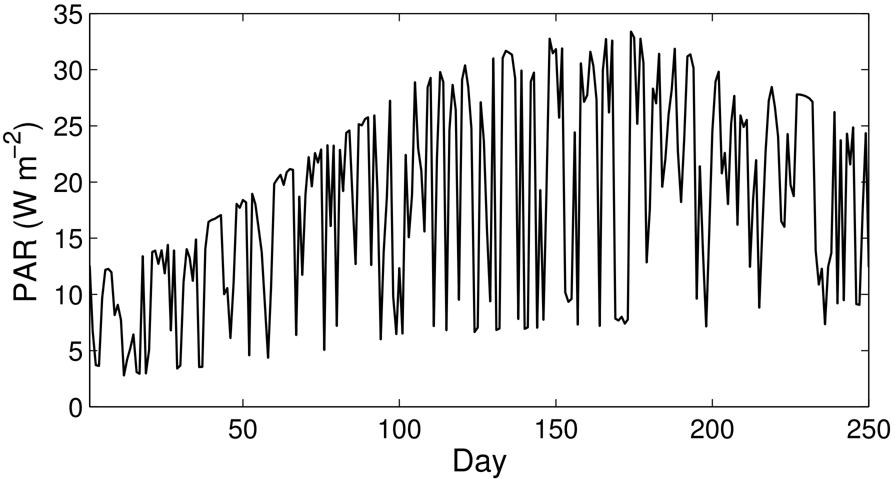

Figure 3.3: Time series of PAR at the water surface

3.3.4 Scenarios

To study the response of the phytoplankton spring bloom to different SPM variations, we explored five scenarios by reconstructing the SPM concentration time series subject to different physical sources (Table 3.1).

Table 3.1: Summary of the tested scenarios. S2* is considered as the standard run.

Scenarios	**SPM forcing frequency**
S1	Constant
S2 *	Monthly with seasonal cycle
S3	Fortnightly with spring-neap cycle
S4	Hourly with tidal cycle
S5	Monthly with episodic storm event

In scenario 1 (S1), a constant SPM concentration was applied to the whole year aiming to remove the seasonality. To explore the possible rang of the spring bloom shift caused by the absence of the SPM variation, we considered three additional cases (S1a, S1b and S1c) with the SPM value assigned to the maximum, minimum and annual mean of the year (Fig. 3.4 (a)).

Scenario 2 (S2), defined as the standard run, employed the MERIS derived monthly average of SPM concentration (Fig. 3.4 (b)). This monthly time series was calculated based on the MERIS images over the period of 2003-2009 to serve as a climatologically seasonal variation. This seasonal pattern was in accordance with the study of Jiang et al. (2000), with higher values in winter-spring and lower values in summer (Fig. 3.5 (a)). $K_d(S2)$ is the corresponding light attenuation coefficient calculated based on Eq. 3.3. Fig. 3.5 (b) exhibits the observed transparency in the Central Bohai Sea in 1982-1983 (Fei, 1986). The corresponding light attenuation coefficient (K_d empirical) was calculated using the empirical relationship $K_d = 1.51 \cdot S^{-1}$ (S is transparency) (Gao et al., 1998). The comparison (Fig. 3.5 (c)) shows that $K_d(S2)$ provides good estimates at low attenuation coefficient levels. The underestimation at higher values was likely due to higher uncertainties in the visual readings of transparency (Tian et al., 2009). In addition, the deviation of the individual year from the climatological mean should also be considered. $K_d(S2)$ shows high correlation with MERIS derived K_{min}. Based on the analysis above, the MERIS derived climatologically monthly mean SPM cooncentration is capable of representing the seasonality in the Bohai Sea.

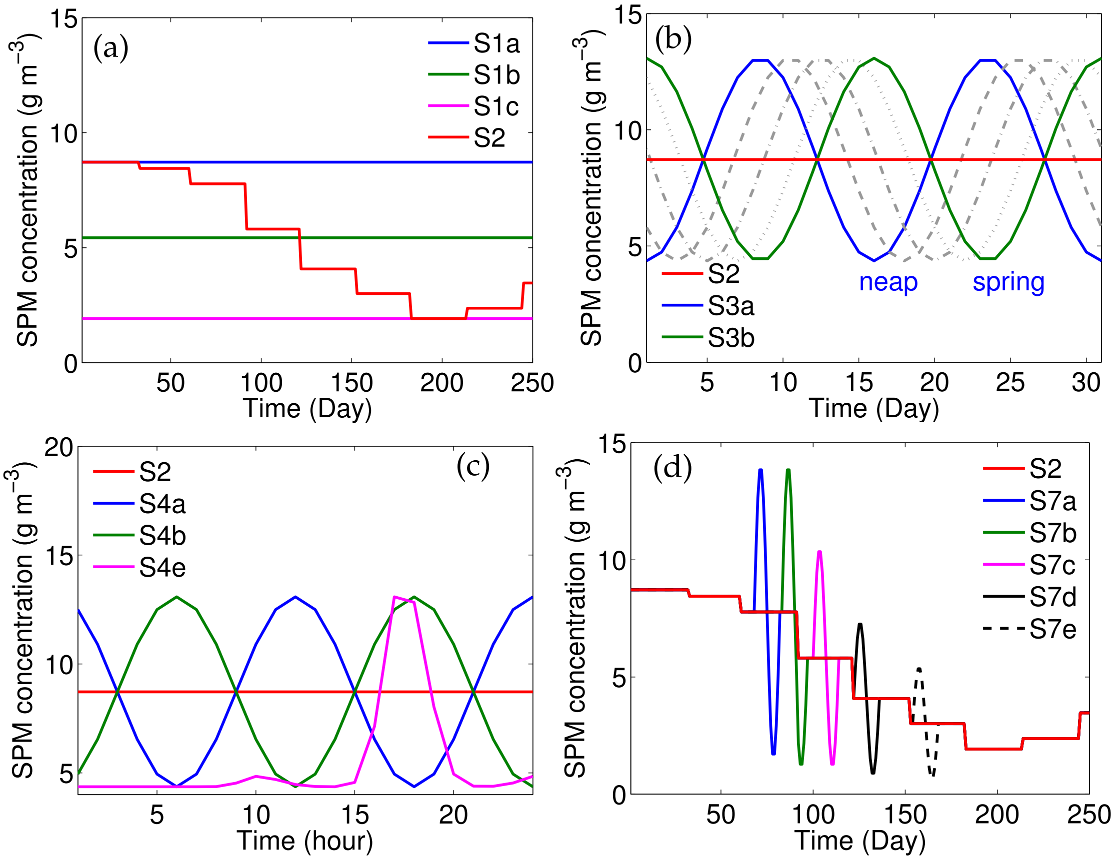

Figure 3.4: Time series of SPM concentration for different scenarios

In Scenario 3 (S3), aiming at exploring the impact of neap-spring fluctuations in the SPM field, we assumed a cosine cycle with a periodicity of half a month, which means the maximum and minimum SPM concentration occur twice a month. The maximum and minimum SPM concentration are set 1.5 and 0.5 times of the monthly mean which is expressed in S2 (Fig. 3.5 (a)). The amplitude was determined based on the observations in Shi et al. (2011) in the Yangtze River Estuary and the Hangzhou Bay of the East China Sea, where the SPM concentration during the spring tides was about $1.5 - 2.5$ times larger than during neap tides. Since the light penetration depends on the phase of the spring-neap cycle, the time series of SPM concentration was defined as a function of the starting phase ϕ shown in Eq. 3.4, where SPM_{daily} is the daily SPM concentration, SPM_M is the monthly mean SPM concentration which is identical with S2. T is the periodicity of the spring-neap cycle, which is defined as half a month for simplicity. t_M is the day of each month. ϕ is the phase lag of the cosine cycle, indicating the starting phase of SPM fluctuation on the first day of each month. Concerning the varying ϕ, eight additional cases (S31-S38) are considered (dashed grey lines), where ϕ was sampled from 0 to 2π with an interval of 0.25 π. Two typical time series of SPM with the ϕ value of 0 (S3a) and π (S3b) are illustrated in Fig. 3.4 (b) for January, indicating a maximum and minimum SPM concentration on the first day of the month, respectively.

$$SPM_{daily} = SPM_M \cdot (1 - 0.5\cos(\frac{2\pi}{T} * (t_M - 1) - \phi)) \tag{3.4}$$

In Scenario 4 (S4), in coastal waters which are characterized by strong tidal forcing, an intratidal variation in SPM dynamics can be introduced by tidal currents (Fettweis et al., 1998; Badewien et al., 2009). SPM concentration increases sharply to the maximum shortly after the current maximum in the middle of the flooding/ebbing period and reaches the lowest level shortly after the high/low tides, leading to a quarter-diurnal (ebb-flood) signal. This fluctuation was also observed in the Bohai Sea (Jiang et al., 2004), as shown in Fig. 3.2 (a). However, due to the asymmetry of the flood-ebb tide, the intra-daily SPM fluctuation was difficult to identify. For instance, Badewien et al. (2009) and Fettweis et al. (2010) all reported a quarter-diurnal (ebb-flood) signal of the SPM variation in the southern North Sea, while Neukermans et al. (2012) found a diurnal SPM variability from the high-temporal-resolution SEVIRI geostationary sensor. The influence of the intra-daily variation of the SPM on the phytoplankton growth was via the combined action with solar radiation. In order to investigate the impact of short-time (hourly) fluctuations in the SPM field, we considered five additional cases (S4 a-e) (Fig. 3.4 (c)). In case S4a and S4b, we used a semi-diurnal cycle of SPM concentra-

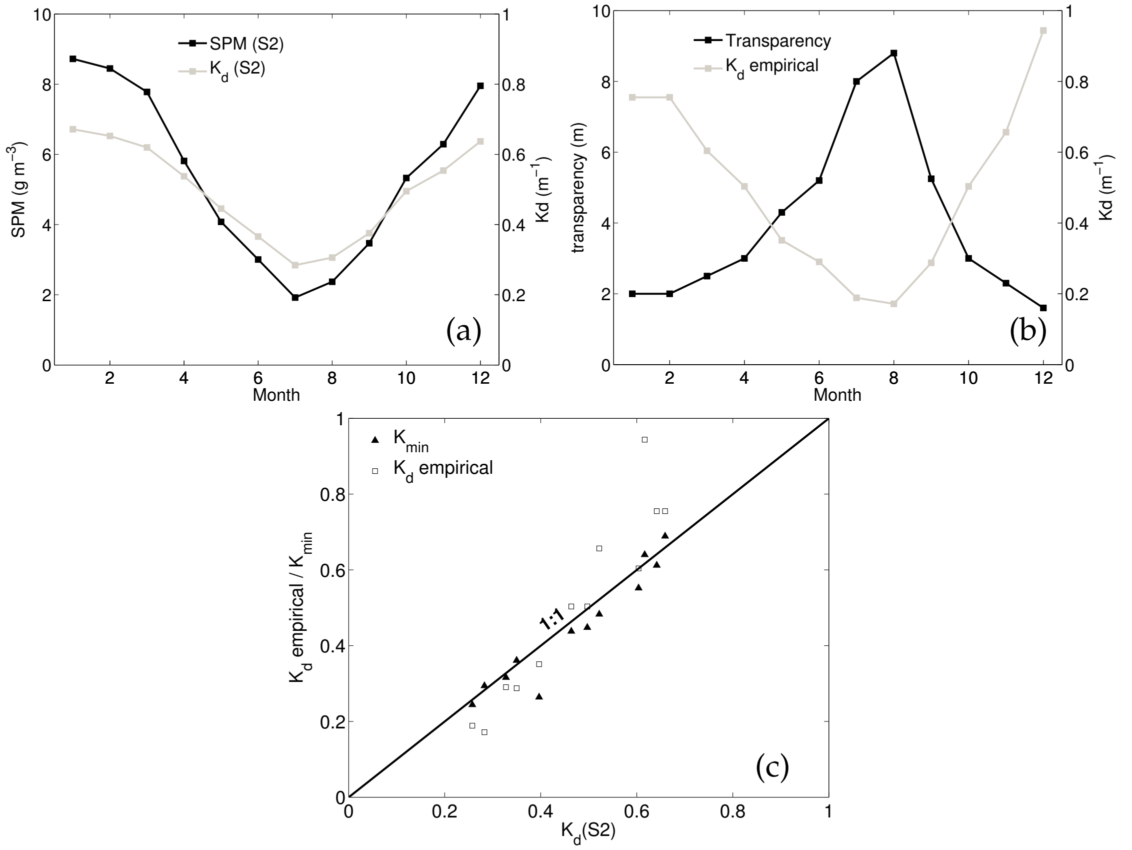

Figure 3.5: (a) MERIS derived climatologically monthly mean SPM concentration and calculated K_d (S2). (b) Observed transparency in 1982-1983 (Fei, 1986) and the corresponding K_d using the empirical relationship $K_d = 1.51 \cdot S^{-1}$, S is transparency (Gao et al., 1998). (c) Phase diagram showing the vertical light attenuation coefficient K_d predicted using SPM versus K_d empirical and the MERIS derived climatic monthly K_{min}.

tion to represent the influence of the diurnal tides, with maximum and minimum value at noon respectively. For cases S4c-d, they are similar with S4a-b but for a quarter-diurnal cycle to represent the effects of the semi-diurnal tides. For case S4e, the SPM concentration was estimated based on Desmit et al. (2005) by expressing the particulate matter content as a function of the local instantaneous current velocity and water depth with the assumption that SPM concentration fluctuated in phase with the tidal current speed:

$$SPM = X \cdot \frac{|u|^5}{z^2} + Y \tag{3.5}$$

where $|u|$ is the current velocity and X, Y are two constant. For all the five cases, the maximum and minimum SPM concentration were 1.5 and 0.5 times of the daily mean used in S2. Based on this assignment, in case S4e the constants X and

Y can be estimated each day.

In Scenario 5 (S5), we considered the effect of the SPM variation caused by strong wind stirring, since the Bohai Sea is often hit by the winter-spring storm produced by cold-air outbreaks (Peng and Wensheng, 2011). Due to the insufficient field observations, especially the lack of high-frequent monitoring during and after the storm period, the response of SPM variations to strong winds is still unclear in the Bohai Sea. However, in the similar coastal regions, it was reported that storm events had a profound influence on the sediment budget, as a continuous long-term measurement of SPM in turbid coastal waters (Wadden Sea) displayed a strong increase of SPM concentration following a storm surge on 9 November 2007 (Badewien et al., 2009). Verspecht and Pattiaratchi (2010) also demonstrated an increase of SPM concentration in the wind-exposed areas. They pointed out that the enlarged bed shear stress would enhance the sediment resuspension and the strong vertical mixing allowed more SPM to be suspended in the water column. Analogously, we can anticipate a remarkable SPM enhancement along with a storm or strong wind event in the Bohai Sea in winter-spring time. Therefore, we set up a series of ”storm scenarios”, assuming a sinusoidal increase of SPM concentration in a period of 7 days, with the highest concentration 1.8 times of the currently monthly mean (The monthly mean see Fig. 3.4 a)). According to Verspecht and Pattiaratchi (2010), a calm period generally follows the passage of the storm, allowing SPM to settle down. Therefore, we assumed a 7-day-period sinusoidal decrease of SPM concentration right after the storm-induced increase, by which we also ensured the whole monthly mean SPM concentration to be unchanged compared with S2. In order to investigate the influence of the SPM variations caused by storms in different periods, we assumed that the 7-day storm occurred far before the standard spring onset time (e.g. on day 68), closely before the spring onset time (e.g. on day 87), during the bloom developing period (e.g. on day 100), during bloom peak period (e.g. on day 122). The corresponding SPM time series are show in Fig. 3.4 (d).

3.3.5 Spring bloom definition

The spring bloom is characterized with respect to its intensity, bloom peak time, onset time and duration (Rey et al., 1987; Platt et al., 2003; Fuentes-Yaco et al., 2007). In this study, we chose the bloom onset time, bloom peak time and bloom intensity to act as the three indices to quantify the blooms.

Analogously to the previous work, we defined the onset of the spring bloom as the time when the phytoplankton biomass (expressed as Chl-a concentration) exceeded a certain threshold (the annual mean, here is 1.5 mg Chl m^{-3}) (Henson et al., 2006; Jo et al., 2007; Peeters et al., 2007; Wu et al., 2007) (Fig. 3.6). In addition, the phytoplankton biomass was required to remain at this elevated level for at least 3 days in order to eliminate temporary increases in phytoplankton resulting from transient events. The spring bloom peak time was defined as the time when the maximum phytoplankton biomass occurred. The bloom intensity was defined as the difference of the maximum and minimum phytoplankton biomass during the study period.

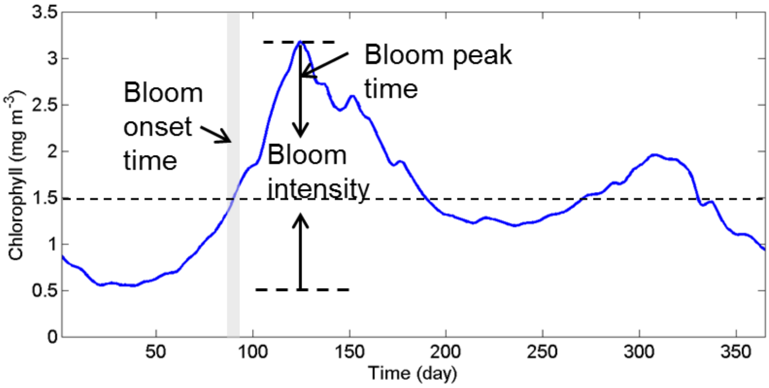

Figure 3.6: Diagram showing the spring bloom definition. The time series of Chl-a concentration is from the standard run, which is driven by the seasonal cycle of SPM concentration (S2). Dashed line shows the threshold of the Chl-a concentration to recognize the bloom period.

3.4 Results

3.4.1 Bloom versus seasonal cycle of SPM

We first investigated S1 to understand the phytoplankton response to the seasonal cycle of the SPM concentration. The high frequent light attenuation fluctuation caused by the daily Chl-a variation was ignored since the magnitude was much smaller than the seasonal cycle. Therefore, we performed a 10-day running mean to K_d (Fig. 3.7). Since SPM was constant, the seasonal variation of K_d was governed by the Chl-a. For all the three cases (S1a-c), the seasonal variations of K_d were weaker than the standard run (S2), which involved the seasonal cycle of the SPM variation.

In Fig. 3.7, high constant SPM concentration in S1a resulted in a delayed phytoplankton spring bloom (both onset and peak time) as compared with the standard run. To further elucidate the mechanism, nutrient (source term) and zooplankton (loss term) were analyzed. In the Bohai Sea, nitrate was found to be the limiting nutrient in spring (Liu and Yin, 2010). Therefore, nitrate was used to represent the nutrient condition. Furthermore, the time of the nutrient depletion was close to the bloom peak time, and the nutrient decreasing rate was an indicator of the phytoplankton growth rate. In S1a, the light penetration was stronger than in the standard run, which resulted in a relatively low nutrient assimilation (hence a lower phytoplankton growth), which caused the later bloom onset time and peak time even though the grazing pressure was weaker before the peak time. In S2a, the bloom onset was earlier even though the phytoplankton growth rate was lower (indicated by the lower nutrient decreasing rate). However, higher underwater light availability in winter-spring period pertained the phytoplankton growth. The consequently higher initial phytoplankton biomass at the beginning of the year contributed to the earlier bloom onset time. The peak time remained unchanged, because of the combined effects of the limited nutrient storage in winter time, the higher grazing pressure and the higher initial phytoplankton biomass. Similar to S2b, the favorable light condition resulted in a quite early bloom onset in S1c. Since the phytoplankton still grew in winter, nutrient could not accumulate in winter. The limited nutrient storage and the high grazing pressure led to a much earlier bloom peak time.

Interestingly, regardless the different levels of the constant SPM concentration, weaker bloom intensities compared with the standard run were found in S1a-c. The mechanisms were different. In S1a, the later bloom peak time was accompanied by an increasing grazing pressure, which resulted in a negative feedback to the phytoplankton bloom development. In S1b and S1c, the limited nutrient storage after the winter time and the higher grazing pressure accounted for the depressed bloom intensity.

The quantitative assessment is displayed in Table 3.2. Without considering the seasonality of the SPM, the spring bloom can be either stimulated or delayed based on the SPM concentration levels. However, the underestimation of the bloom intensity is likely to be independent of the SPM concentration.

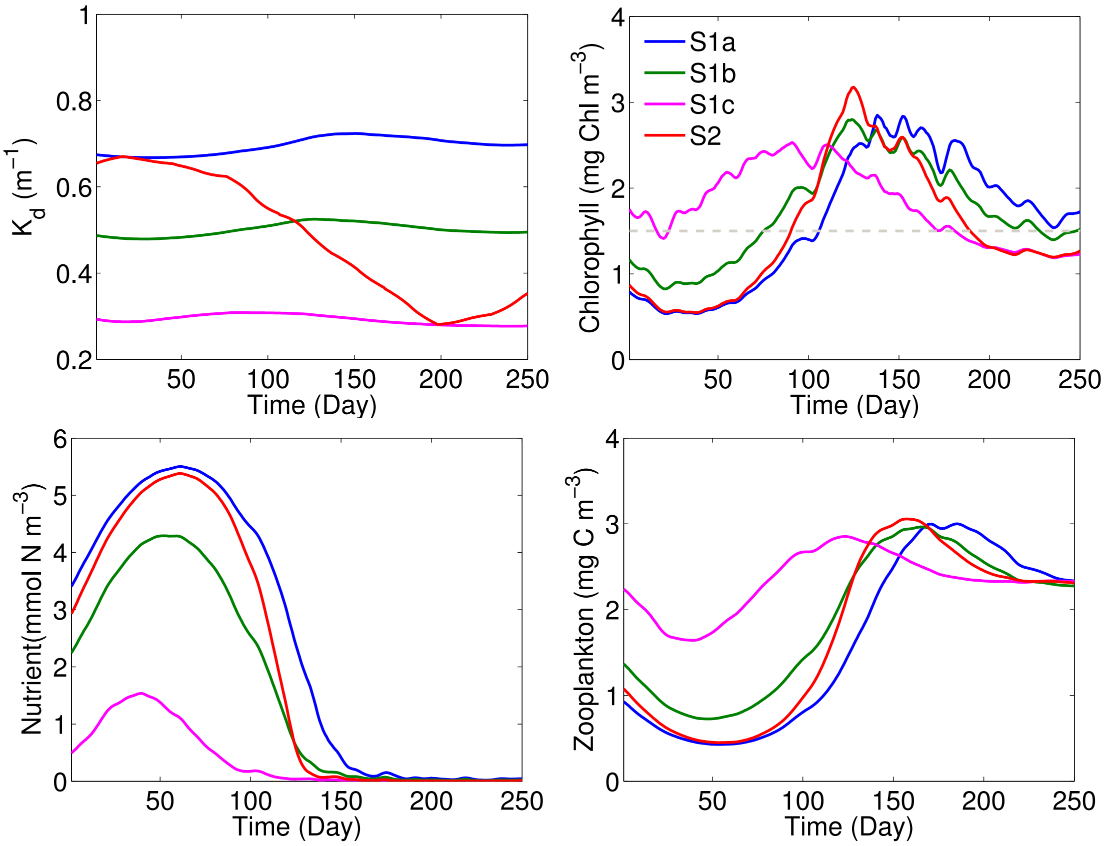

Figure 3.7: Time series of light attenuation coefficient K_d, phytoplankton biomass (Chl-a), nutrient concentration and zooplankton biomass for the first 250 days of 2006 under S1 and S2. Blue lines (S1a) present the case forced with a temporally constant SPM concentration defined as the maximum of the year. Green lines (S1b) present the case with the constant SPM concentration of the annual mean. Magenta lines (S1c) present the case with the constant SPM concentration defined as the minimum of the year. Red lines (S2) stand for the standard run, which was forced by the seasonal cycle of SPM, as was expressed by monthly-averaged concentration. Dashed line shows the threshold of the Chl-a concentration to recognize the bloom period.

3.4.2 Bloom versus neap-spring cycle of SPM

Fig. 3.8 shows the corresponding feedback of the phytoplankton spring bloom when considering the neap-spring cycle of SPM concentration in addition to the seasonal cycle. These comparisons revealed two consistent features. First, in addition to the seasonal evolution, there were sub-fluctuations in the phytoplankton biomass. Second, both cases had an earlier bloom onset time. Different patterns were also observed. In S3a, the bloom onset was later than in S3b, even though both were stimulated compared with S2. The bloom intensity was elevated in S3a but was depressed in S3b as the bloom peak was destroyed. As a consequent, the bloom peak time in S3a seemed unchanged while in S3b the bloom reached the peak earlier.

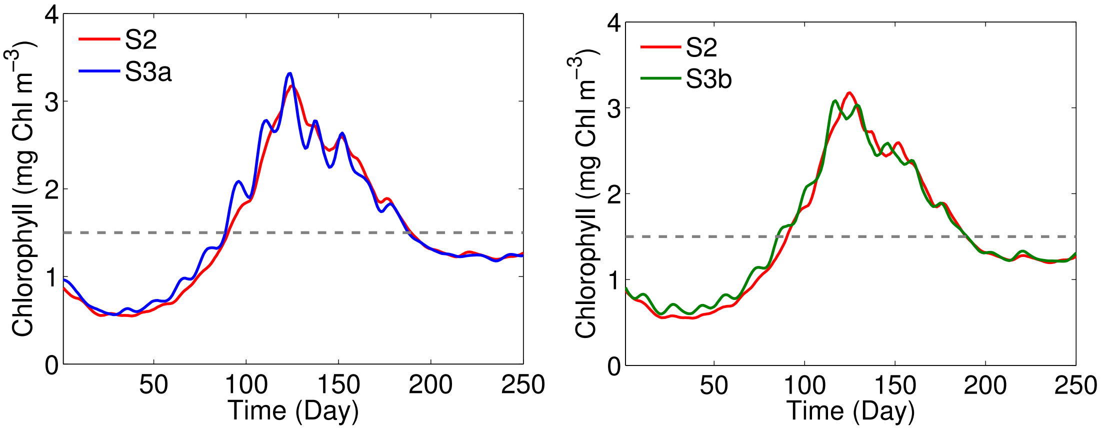

Figure 3.8: Time series of phytoplankton biomass (Chl-a) under the two typical cases in scenario S3 as compared with standard run (red line). Dashed lines show the threshold of the Chl-a concentration to recognize the bloom period.

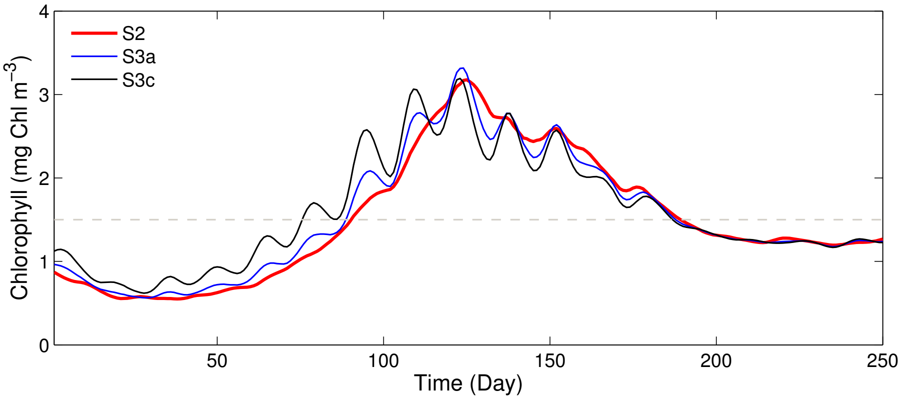

Figure 3.9: Time series of phytoplankton biomass in different cases. The red line stands for the result of the standard run. The blue line stands for S3a, with the neap-spring fluctuation the same order with the monthly mean. The black line represents the results of the additional case similar with S3a, but a SPM fluctuation 1.6 times of the monthly mean. Dashed line shows the threshold of the Chl-a concentration to recognize the bloom period.

In general, the phytoplankton had higher biomass when considering the neap-spring cycle of SPM concentration, which can be seen in Fig. 3.8. The higher phytoplankton biomass during the development phase of the bloom seemed independent of the phase and amplitude of the SPM neap-spring cycle. This results was further illustrated in Fig. 3.9. An additional case with the same phase as S3a but an intensified amplitude of the SPM variation was compared with S3a. In both cases, the phytoplankton biomass was higher than S2. The enhancement was proportional to the amplitude of the SPM variation.

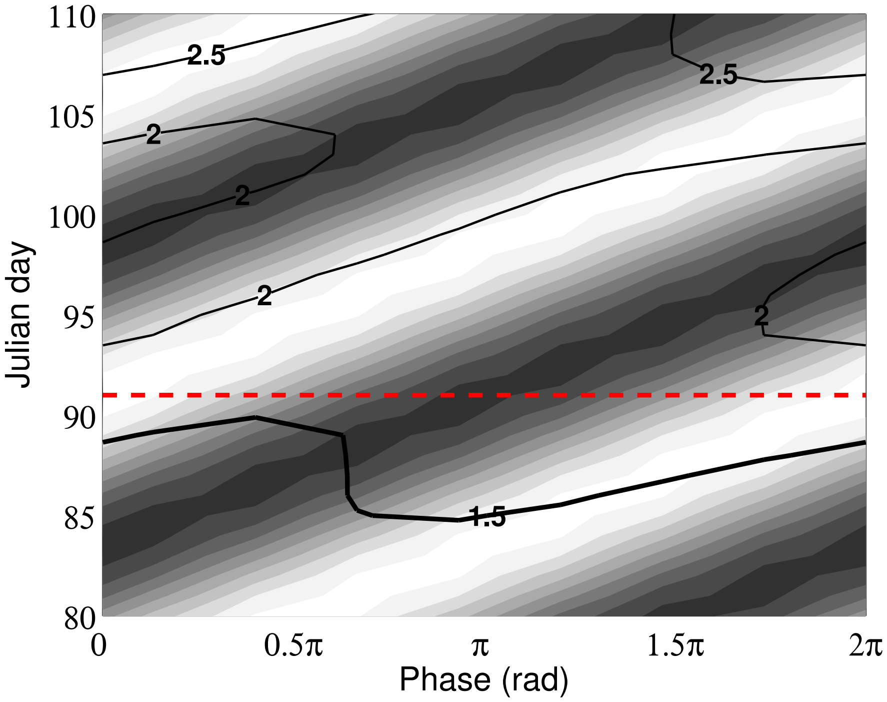

Figure 3.10: Simulated phytoplankton biomass (line contours, mg Chl m^{-3}) and daily-averaged neap-spring index (shaded) as a function of the starting phase (x-axis) expressed in Eq. 3.4. The X-axis stands for the different cases expressed by different starting phases. The Y-axis stands for the day of the year. Along with the Y-axis is the time series of phytoplankton biomass for each case as shown by the contours. The bold black line indicates the threshold Chl-a concentration for defining the spring bloom onset. The red dashed line stands for the bloom onset time of the standard run S2. The shaded contouring illustrates neap tides (white) and spring tides (dark).

The response inconsistency of the bloom onset and the bloom peak implied the dependence of the bloom development on the neap-spring tidal conditions. Fig. 3.10 shows the relationship between the neap-spring tidal conditions and the bloom onset. All the cases showed earlier bloom onset time when compared with the standard run (red dashed line). This conclusion can be also derived from Table 3.2. However, the comparison within the cases revealed the following results: neap tides before the bloom initiation (around day 83) were likely to accelerate the bloom development while spring tides were likely to impede spring bloom development.

Fig. 3.11 is similar to Fig. 3.10 but for the relationship between the neap-spring tidal conditions and the bloom peak development. Neap tides before the bloom peak development (around day 113) were likely to accelerate the peak development while spring tides would impede or destroy bloom peak development.

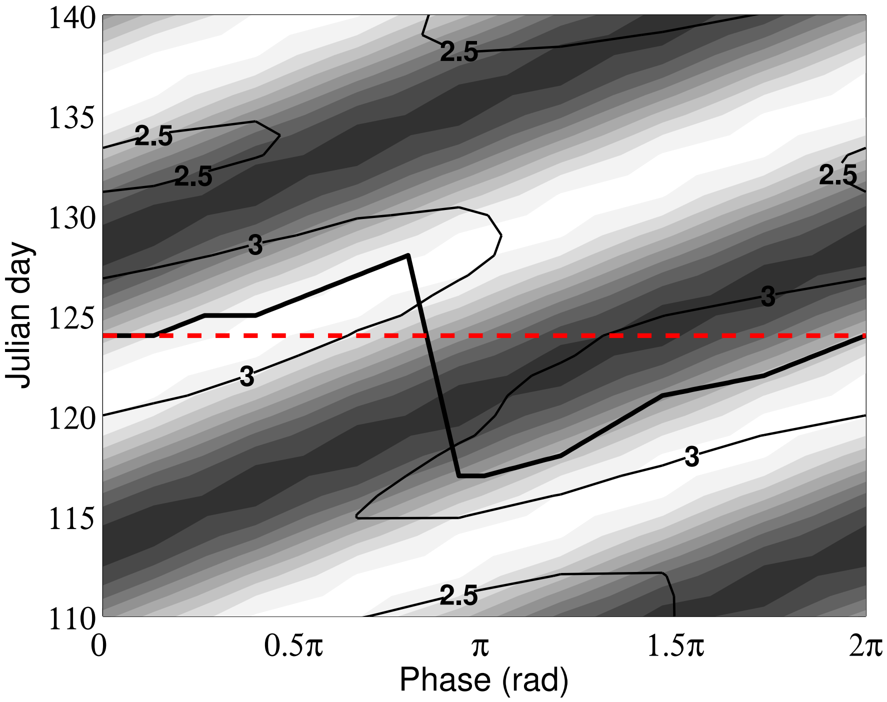

Figure 3.11: Simulated phytoplankton biomass (line contours, mg Chl m^{-3}) and daily-averaged neap-spring index (shaded) as a function of the starting phase (x-axis) expressed in Eq. 3.4. The X-axis stands for the different cases expressed by different starting phases. The Y-axis stands for the day of the year. Along with the Y-axis is the time series of phytoplankton biomass for each case as shown by the contours. The bold black line indicates the bloom peak starting time. The red dashed line stands for the bloom peak time of the standard run S2. The shaded contouring illustrates neap tides (white) and spring tides (dark).

3.4.3 Bloom versus hourly fluctuation of SPM

Fig. 3.12 illustrates the possible response of phytoplankton spring bloom to the diurnal-tidally resolved SPM fluctuation. This fluctuation with a maximum at noon (S4a) did not show significant alternation of the spring bloom. The other case with the minimum SPM concentration at noon (S4b) showed an earlier bloom onset time because of the relatively high phytoplankton biomass before the bloom initiation. For both cases, the bloom peak time and bloom intensity were unaffected. These different responses also illustrated the importance of the interaction between daily resolved solar radiation with the short-term SPM fluctuation.

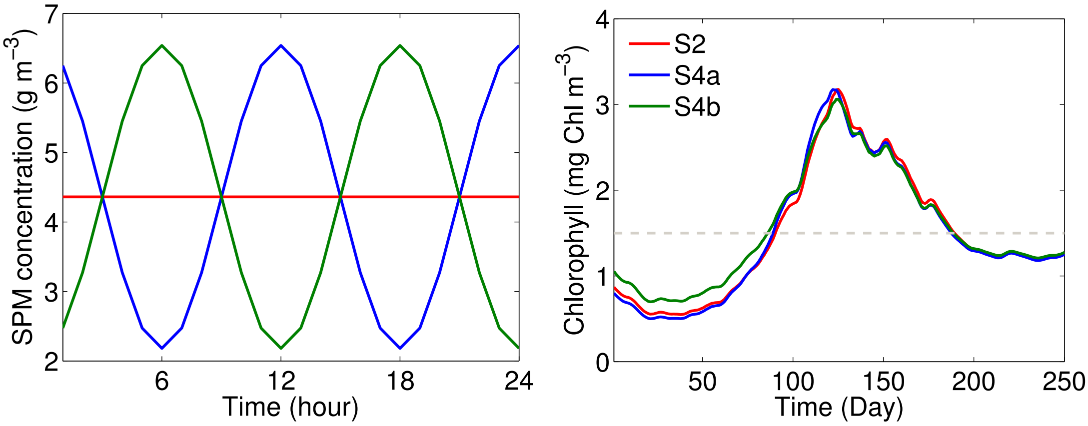

Figure 3.12: Hourly variation of SPM concentration within one day (left panel). Red dashed line stands for the daily SPM in S2. Blue line (S4a) stands for the case with an additional diurnal-tidally resolved SPM fluctuation compared with S2. In this case, maximum SPM concentration appears at noon. Green line (S4b) is the same with S4a but with the minimum value at noon. Daily phytoplankton biomass (right panel) showed the corresponding feedbacks. Dashed lines show the threshold of the Chl-a concentration to recognize the bloom period.

Fig. 3.13 illustrates the possible response of phytoplankton spring bloom to the semi-diurnal-tidally resolved SPM fluctuation. Unlike the case of S4a-b, both cases displayed no significant deviation of the phytoplankton biomass. The comparison of S4a-b with S4c-d revealed that on the hourly scale, lower frequency of the fluctuation would result in a larger bias. The case S4e shows a persistently higher phytoplankton biomass before the bloom peak time (Fig. 3.14).

3.4.4 Bloom versus episodic fluctuation of SPM

Under this scenario, we considered a storm occurring in different periods. According to the response patterns of the phytoplankton spring bloom, those storms were classified into five categories (Fig. 3.15).

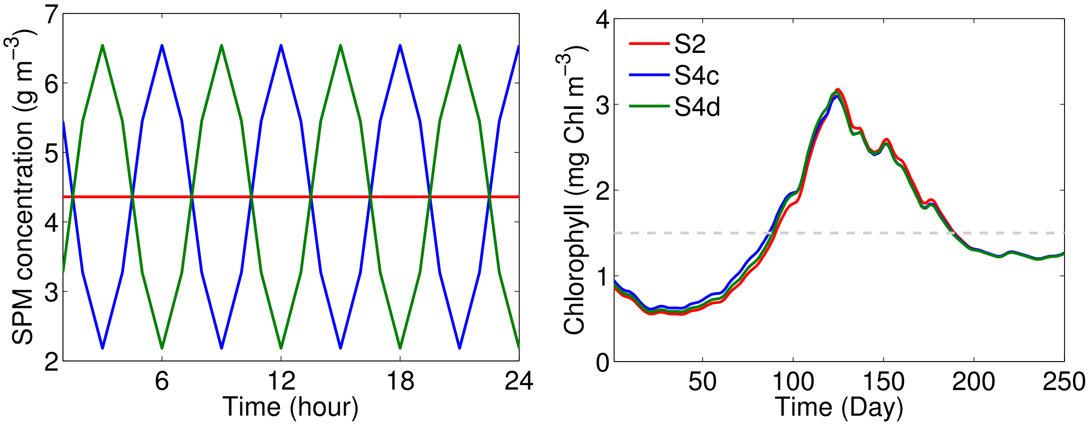

Figure 3.13: Similar with Fig. 3.12 but for an additional semi-diurnal-tidally resolved SPM fluctuation as shown by S4c and S4d. Dashed lines show the threshold of the Chl-a concentration to recognize the bloom period.

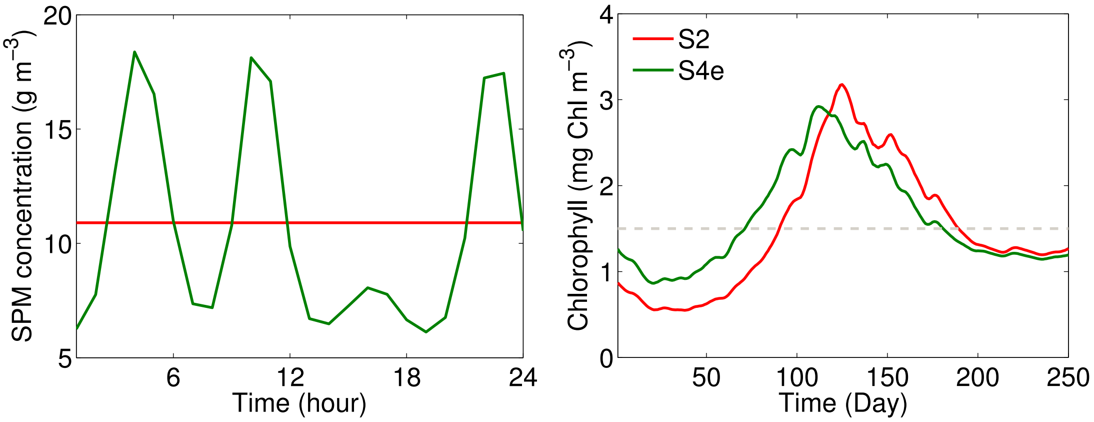

Figure 3.14: Similar with Fig. 3.12 but for an additional SPM fluctuation that depends on the local instantaneous current velocity and water depth. Dashed line shows the threshold of the Chl-a concentration to recognize the bloom period.

The analysis of the five categories revealed two general features of the bloom response. First, the 7-day wind slack induced more remarkable influence on the spring bloom development than the 7-day storm event when the duration and magnitude of the phytoplankton biomass deviation were considered. Second, in spite of the storm perturbation, the spring bloom would finally recover to the standard level.

S5a shows a storm event happening before the bloom initiation. The phytoplankton biomass decreased after the storm formation for a short-term period and then turned to a long-lasting rapid growth. This response led to an earlier boom onset. The bloom peak time was unaffected. The bloom intensity was slightly suppressed. With respect to the standard run, a similar response of the spring bloom was captured when the storm happens during the period from day 48 to day 82 of the year (Figure not shown). That means the storm could influence the spring bloom as long as 43 days after its formation (considering the bloom onset time of the standard run, day 91). Table 3.2 summarizes the possible bloom onset time under the influence of the early storms, ranging from day 83 to day 90, leading the bloom onset time up to 8 days earlier.

S5b shows that a storm happening on day 87 resulted in a delayed bloom onset with a suppressed bloom intensity. Similar response was captured when the storm happens during the period from day 83 to day 91 of the year. This condition led to the bloom onset time ranging from day 92 to day 95, up to 4 days later than the standard run. The bloom intensity was around 2.48-2.49 mg Chl m^{-3}, about 0.13 mg Chl m^{-3} lower than the standard run (Table 3.2).

S5c represents an earlier bloom peak time and an enhanced bloom intensity caused by the storm happening on day 100. A similar response was captured when the storm happens during the period from day 95 to day 110 of the year. The possible peak time can be up to 11 days earlier than the standard run (day 125 of the year). The bloom intensity can be enhanced to 3.19 mg Chl m^{-3}, about 22% higher than the standard run (Table 3.2).

S5d is similar to S5c but for a later bloom peak time. A storm happening during the period from day 115 to day 118 could cause a similar response. As is shown in Table 3.2, the 4-day delayed bloom peak time was corresponding with a 14% enhancement of the bloom intensity.

S5e shows that a storm happening around the bloom peak period did not induce notable perturbation to the spring bloom, only the bloom peak was suppressed to some extent.

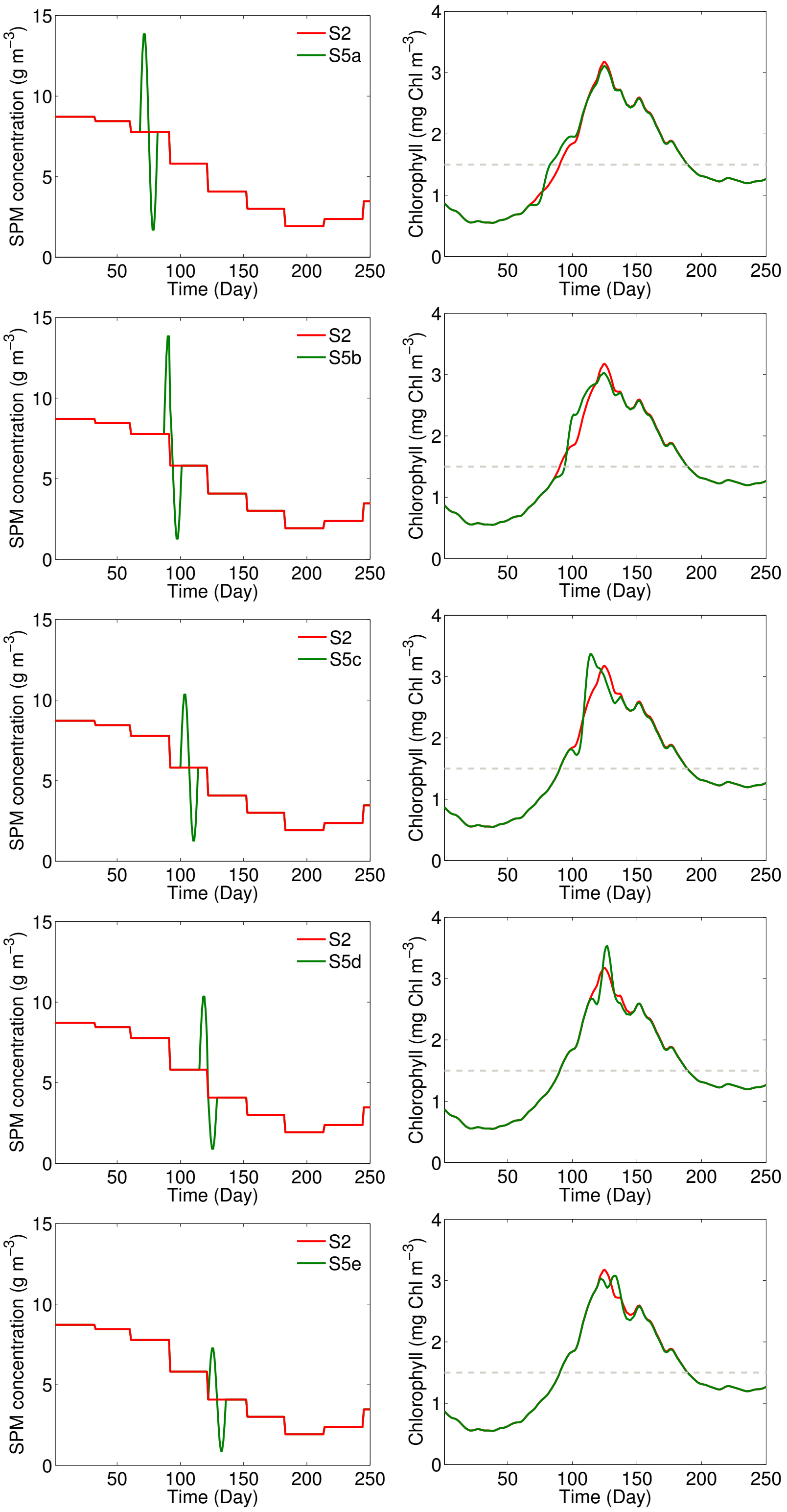

Figure 3.15: The time series of SPM concentration and phytoplankton biomass under S5 (green lines) with a storm happening during different time periods. The storm lasts for 7 days, which is followed by a 7-day wind slack represented by a sinusoidal decrease of SPM. The corresponding result is compared with the standard run (S2, red lines). From top to down, the storm happens on day 68, 87, 100, 115, 122, respectively. Dashed lines show the threshold of the Chl-a concentration to recognize the bloom period.

Table 3.2: The spring bloom characteristics of each scenario. Note in S3, ϕ refers to Eq. 3.4

Scenario	Case	Bloom onset time (day)	Bloom peak time (day)	Bloom intensity ($mgChlm^{-3}$)	Note
S1	S1a	106	138	2.31	
	S1b	76	124	1.97	
	S1c	23	91	1.34	
S2 †	S2	91	125	2.62	
S3	S31(S3a)	89	124	2.75	$\phi = 0$
	S32	90	124	2.75	$\phi = 0.25\pi$
	S33	90	125	2.65	$\phi = 0.5\pi$
	S34	86	127	2.55	$\phi = 0.75\pi$
	S35(S3b)	85	117	2.48	$\phi = \pi$
	S36	86	118	2.53	$\phi = 1.25\pi$
	S37	87	121	2.66	$\phi = 1.5\pi$
	S38	88	122	2.72	$\phi = 1.75\pi$
S4	S4a	87	125	2.36	
	S4b	89	122	2.67	
	S4c	89	124	2.57	
	S4d	87	124	2.48	
	S4e	72	112	2.06	
S5	S5a	83-90	125	2.49-2.63	
	S5b	92-95	124-125	2.48-2.49	
	S5c	91	114-123	2.82-3.19	
	S5d	91	127-129	2.86-2.98	
	S5e	91	133	2.53	

3.5 Discussion

3.5.1 Model deviation related with the seasonal cycle of SPM

In deep waters, the spring bloom development is closely related to the stratification, given that the spring bloom can not initiate until the upper mixed layer depth is shallower than some critical depth (e.g. Sverdrup, 1953; Platt et al., 1991). In shallow waters, the water column is well mixed over the year. Underwater light rapidly attenuates with depth, making the photosynthesis confined to a relatively narrow photic zone. Therefore, the phytoplankton spring bloom is highly depending on the underwater light conditions.

Fig. 3.7 shows that the omission of the SPM seasonality will underestimate the seasonal variation of the underwater light, which in turn alters the seasonal pattern of the nutrient-phytoplankton-zooplankton interaction. S1c produces an unrealistic phytoplankton spring bloom due to the assumption of low SPM over the year, leading to a significant model bias. Nevertheless, the result demonstrated the possible deviation caused by the arbitrary treatment of the SPM variation in previous model simulations. Because of sparse observations, the previous ecosystem model studies in the Bohai Sea did not fully consider the SPM variation (Table 3.3). Liu and Yin (2007a) have pointed out the importance of SPM in predicting the spring bloom when they found the absence of SPM could induce a large bias of the phytoplankton spring bloom compared to their earlier works in Liu and Yin (2006). The choice of a constant SPM concentration can also lead to a large model bias, as the phytoplankton spring bloom is very sensitive to the SPM concentration level, which is demonstrated by the case studies S1a-c.

Table 3.3: Representations of light attenuation coefficient in the previous Bohai Sea ecosystem models. S is water transparency observed once a month during May, 1982-May, 1983. K_w is light attenuation coefficient due to the seawater absorption. K_b represents background light attenuation accounting for the seawater and resuspended sediments. ε_{Chl} is the light extinction coefficient of phytoplankton.

Reference	Light attenuation (K_d)	Parameters
Gao et al. (1998), Wei et al. (2004b)	$K_d = 1.51/S$	S: monthly observation
Liu and Yin (2006)	$K_d = K_w + \varepsilon_{Chl} \cdot \mathrm{Chl}$	$K_w = 0.04$
Liu and Yin (2007a)	$K_d = K_b + \varepsilon_{Chl} \cdot \mathrm{Chl}$	$K_b = 0.15$

3.5.2 Neap-spring tidal effects

The relationship between phytoplankton fluctuations with the neap-spring cycle has been widely discussed in terms of tidal mixing. Phytoplankton spring blooms at neap tides are mostly attributed to the stratification caused by the reduced tidal currents (e.g. Winter et al., 1975; Cloern and Nichols, 1985; Roden, 1994; Sharples, 2008). Our results showed another impact of the neap-spring cycle on the phytoplankton variation in terms of the modulation of the underwater light conditions by means of the SPM fluctuations.

The fortnightly sub-fluctuation of phytoplankton displayed in Fig. 3.8 is clearly related to the SPM neap-spring cycle. Reduced turbidity during calm conditions at neap tides provides suitable light conditions for phytoplankton growth, while an enhanced SPM concentration that is related to the strong tidal current at spring tides is likely to impede the growth. However, the effect of the neap-spring cycle of the SPM is asymmetric. The accelerated phytoplankton increase results in a positive bias of the phytoplankton biomass compared with the standard run. The enhanced SPM at spring tides leads to a drop of the phytoplankton biomass towards the seasonal level. However, the decrease is not enough to lead to a negative bias compared with the standard run. This asymmetry is better illustrated in Fig. 3.9 by the results of S3c, in which the SPM fluctuation is stronger. The acceleration of the phytoplankton growth is more efficient than the repression. This result emphasizes the importance of the light in stimulating the phytoplankton growth in spring, which is also observed in other modeling analysis and the laboratory work (personal communication with Dr J.E.E. van Beusekom). Overall, the neap-spring fluctuation of the SPM is favorable for the phytoplankton spring bloom development, which is also reflected by the earlier spring bloom onset time.

The two tested cases in Fig. 3.9 (S3a and S3c) produced similar temporal phytoplankton developments, however, with distinct differences in the spring bloom onset time, as well as in the phytoplankton biomass. In S3c, the higher fluctuation of SPM presents intensified turbidity at spring tides and stronger light penetration at neap tides. This amplified light attenuation oscillation with a neap-spring cycle leads to higher phytoplankton biomass before the bloom peak. These two cases can be treated as positions with different light regimes. In stronger tidal regions (as represented by S3c), the neap-spring tidal will introduce amplified short-term fluctuation of the phytoplankton biomass as well as an earlier bloom development.

3.5.3 Tidal regimes in the Bohai Sea

Tidally induced high frequency interactions between light and phytoplankton growth in coastal shallow waters have gained increasing attention in the latest years (Lunau et al., 2006; Byun et al., 2007). Desmit et al. (2005) emphasized the necessity to consider the interference between solarly and tidally driven physical forcing functions by operating the model at a high time resolution, because he found remarkable errors when the temporally resolved light penetration that was linked to the tidal cycle of solids settling and resuspension was neglected in the model simulation. However, in the Bohai Sea, we found no significant bias when dismissing the semi-diurnally resolved SPM fluctuation (Fig. 3.13). A bias is likely to be caused at diurnal-dominated regions (Fig. 3.12) as a result of the combined action of the solar cycle and the high frequency of underwater light fluctuation. Therefore, the high frequency of SPM fluctuation at semi-diurnal tidal regions can be ignored while at the regions dominated by diurnal tide, the influence of the hourly SPM fluctuation should be carefully evaluated.

In order to quantitatively classify the tidal type in the Bohai Sea, the number F is employed, defined as:

$$F = \frac{a_{K_1} + a_{O_1}}{a_{M_2} + a_{S_2}} \tag{3.6}$$

Where a_* is the tidal constituent amplitude. Where F is less than 0.25, the tide is classified as semi-diurnal; Where the number is from 0.25 to 2, the tide is mixed but mainly semi-diurnal; where the number is from 2.0 to 4.0, the tide is mixed but mainly diurnal; where the number is greater than 4.0, the tide is diurnal. Fig. 3.16 shows the distribution of the tidal type in the Bohai Sea, in which most parts are dominated by semi-diurnal or quasi semi-diurnal tides. Only limited regions near the coast of Qinghuangdao and the Yellow River mouth are characterized by diurnal tides.

In case S4e, the SPM fluctuation is estimated using the concept of maximum transport capacity, which is suitable in strongly tidal shallow regions (Desmit et al., 2005). The application to the Bohai Sea needs an accurate validation in combination with a large amount of observations.

3.5.4 SPM settling during wind slacks

The effect of wind on the SPM variations is very complicated and can not be explained simply with a clear relationship. The wind direction and the advection of water masses, the previous history and the availability of fine-grained sediments in fluffy layers are all factors influencing the SPM signal. In spite of those difficulties, we only adopt the concept that high winds would lead to an increase of SPM concentration whereas in the following wind slack periods the SPM would settle down.

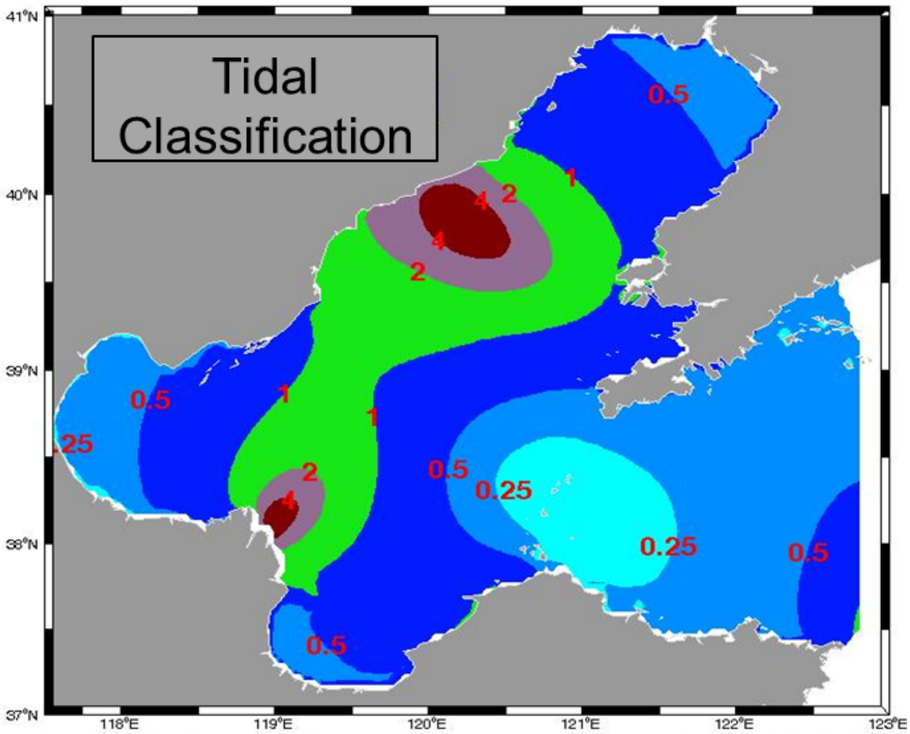

Figure 3.16: Map showing the tidal type distribution in the Bohai Sea. (Zheng, personally communication)

Our simulation shows a profound effect of the SPM decreasing on the phytoplankton spring bloom in terms of the bloom duration and magnitude (Fig. 3.15). Tian et al. (2011) have found in the German Bight the similar effect of the wind slack on the spring bloom formation. They observed a period of high wind speed preceding the spring bloom and a following wind slack at the bloom period. By settling of SPM, the wind slack effectively ensures deeper light penetration in the shallow coastal waters, which significantly releases the light limitation for the phytoplankton growth (May et al., 2003).

3.6 Conclusion

In this chapter, we investigated the possible response of the phytoplankton spring bloom to different SPM variations. We conducted idealized scenario simulations based on the limited observations that reveal the typical SPM variation time scales. Fig. 3.17 summarizes all the possible deviations of the spring bloom from the standard run, which is driven by the seasonal cycle of SPM concentration. The largest deviation occurs when constant SPM is involved in the simulation.

Remarkable deviation can also be derived when the tidally resolved SPM field is used. The neap-spring cycle of SPM concentration is likely to cause an earlier bloom onset time. The bloom peak development is highly depending on the neap-spring tidal conditions. Episodic fluctuations of the SPM field caused by storm events affect the spring bloom, mostly because of the SPM settlement during the wind slacks. This work is a first trial to help understand the possible mechanisms of the interaction between different underwater light regimes and the phytoplankton spring bloom dynamics. We expect further detailed observations and model advancements to improve our understanding.

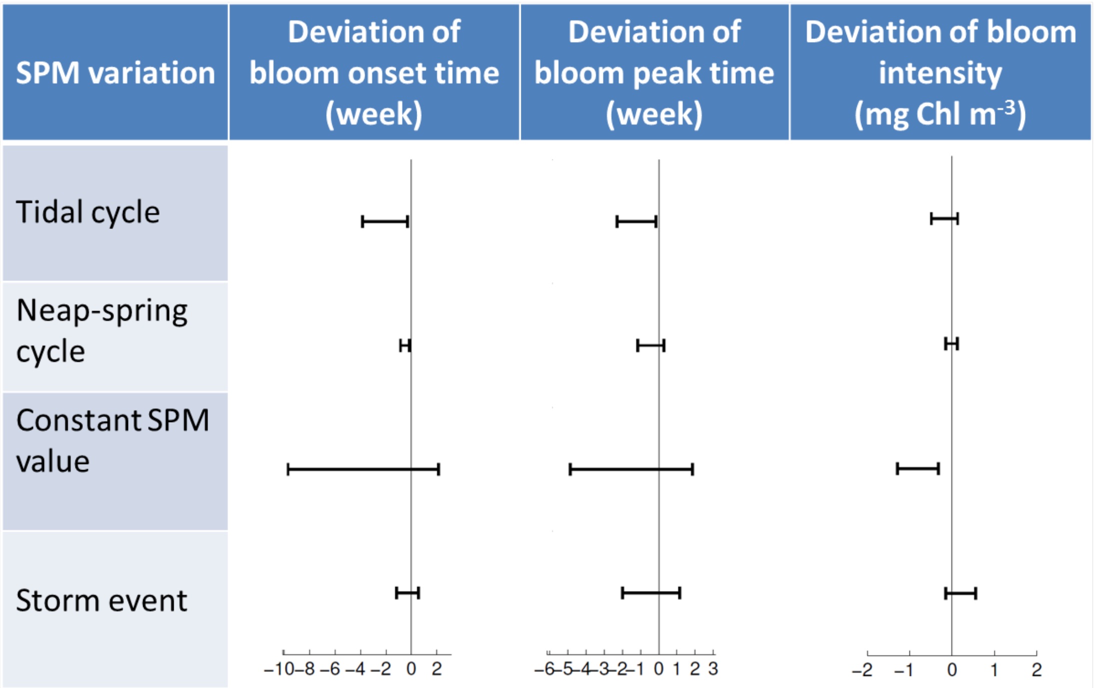

Figure 3.17: The summary of the response of the phytoplankton spring bloom to different SPM variations. Bars show the deviation of each bloom indices from the standard run.

Chapter 4

The coupled hydrodynamic-ecosystem model HAMSOM-ECOHAM: Model description and validation

4.1 Abstract

This chapter presents the setup and the results of HAMSOM-ECOHAM, a three-dimensional coupled hydrodynamic-ecosystem model dedicated to simulate the the annual cycle and spatial distribution of phytoplankton and nutrients in the Bohai Sea. The ecosystem model ECOHAM is based on lower trophic level interactions taking into consideration of two phytoplankton and two zooplankton components. The dynamics of the phytoplankton components are governed by the availability of nutrients (nitrate, ammonium, phosphate and silicate) and light, as well as the temperature influence. The ecosystem model is coupled to a nonlinear three-dimensional baroclinic model HAMSOM.

The model was integrated for 2006. Model validation was first shown by comparing time series of model simulated phytoplankton biomass and nutrient concentrations with in situ data in two regions with different physical conditions. This comparison indicated that the model was able to reproduce the seasonal dynamics of phytoplankton and nutrients in the Bohai Sea, especially the development of the spring bloom. In regions close to the Yellow River mouth, the model produced lower Chl-a concentration in early spring and a consequently later sea-

sonal increase. As a general trend, the Chl-a concentration was overestimated during the summer-autumn period. The seasonal evolution of the two phytoplankton components indicated the dominance of diatoms in spring and the co-existing of diatoms and the other phytoplankton species in summer-autumn time. Comparisons between the monthly averaged surface Chl-a and nutrient concentrations of the model simulation with in situ data were used to assess the accuracy of the simulated spatial distribution. In general the model was able to reproduce the spatial patterns of the Chl-a and nutrients with nevertheless discrepancies in the three bays. The simulated phosphate showed inverse pattern with the observations in 1982 and 1992 but agreed well with the observations in 2008, possibly because of the long-term change of the nutrient regimes during the last 30 years.

4.2 Introduction

Fig. 4.1 shows the monthly composites of MERIS-derived light attenuation coefficient (K_{min}) and SPM from March to May in 2006. Remarkable spatial gradient of K_{min} suggests that the Bohai Sea is dominated by different light regimes. High spatial correlations between K_{min} and SPM suggest that the Bohai Sea is optically dominated by SPM. In Chapter 3, we investigated the influence of the SPM variations on the phytoplankton spring bloom focusing on one single station. In regarding to the different light regimes in the Bohai Sea, the further investigation on the spatial pattern of the phytoplankton spring bloom is essential, which requires an extension of the one-station analysis to a three-dimensional exploring. Therefore, a three-dimensional model simulation is required.

Several modeling efforts have already been performed in the Bohai Sea to address different questions in concern. Gao et al. (1998) compared the annual cycles of primary production in different regions by using a vertically integrated NPZD model. Liu and Yin (2007b) investigated the nutrient-phytoplankton dynamics using a coupled model in which the biological model is a simple NPZD module. Wei et al. (2004b) used an earlier version of ECOHAM to study the phytoplankton dynamics as well as the nutrient budgets in the Bohai Sea. However, none of the existing models was found to be appropriate for the aims of the thesis. For example, some of these models involve only one nutrient cycle and hence might not be flexible enough for simulating phytoplankton under different nutrient limiting conditions (Liu and Yin, 2006, 2007b). The main point is that these models paid less attention on the representation of the underwater light variability as well as the linkage with the SPM variations. Gao et al. (1998) and Wei et al. (2004b) calculated the light attenuation coefficient, which is the key factor for determining the underwater light climate, as a linear function of water transparency, which was only distinguished by four regions. Liu and Yin (2006, 2007b) considered the temporal variation of light attenuation only as a function of phytoplankton.

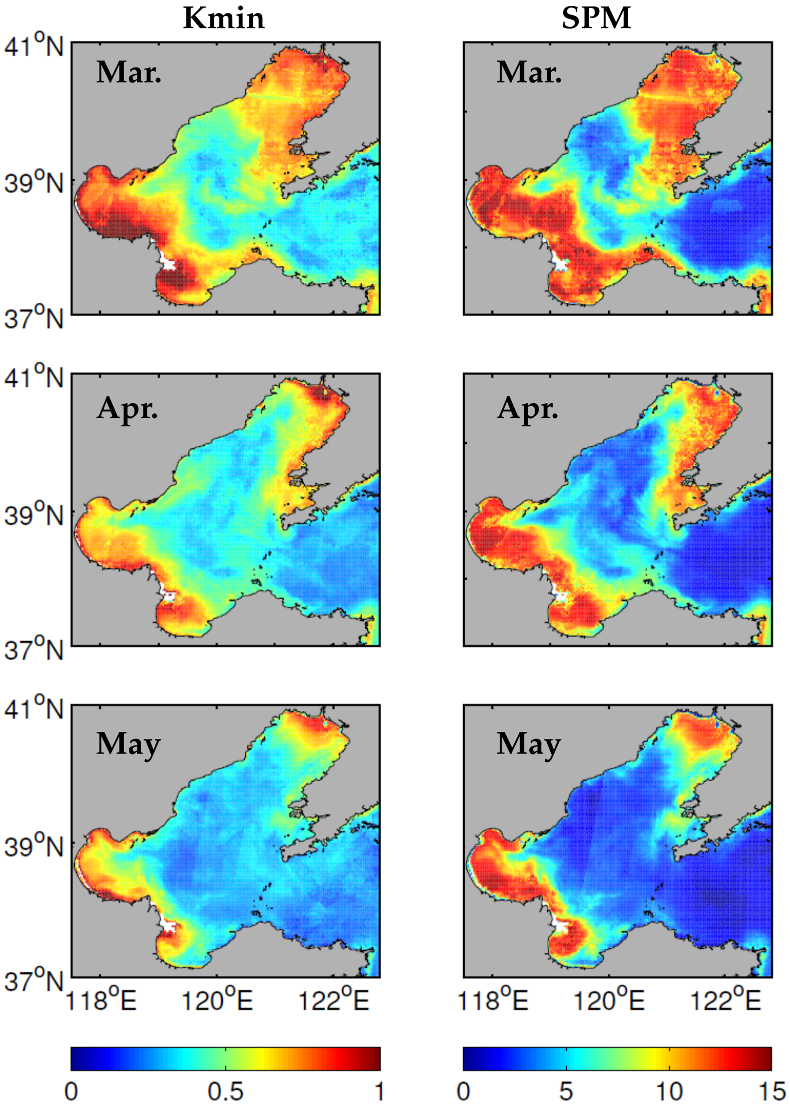

Figure 4.1: Monthly evolution of K_{min} (left panels, m^{-1}) and SPM (right panels, g m^{-3}) in 2006 derived from MERIS images.

In this chapter, the goal is to adopt a proofed model of sufficient complexity to resolve the temporal and spatial variations of the phytoplankton and nutrients, especially for the simulation of the phytoplankton spring bloom, to lay a foundation for the study of the influence of the SPM variations on the spatial patterns of the phytoplankton spring bloom. In addition, this model should be able to examine the effects of underwater light variations, including SPM variations for scenario testing. Here we concentrate on the model-setup and validation.

4.3 Model description

The coupled hydrodynamic-ecosystem model HAMSOM-ECOHAM was developed for the Bohai Sea to include the interactions of water masses, nutrients and plankton biomass. In the following, the description is separated into a description of the hydrodynamic and ecosystem components, a description of the model configuration as well as a description of the model parameterization. The interaction of the coupled model is illustrated in Fig. 4.2.

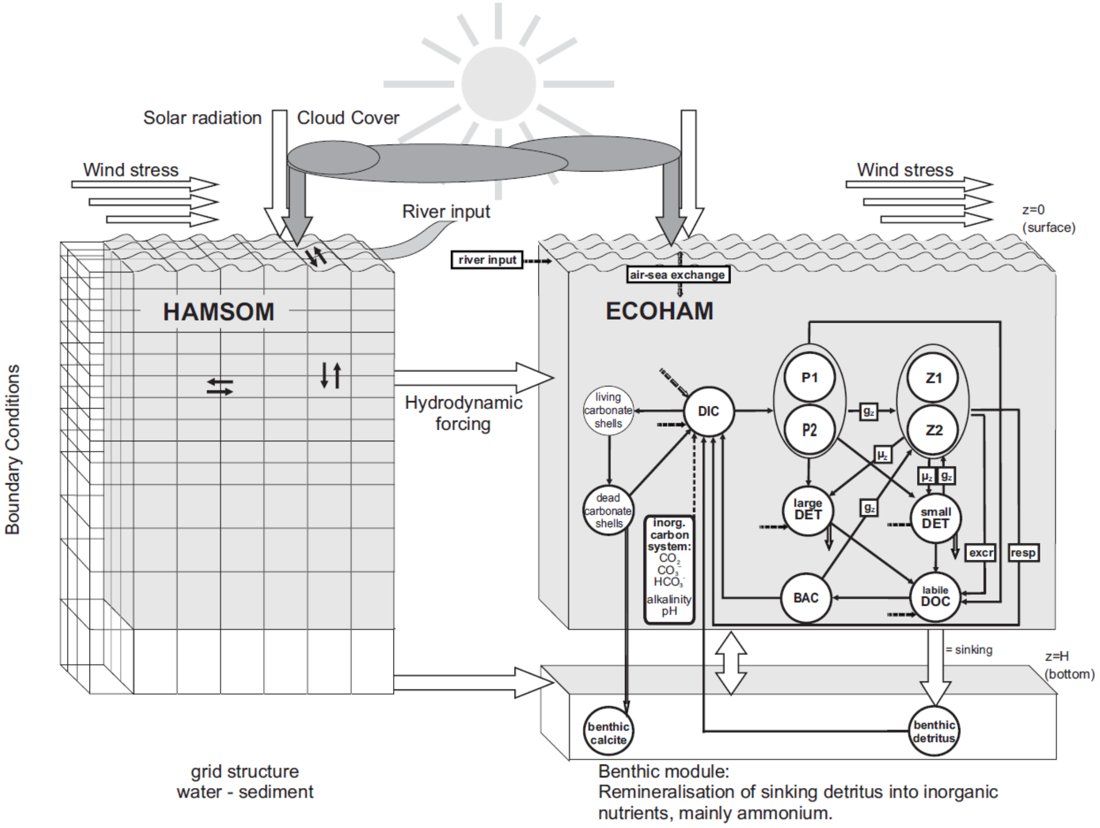

Figure 4.2: Conceptual diagram of the three-dimensional coupling of the hydrodynamic and ecosystem model showing the physical transport within grid cells and local ecosystem processes in each grid cell for the example of the carbon cycle (Stegert et al., 2009, see Fig.2 modified)

4.3.1 The hydrodynamic model

The hydrodynamic component of the coupled model is based on the nonlinear primitive equation model HAMSOM (HAMburg Shelf Ocean Model). HAMSOM has been developed in the Institute of Oceanography at the University of Hamurg and has been applied to several regions (e.g. Alaee et al., 2004; Pohlmann, 2006; Schrum et al., 2006; Meyer et al., 2011). General characteristic of the model can be found in Backhaus and Hainbucher (1987) and Pohlmann (1996). This model has also been successfully applied in the Bohai Sea to investigate the hydro- (Hainbucher et al., 2004; Wei et al., 2004a) and thermal-dynamics (Huang et al., 1999).

The model variables, including temperature, salinity, horizontal and vertical advection as well as turbulent mixing, are provided to the ecosystem model. Daily averaged results are stored for driving the ecosystem model in offline mode for the period of 2001-2006.

4.3.2 The ecosystem model

The ecosystem model ECOHAM (ECOsystem model, HAMburg) is a lower trophic model that was initially developed for the North Sea ecosystem in the Institute of Oceanography, University of Hamburg. The model has been continuously improved during the last 20 years by being used to investigate various ecological/biogeochemical questions (ECOHAM1, Moll 1998, Skogen and Moll 2005; ECOHAM2, Moll and Stegert 2007; ECOHAM3, Pätsch and Kühn 2008, Stegert et al. 2009; ECOHAM4, Lorkowski et al. 2012). In this study, we employed the version that is described in Lorkowski et al. (2012), where the detailed explanations of biological processes and their parameterizations can be found. The general model concept is described as follows.

ECOHAM includes interactions between 34 state variables, which consists of four nutrients (nitrate, ammonium, phosphate, silicate), two phytoplankton groups (diatoms and the other phytoplankton species referring to as flagellate), two zooplankton groups (micro- and mesozooplankton), bacteria, two fractions of detritus (fast and slowly sinking), labile dissolved organic matter, semi-labile organic carbon, oxygen, dissolved inorganic carbon and total alkalinity. Dissolved and particulate matter (C, N, P, Si) have variable ratios. The model employs three biogeochemical cycles for the nutrients: the nitrogen cycle, the phosphorus cycle and the silica cycle, so that it can cover the main macro-nutrient-limiting phytoplankton production in coastal waters. The dynamics of the two phytoplankton functional groups, diatoms and all the rest, mainly flagellates, are simulated based on their respective physiological characteristics. The fate of the two zooplankton functional groups is estimated according to their specific feeding behavior. The flow of nutrients and biomass in the model is calculated based on the concept of Redfield stoichiometry, with a fixed ratio of C:N:P applied for the phytoplankton groups (C:N:P=106:16:1). Carbon is used as the currency in the simulation. Chl-a concentration is diagnostically calculated from the simulated phytoplankton biomass in carbon unit, assuming a constant ratio of 38 mg C: 1 mg Chl as observed in the Bohai Sea (Wei et al., 2004b). In the following analysis, Chl-a concentration is used to represent the phytoplankton biomass.

4.3.3 Model setup

In this study, the model grid configuration is adjusted slightly from the previous applications (Huang et al., 1999; Wei et al., 2004a). The study area covers 37.0 ^{o} - 41.25 ^oN, 117.25 ^{o} -123 ^oE. The horizontal resolution is 5 $'$ both in latitude and longitude. Vertically, 19 layers are set up with the thickness increasing towards the bottom. The surface layer thickness is time-varying due to the free surface elevation, with a mean thickness of 4m. The underlying layer thickness is 3*12, 5*6m from top to bottom. The ecosystem model has the same grid configuration with the coupled hydrodynamic model.

Initially, the currents are simply set to zero. Since the Bohai Sea is well mixed in winter, temperature and salinity are both taken to be uniform, as 20 ^{o} C and 34 respectively for the initial condition. The biological compounds are specified homogeneously according to Liu and Yin (2007a), with the concentrations of nitrate, ammonia, phosphate, zooplankton and detritus set to be 3.55, 0.71, 0.5, 0.2, 0.2 $mmol\ m^{-3}$, and the phytoplankton biomass 1 $mg\ Chl\ m^{-3}$.

The open boundary is placed in the North Yellow Sea, far away from the study area, to avoid possibly unexpected open boundary effects due to the inconsistency of the simulation and the input boundary conditions. The open boundary conditions, including the monthly temperature and salinity, are provided by the World Ocean Atlas 2009 (WOA09). The sea surface elevation at the open boundary is obtained by means of harmonic analysis, with 11 dominant tidal constituents (Q1,O1,P1,K1,N2,M2,S2,K2,Mf,Mm,M4,MS4 and Mn4) considered. For nutrients, phytoplankton biomass and zooplankton biomass, the seasonal variations are derived from marine atlas (Zhang et al., 1991).

Instead of using the sparse oceanographic stationary observations (only 4 stations, see Huang et al. (1999)), we obtained the meteorological forcing from the ERA-Interim database (Dee et al., 2011). The forcing consists of six-hourly fields of air temperature, relative humidity, cloud coverage, wind speed and wind stress in 2 dimensions for the year 2006. In HAMSOM, surface fluxes were calculated by the bulk formula according to Large and Yeager (2009). The simulated three-dimensional temperature, salinity, advection flow field and turbulent mixing were provided to the biological simulation. The 2-hourly short wave radiation at the water surface were calculated as a function of the local latitude θ, time t, solar constant set to 1368.0 $W\ m^{-2}$ and the six-hourly cloudiness from the ERA-Interim database, taking into account the effect of surface albedo (Beriland, 1960; Budyko, 1974). The SPM concentration was the monthly composites derived from the MERIS data averaged over 2003 to 2009. This data was further interpolated spatially to each grid point of the model. The model was integrated for the year 2006 with five years of spin-up in order to reduce the sensitivity of the results to initial conditions.

More than 17 rivers enter the Bohai Sea. The Yellow River, carrying more than 50 percent of the total fresh runoff, is the largest one (Zhao et al., 2002). In this study, we only considered the Yellow River inputs. The monthly freshwater discharge was taken from the Yellow River Sediment Bulletin in 2009 (Yellow River Conservancy Commission of MWR, 2009). The monthly runoff (Fig. 4.3, the bottom panel) was further distributed to each second assuming a consistent runoff within each month. For the inorganic nutrients (nitrate, ammonia, phosphate and silicate), daily loads were derived from the monthly measurements at Shengliqiao Station, near the Yellow River mouth from January to December, 2009 (S. Liu, personal communication, Fig. 4.3, the top four panels).

4.3.4 Ecosystem model parameterization

The model adaptation to the Bohai Sea started with the ECOHAM parameterization. The parameter optimization was based on a one-dimensional model setup and consists of three steps. First, we used the parameters of the North Sea in ECOHAM4 (Lorkowski et al., 2012) as the starting point to do the model sensitivity analysis. The model-sensitive parameters were determined via the model

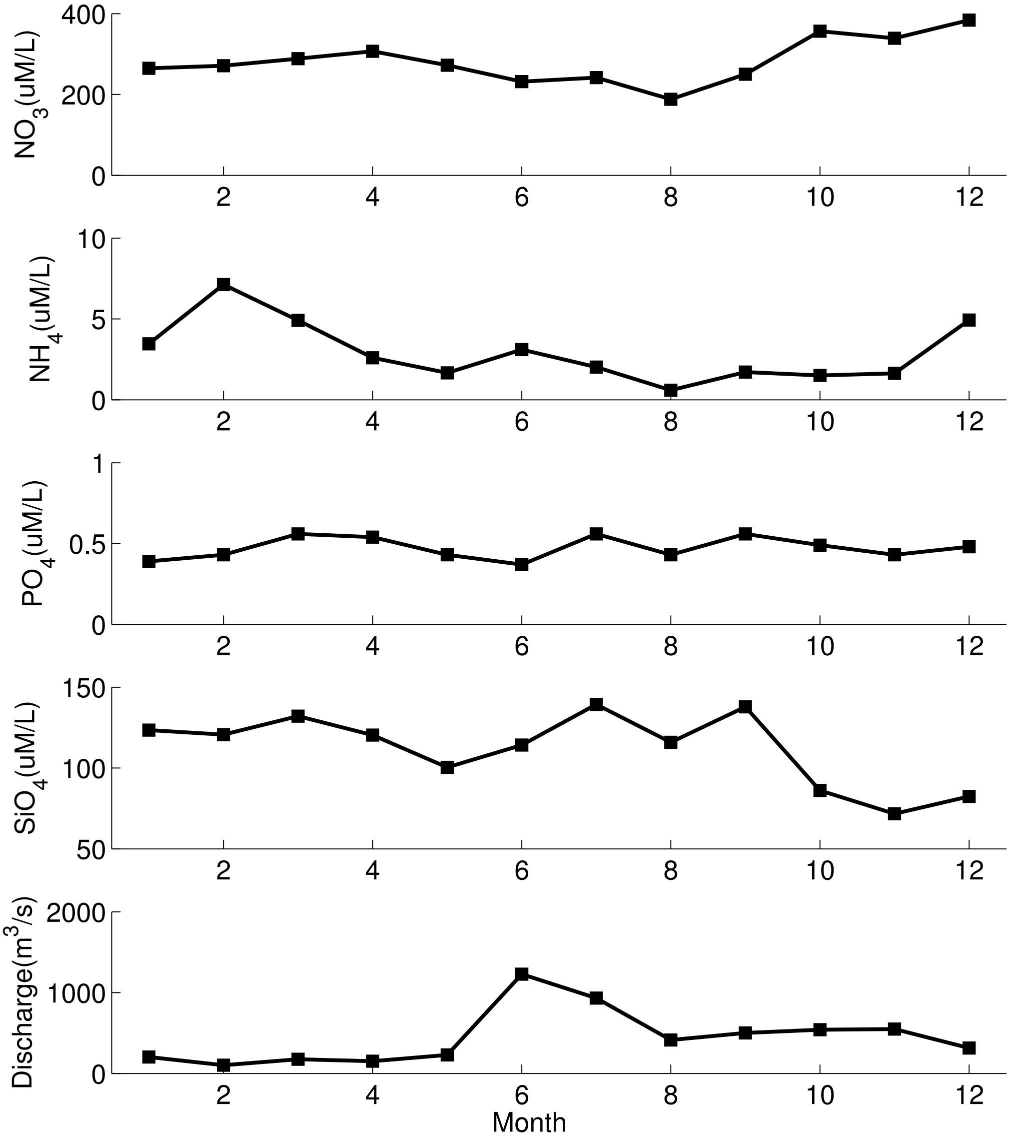

Figure 4.3: Monthly loads of the Yellow River in 2009. From top to down are nitrate, ammonia, phosphate, silicate and freshwater discharge.

sensitivity analysis based on (Fasham et al., 1990), as expressed in Eq. 4.1, where S stands for the normalized sensitivity, ΔF is the deviation of the annual Chl-a induced by the parameter variation ($\Delta Para$). Here eight parameters that are related with the phytoplankton growth or loss are listed in Table 4.1. In terms of the simulated annual Chl-a, the model is most sensitive to the maximum growth rates of phytoplankton (v_{p1} and v_{p2}) and robust to the half-saturation constant of nutrients taken by the phytoplankton (K_1 , K_{21}, K_{21}, K_{22}).

For the second step, a cost function (Eq. 4.2) was set up to evaluate the model deviation from the observations. E stands for the model deviation, Sim and Obs are monthly model simulations and observations respectively. In order to choose the best parameter ranges, we run the model recursively along with the parameter variations, with the aim of minimizing the discrepancy between the simulated times-series of Chl-a and the observed data. The model deviations which were varying with the variation of each parameter are show in Fig. 4.4.

After having found the best parameter ranges, we manually adjusted the parameters within these fixed ranges to obtain the best fit to observed bloom characteristics like maximum, minimum and slop increase in phytoplankton biomass. The final best set of biological parameters was then used for the standard simulation. The detailed explanations of the model parameters used in this study are listed in Table D.1.

$$S = \frac{\Delta F/F}{\Delta Para/Para} \tag{4.1}$$

$$E = \sum_{i=1}^{12}(Sim_i - Obs_i)^2 \tag{4.2}$$

Table 4.1: Model parameter used for sensitivity analysis

Parameter	min value	middle value	max value	Sensitivity (%)
v_{p1}	0.55	1.1	1.65	21.62 ∼ 42.68
v_{p2}	0.2	0.4	0.6	2.43 ∼ 20.46
K_1	0.25	0.5	0.75	-1.98 ∼ -1.36
K_{21}	0.25	0.5	0.75	-4.65 ∼ -4.63
K_{22}	0.025	0.05	0.075	0.65 ∼ 2.9
K_p	0.025	0.05	0.075	-1.69 ∼ -0.86
μ_{11}	0.0175	0.035	0.0525	-15.21 ∼ -14.93
μ_{12}	0.0175	0.035	0.0525	-12.61 ∼ -10.91

4.3.5 Observational datasets

Sea surface temperature (SST) data derived from the Modular Ocean Data Assimilation System (MODAS) from 2001 to 2006 were used to compare with the model simulation. The MODAS provides improved temperature and salinity fields over the global ocean by assimilating near-real-time observations. Detailed evaluation

Table 4.2: Data sets used for validation of model results for seasonal cycle nutrients and Chl-a

Data set name	Parameters	Periods and frequency	Spatial coverage	Reference
BH82	Nutrients; Chl-a	1982.05-1983.05 (monthly for Chl-a and seasonally for nutrients)	Central Bohai Sea; Bohai Bay; Laizhou Bay	Fei (1991); Tang and Meng (1997)
BH92	Nutrients; Chl-a	1992.08; 1992.10; 1993.02; 1993.05	Central Bohai Sea; Bohai Bay; Laizhou Bay	Tang and Meng (1997)
Sino-German	Nutrients; Chl-a	1998.09; 1999.05	Central Bohai Sea	Sündermann and Feng (2004);Wei et al. (2004b)
Cruise 2008	Nutrients	2008.08-09	Whole Bohai Sea	Liu et al. (2011)
Cruise 2010a	Nutrients; Chl-a	2010.06; 2010.08; 2010.10	Central Bohai Sea; South part of Liaodong Bay	D. Guo, Personal communication
Cruise 2010b	Nutrients; Chl-a	2010.04	Central Bohai Sea; North Yellow Sea	D. Liu, Personal communication
Cruise 2011	Nutrients	2012.02; 2012.08; 2012.10	Transect	D. Guo, Personal communication
Cruise 2012	Nutrients; Chl-a	2012.05	Central Bohai Sea; North Yellow Sea	D. Liu, Personal communication
Mornitor99	Nutrients; Chl-a	1998.07-1999.09 (monthly)	Changdao Station	Wei et al. (2004b)

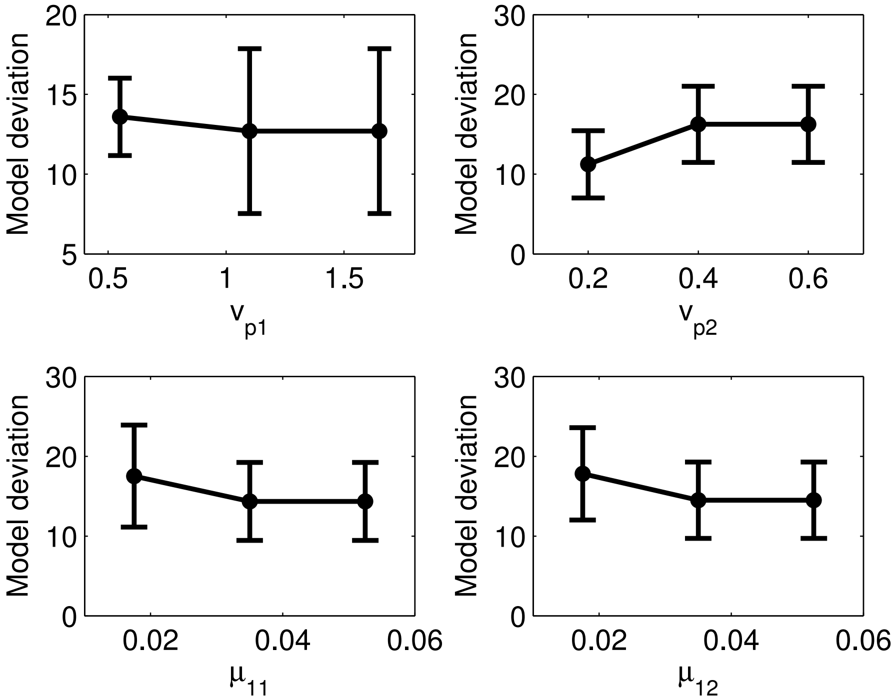

Figure 4.4: Model deviation along with the parameter changes. For each panel, the parameter indicated by the x-axis is variable while the other three parameters are kept as the optimal value. The y-axis stands for the model discrepancy between the simulated times-series of Chl-a and the observed data calculated by Eq. 4.2

of the MODAS performance is discussed in Fox et al. (2002). Here in this study monthly averaged data with horizontal resolution of $1/8^o$ were selected for the model validation.

In the Bohai Sea, for the validation of the biological compounds simulation, climatic data from field sampling are not available because of the sparse measurements. The commonly used climatic data sets, the World Ocean Atlas (WOA), is too coarse to provide a sufficient resolution to validate both the spatial and temporal characteristics of the model results. Despite that several cruise investigations have been conducted in the last three decades, similar with the conditions in the North Sea, significantly systematic uncertainties are caused by the fact that limited available observations are not equally or even normally distributed in space nor in time (Schrum et al., 2006). In spite of the problems, those investigations provide at the moment the best database guess on average seasonal nutrient and phytoplankton dynamics and hence will be used for validation purpose. The corresponding information of the observations can be found in Table 4.2.

In order to assess the model ability to reproduce the seasonal dynamics of the ecosystem, the study area is divided into eight boxes to demonstrate different hydrodynamic regimes (Fig. 4.5). For each box, the daily regional average of the model results are compared with the monthly in situ data. A primary quality control of the observations has lead to the discard of extreme values prior to the comparison. Since large variabilities among those measurements make it rather difficult to get reasonable statistical patterns for the seasonal nutrient and phytoplankton dynamics by simply integrating the database, each data set with the simple statistic characters (mean, maximum, minimum) are listed within each box. Here it is worthwhile to note that the insufficient observations do not allow the normal statistic analysis such as the standard deviation. Therefore, the maximum and minimum values are used to illustrate the possible range of variation. Taking into consideration of the measurement consistency, the BH82 and BH92 data are used for the spatial distribution comparison.

4.4 Model results and validation

4.4.1 Temperature

The basic step in the validation of an ecosystem model is the validation of the hydrodynamics because discrepancies in the physical simulation increase the uncertainty of the modeled biological processes (Stegert et al., 2009). The circulation pattern simulated using HAMSOM has been reported in Wei et al. (2004a). Our model results agree well with those analyses (Figure not shown). Since temperature is important for the annual cycle of phytoplankton, here we only analyze the simulated sea surface temperature (SST).

The simulated annual cycles of SST for different parts of the Bohai Sea (Fig. 1.2) are shown in Fig. 4.6 compared with MODAS data (Fox et al., 2002). The annual cycles of SST in the four regions indicate an identical seasonality, which is characterized by lowest values in winter (February) and highest values in summer (August). The SST in winter is about 0 ^{o}C. After an increase in the spring time, the SST reaches the highest value in summer. At this time, the SST can be as high as 26 ^{o}C. Since August, SST starts to decrease to the winter level.

The simulated annual cycle of SST in the four parts agrees well with the obser-

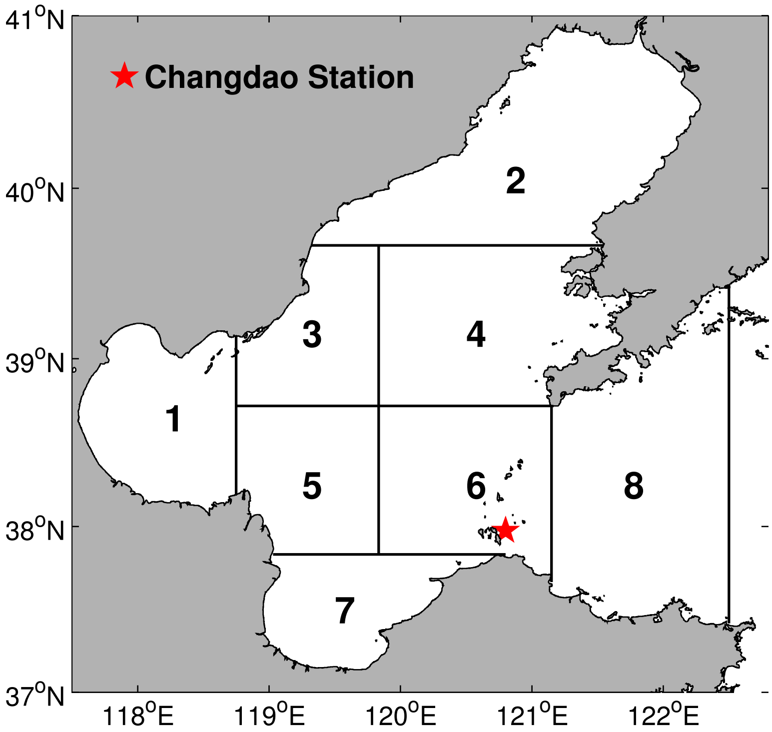

Figure 4.5: Box configuration for the Bohai Sea based on different hydrodynamic conditions. Box1 (the Bohai Bay) and Box5 are regions which are heavily affected by the Yellow River inputs. Box2 (the Liaodong Bay), Box3, Box4, Box6 and Box7 (the Laizhou Bay) are regions which are less influenced by the Yellow River inputs. Box8 is the box outside the Bohai Sea which is treated as the boundary box. Note here Box3-6 stand for the Central Bohai Sea. Red star represents the location of the monitoring station, Changdao Station, with monthly measurements for 15 months in 1998-1999.

vations. The model shows an accurate predication of the SST in summer-autumn time. In winter, accurate predictions are found in February in shallow waters (the Bohai Bay and the Laizhou Bay) while in March in deep waters (the Liaodong Bay and the Central Bohai Sea). Model discrepancies occur during the period of March-July, with an overestimation of 3 ^{o}C. During November to January, the simulated SST is about 1.5 ^{o}C lower than the observations.

By comparing the monthly SST in four regions between the model simulation and the observations, the HAMSOM performance of simulating the temperature is evaluated. Despite the bias from the observations, HAMSOM is capable of reproducing the seasonal cycle of temperature, with accurate predictions in summer-autumn period. During spring time, the bloom development is mainly governed by the underwater light. Therefore, despite the bias from the observations, the simulated temperature seasonal variation can be provided to the ecosystem model.

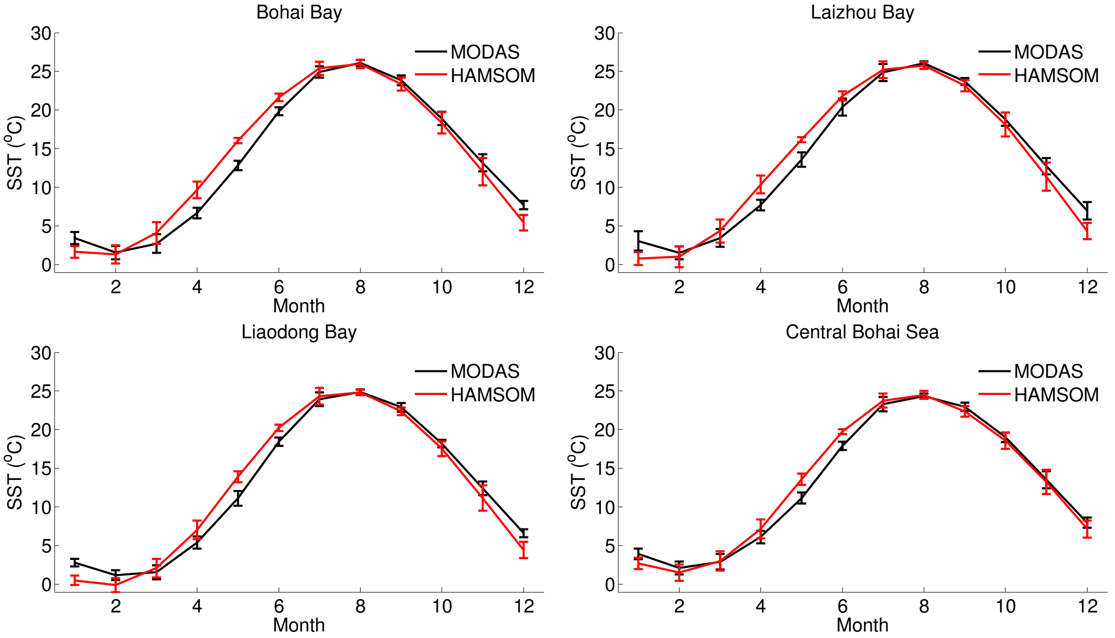

Figure 4.6: Comparison of annual cycle of SST in the four parts of the Bohai Sea between the simulation and the observation. Red lines stand for model result and black lines stand for observation (MODAS data). Solid lines represent the interannual mean of 2001-2006. Bars show the standard deviation caused by the interannual variation.

4.4.2 Seasonal cycle of phytoplankton and nutrients

The model performance to reproduce the seasonal dynamics of nutrients and phytoplankton is evaluated by comparing the monthly mean model results with a set of in situ data (Fig. 4.7). The model validation is presented in two regions which are used to demonstrate the influence of different hydrodynamic regimes. Box5 stands for areas which are heavily influenced by the river input. Box6 is an example of less influence of the river input. Both the in situ measurements and model results are presented in the surface layer for all the compared variables.

The observed Chl-a exhibits high variabilities not only among datasets (comparing error bars in different colors in Fig. 4.7) but also among stations within each dataset (shown as a big distance between the dot and the upper/lower line of each error bar in Fig. 4.7). In both boxes, the variabilities are higher during summer time than in winter and early spring. In spite of the high variability, we can derive the general seasonal patterns of Chl-a. In Box5, high concentrations of Chl-a are found in summer-autumn time (from July to October), low concentrations are in winter and late spring (June). The spring maximums of Chl-a concentration are found in March-May based on different datasets. In Box6, spring blooms can be identified by the datasets of BH82 and Monitoring observations. The spring maximums of Chl-a concentration are observed in March and April, which are followed by a decrease of Chl-a concentration during May-June. High concentrations of Chl-a in summer-autumn time suggest long-lasting summer-autumn blooms which are followed by a decreases since October. In Box5, the model simulation shows the seasonal pattern of high Chl-a concentration in summer-autumn time and the seasonal decrease from October. In early spring, the simulated Chl-a concentration is underestimated, which results in a later increase in spring. The decrease of Chl-a concentration before the summer-autumn blooms can not be captured by the simulation. In summer-autumn time, the Chl-a concentration is overestimated. In Box6, the model produces the general annual cycle of Chl-a, which is characterized with low concentration in winter, spring bloom onset in March and April, spring bloom decay in May, persistent high concentrations during summer-autumn bloom period and the seasonal decrease since October. Major discrepancies are found from May to October, when the Chl-a concentrations are overestimated. Similar to the simulation in Box5, the decay of the spring bloom is not well captured by the model simulation.

High variabilities of nitrate concentration are observed all over the year in Box5 from the in situ data. The datasets of BH82, BH92 and Sino-German provide us a synoptic overview of the seasonal cycle, which is characterized with high concentrations in winter and low concentrations in summer. The high variability observed in Cruise 2008 indicates the influence of the river inputs. Our model results agree well with the observations in winter (February) and autumn (October) but show overestimations in spring (April) and summer (August). The high concentrations in July seem to be the consequence of the river inputs. In Box6, the datasets exhibit an identical seasonality of the nitrate concentration, even though the monitoring observation gives an higher estimation than the others. This seasonal variation is well reproduced by the model, as the model results are in the range of uncertainties which are estimated from the observations.

Monthly mean phosphate shows similar seasonal cycles between model results and observations, which are characterized by high concentrations in winter, sharp decreases after the spring bloom maximum, low concentrations in summer and increases starting from late autumn. Discrepancy happens in the simulation in Box6 as overestimation is found when the model simulation is compared with the monitoring data. This deviation reveals possible interannual variability.

The observed silicate concentrations show a high variability among datasets. In Box5, the seasonality varies with different observations, which seems to be subject to the interannual variability of the river inputs. In Box6, the observations show an consistency of the annual cycle, even though there exist big differences of the concentration level among the datasets. The annual cycle is characterized with high concentrations in autumn and winter while low concentrations in summer. In both boxes, the simulated silicate concentrations agree well with the observations of BH82, which indicates a comparable silicate environment of the simulation with that in 1982.

Similar comparisons of the seasonal cycle of Chl-a and nutrients in the other regions are listed in Appendix. E. Based on the analysis above, we can conclude that in regions of less influence from the river inputs, the model is able to simulate the seasonal increase of Chl-a in spring. The spring bloom onset and the bloom maximum are well captured by the model when comparing with the monitoring observations. In regions which are strongly influenced by the river inputs, the model reproduces lower Chl-a concentrations in early spring and a consequently later seasonal increase. In both regions the model overestimates the Chl-a concentrations in summer-autumn period and underestimates of the spring bloom decay. The general annual cycles of nutrients can be reproduced by the model simulation.

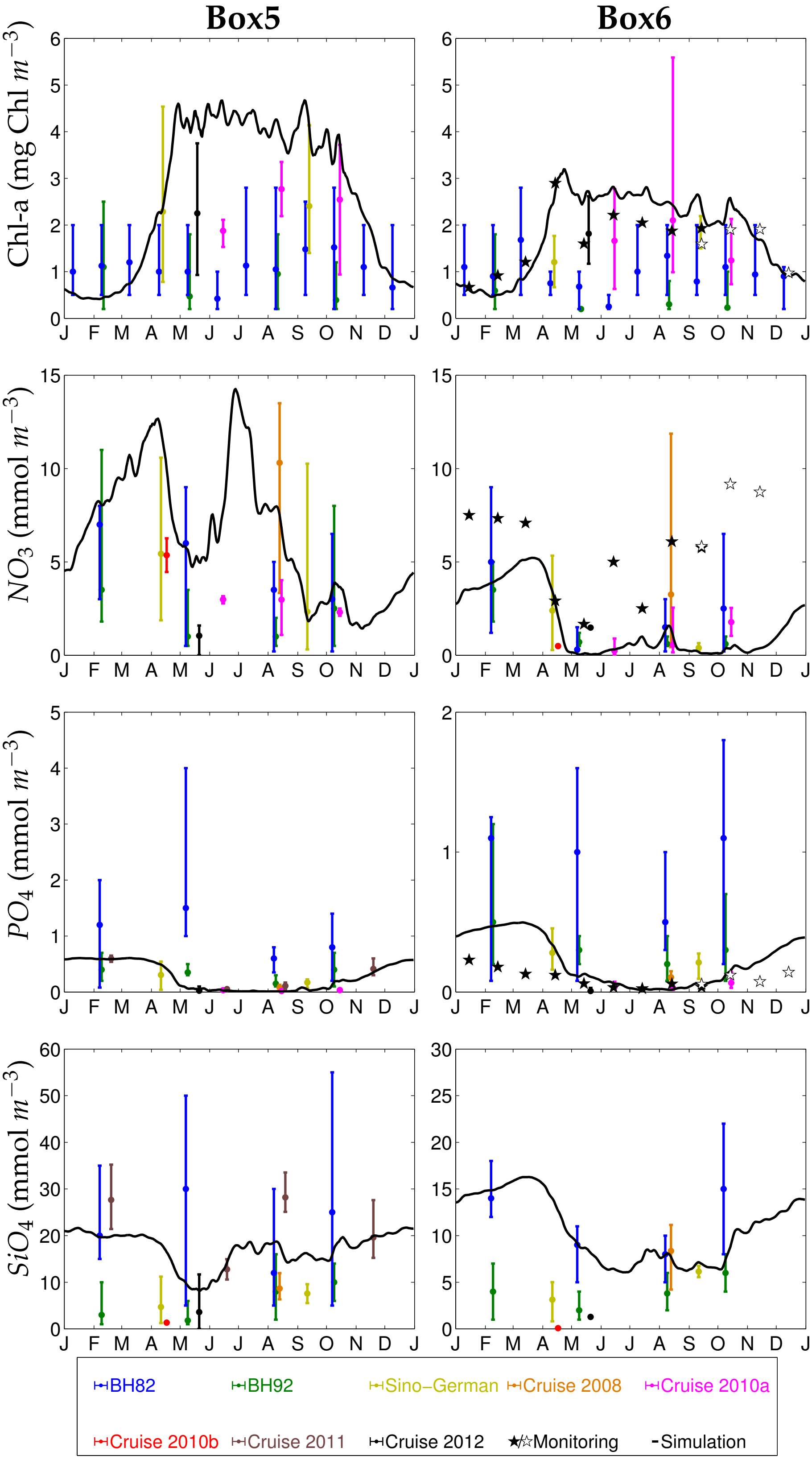

Figure 4.7: Validation of seasonal cycles of Chl-a and nutrients for Box5 and Box6 shown in Fig. 4.5. Error bars stand for different cruise observations labeled by different colors. Dots of the error bars stand for the spatial average of each cruise investigation. The bars show the maximum and minimum of each cruise. For a clearer view, the monthly means of each data set were shifted by 2 days. Pentagram stands for monitoring measurements at Changdao Station. The filled ones are measurements in 1999 while the others in 1998. Bold black lines show the daily model results averaged over the box.

4.4.3 Phytoplankton succession

In this section, the simulated seasonal dynamics of the phytoplankton succession is discussed by analyzing the model results at Changdao Station (Fig. 4.8). Taking into account the total phytoplankton biomass (in Chl-a), the model captures well the seasonal cycle by reproducing accurate spring bloom development and consistent Chl-a concentrations in summer-autumn time. The reasonable model performance enables the analysis of the phytoplankton succession.

As is show in Fig. 4.8, the spring phytoplankton bloom commences in March and reaches its maximum with values up to 3 $mgChlm^{-3}$ in the middle of April. This first phytoplankton maximum consists mainly of diatoms with low biomass of the other species (represented by flagellate). Diatoms remain being the dominant phytoplankton group until June when the diatom biomass has already decreased. The following high phytoplankton biomass is a effect of the coexisting of diatoms and the other species which are dominated by flagellates. This result agrees well with the observations in the Central Bohai Sea , the Bohai Strait and adjacent waters in 1998/1999 (Sun et al., 2002; Wei et al., 2004b).

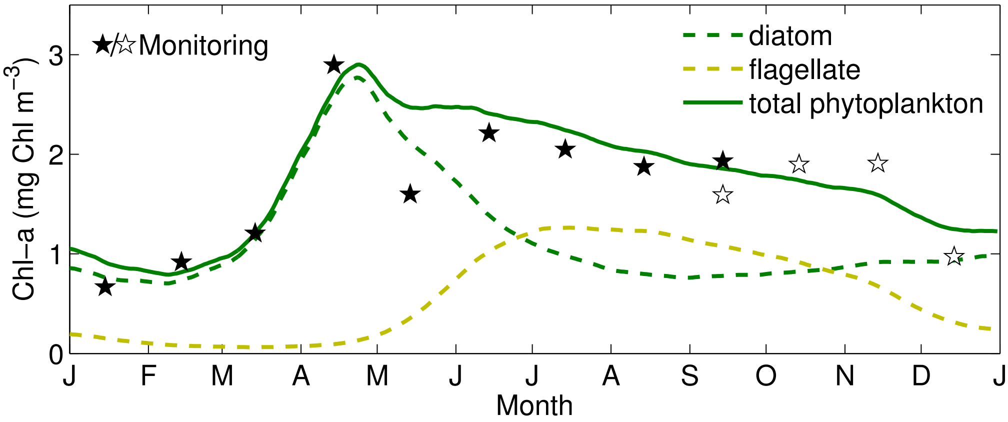

Figure 4.8: The seasonal dynamics of the surface phytoplankton biomass at Changdao Station (Shown in Fig. 4.5). Model results (lines) are compared with monthly observations in 1998 (white pentagram)/1999 (black pentagram) in this location. See description of the observation in Table 4.2. Here note that the concept of flagellate is used to represent the total biomass of the rest phytoplankton species exception for diatoms.

4.4.4 Spatial pattern of phytoplankton and nutrients

Now we concentrate on comparing the simulated spatial patterns of Chl-a and nutrients during the four seasons. The simulated spatial distribution of the surface Chl-a, nitrate and phosphate over th Bohai Sea are compared with the observations in 1982/1983 and in 1992/1993. The plots show the monthly means of February, May, August and October, to represent the four seasons.

The observed Chl-a distribution shows a significant onshore-offshore gradient associated with riverine nutrient inputs (Fig. 4.9, middle and right panels). High Chl-a concentrations are found in the Laizhou Bay, the Bohai Bay, the Yellow River mouth and the adjacent coastal areas. The Central Bohai Sea, especially the north part, is characterized by low concentrations. The model simulation captures the regional character well, with simulated high concentration extended from the Yellow River mouth to the Laizhou Bay and the Bohai Bay (left panels). Nevertheless, discrepancies can be found in each season. In February, simulated highest concentrations are constrained at the narrow zones along the coastal line, possibly caused by the shallow depth. In May and August, the model simulation fails to reproduce high values at the top of Liaodong Bay and Bohai Bay as well as the south part of the Laizhou Bay. This underestimation can be explained by the ignorance of the other river discharges (e.g. the Liaohe River draining to the Liaodong Bay, the Haihe River to the Bohai Bay, shown in Fig. 1.2; the Xiaoqinghe draining to the Laizhou Bay, not shown).

The spatial distribution of nitrate is characterized by high concentrations near the river mouth and the limited coastal areas that are heavily influenced by the human activity. The general pattern of the simulation agrees well with the observations. In February, the highest concentration appears in the Laizhou Bay while the lowest concentration is found in the Liaodong Bay. In May and August, high concentrations are constrained in the Yellow River plume area, leaving low concentrations in large areas of the Central Bohai Sea and the Liaodong Bay. In October, relatively high concentrations are found near the Yellow River mouth and the northeast part of the Central Bohai Sea. Model discrepancies are also observed. In May, the patches of observed high nitrate concentration in the Bohai Bay and Liaodong Bay are not captured by the simulation. Similar conditions occur in October in the east part of the Laizhou Bay as show in BH82 datasets and in the top of the Bohai Bay as show in BH92 dataset (Fig. 4.10).

Fig. 4.11 shows the comparison of the surface phosphate distribution. Large discrepancy occurs not only between simulation and observations, but also between observations of different years (middle and right panels). This inconsistence probably indicates the high interannual variability. The model results show high phosphate concentrations in the Bohai Bay and the Laizhou Bay in February, which can partly resemble the observation of BH82. In May, August and October, the model results present inverse patterns with the observations. However, the simulated spatial pattern in August agrees well with the observations in 2008 provided by Liu et al. (2011), which demonstrate a large area of low phosphate concentrations in the Central Bohai Sea while high concentrations in the top Bohai Bay and the Liaodong Bay. Such inconsistency reveals the change of nutrient regimes during the last 30 years (Zhang et al., 2004).

Fig. 4.12 shows the comparison of the surface silicate distribution. The simulation in February shows a good agreement with observations, which is characterized a significant gradient from the Yellow River mouth to the northeast of the Central Bohai Sea. Discrepancies is found in May. The concentrations in the Liaodong Bay are underestimated because of the neglect of the Daliaohe River inputs. In August and October, the model simulation agrees well with the observations, with low values in the Central Bohai Sea.

In summary, the model simulates well the spatial patterns of the Chl-a and nutrients. Discrepancies are mostly found in the three bays, possibly because the model only considered the Yellow River inputs and neglected the other rivers. The simulated phosphate concentration in the Central Bohai Sea is lower than the observations in BH82 and BH92, but agrees well with the recent observations in 2008. This indicates a long-term change of the nutrient regimes during the last 30 years.

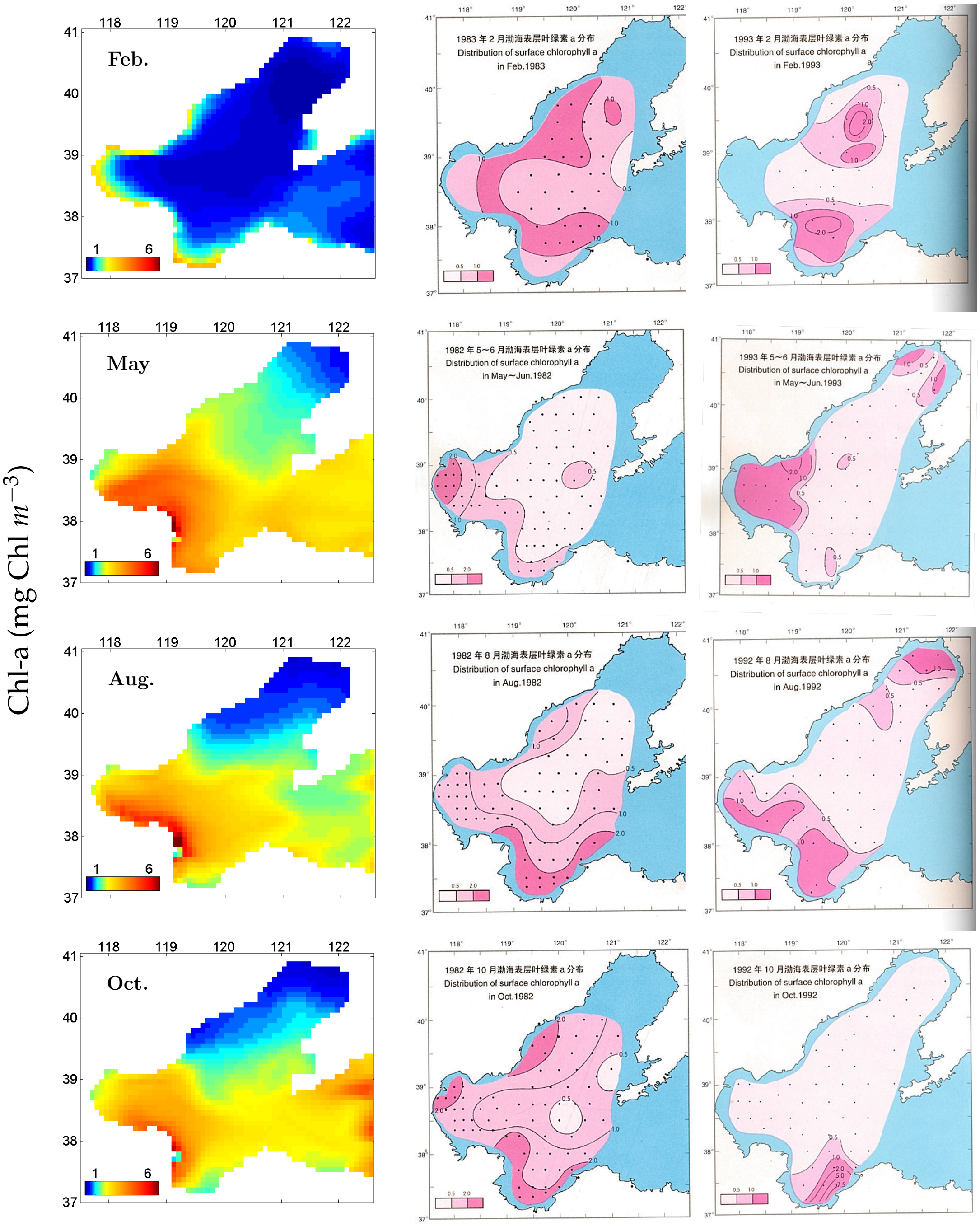

Figure 4.9: Left panel: monthly mean surface Chl-a concentration derived from model simulation. Middle panel: monthly observed surface Chl-a concentration in 1982/1983. Right panel: monthly observed surface Chl-a concentration in 1992/1993. The middle and right panels are taken from Tang and Meng (1997).

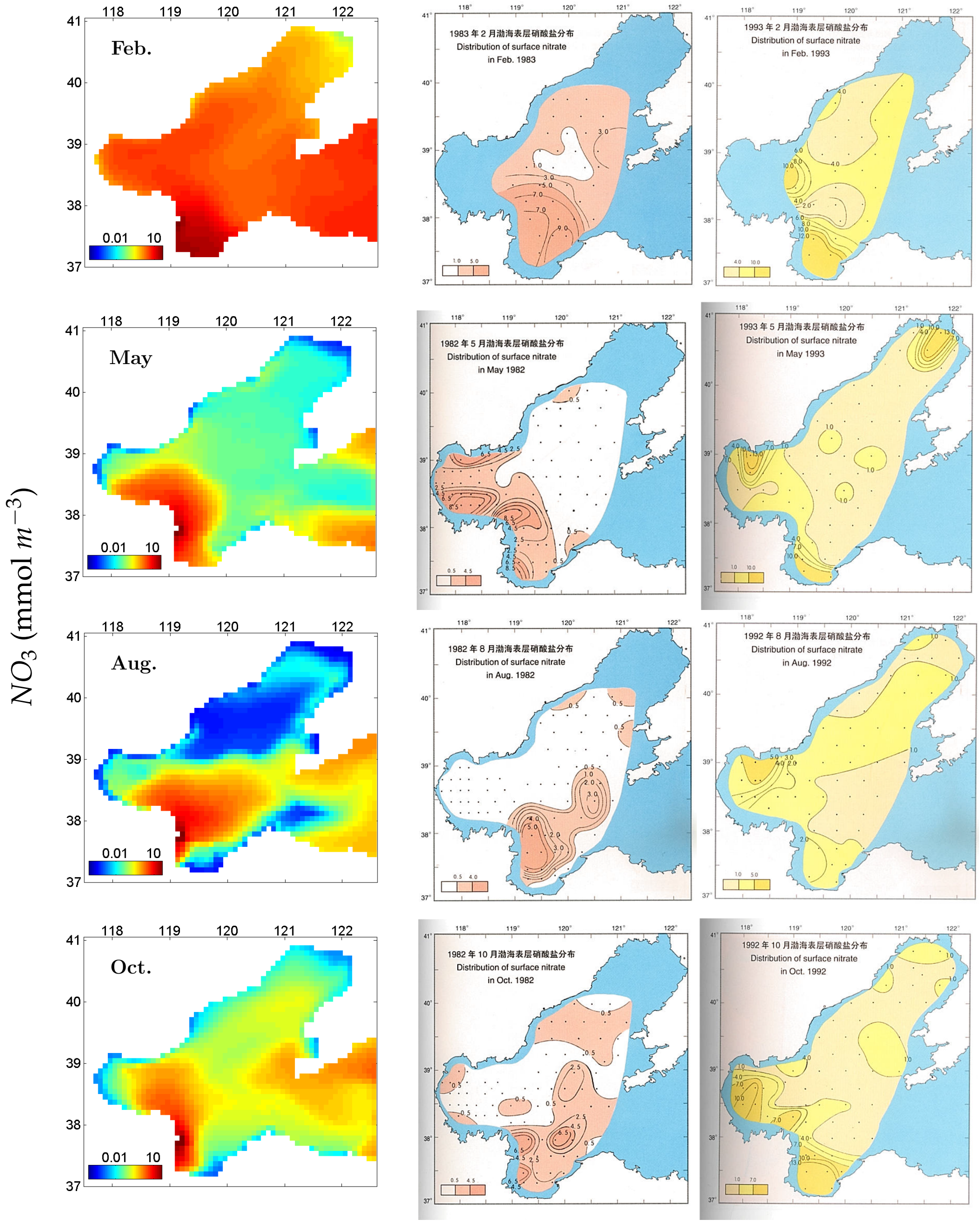

Figure 4.10: Left panel: monthly mean surface nitrate concentration derived from model simulation. Middle panel: monthly observed surface nitrate concentration in 1982/1983. Right panel: monthly observed surface nitrate concentration in 1992/1993. The middle and right panels are taken from Tang and Meng (1997).

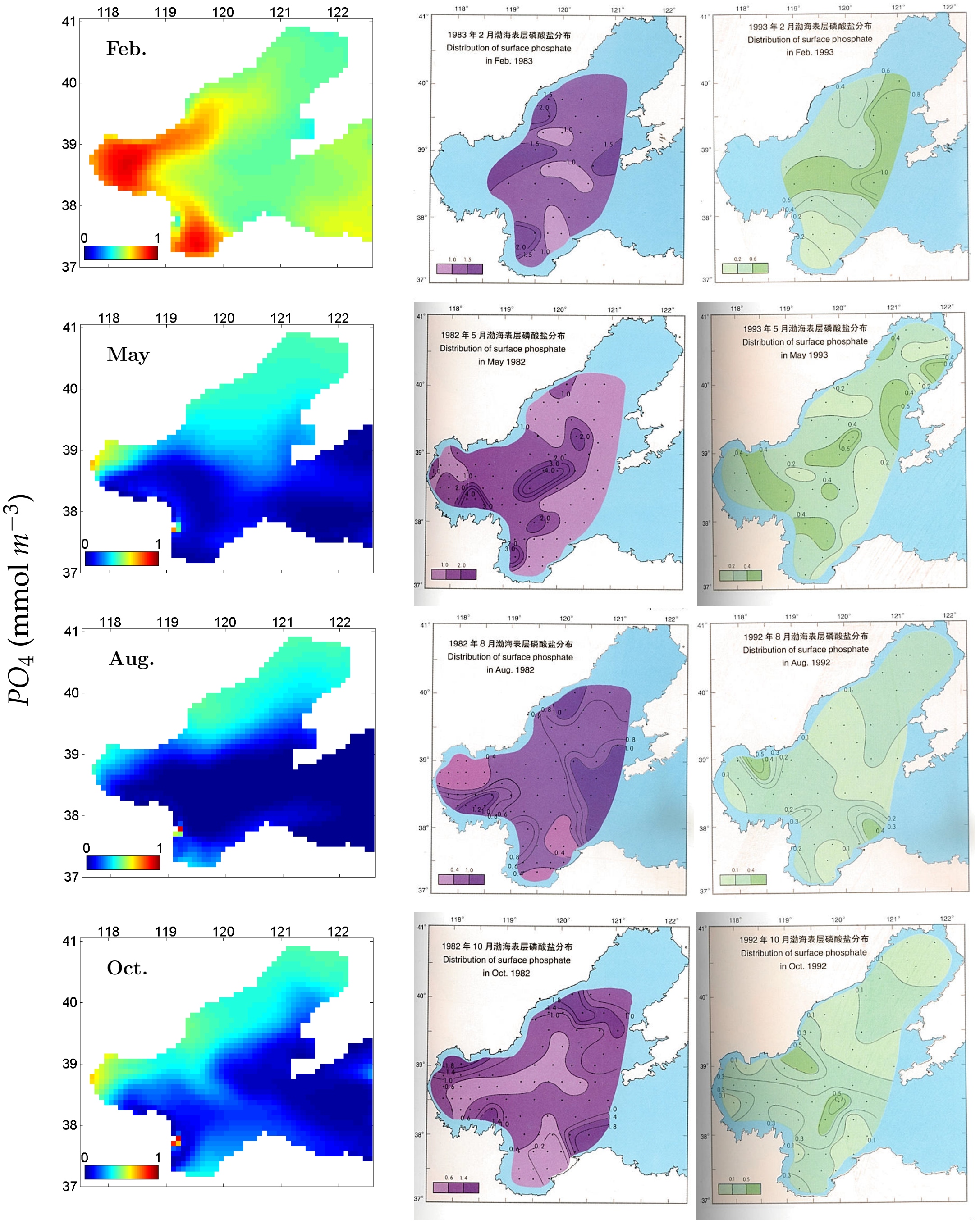

Figure 4.11: Left panel: monthly mean surface phosphate concentration derived from model simulation. Middle panel: monthly observed surface phosphate concentration in 1982/1983. Right panel: monthly observed surface phosphate concentration in 1992/1993. The middle and right panels are taken from Tang and Meng (1997).

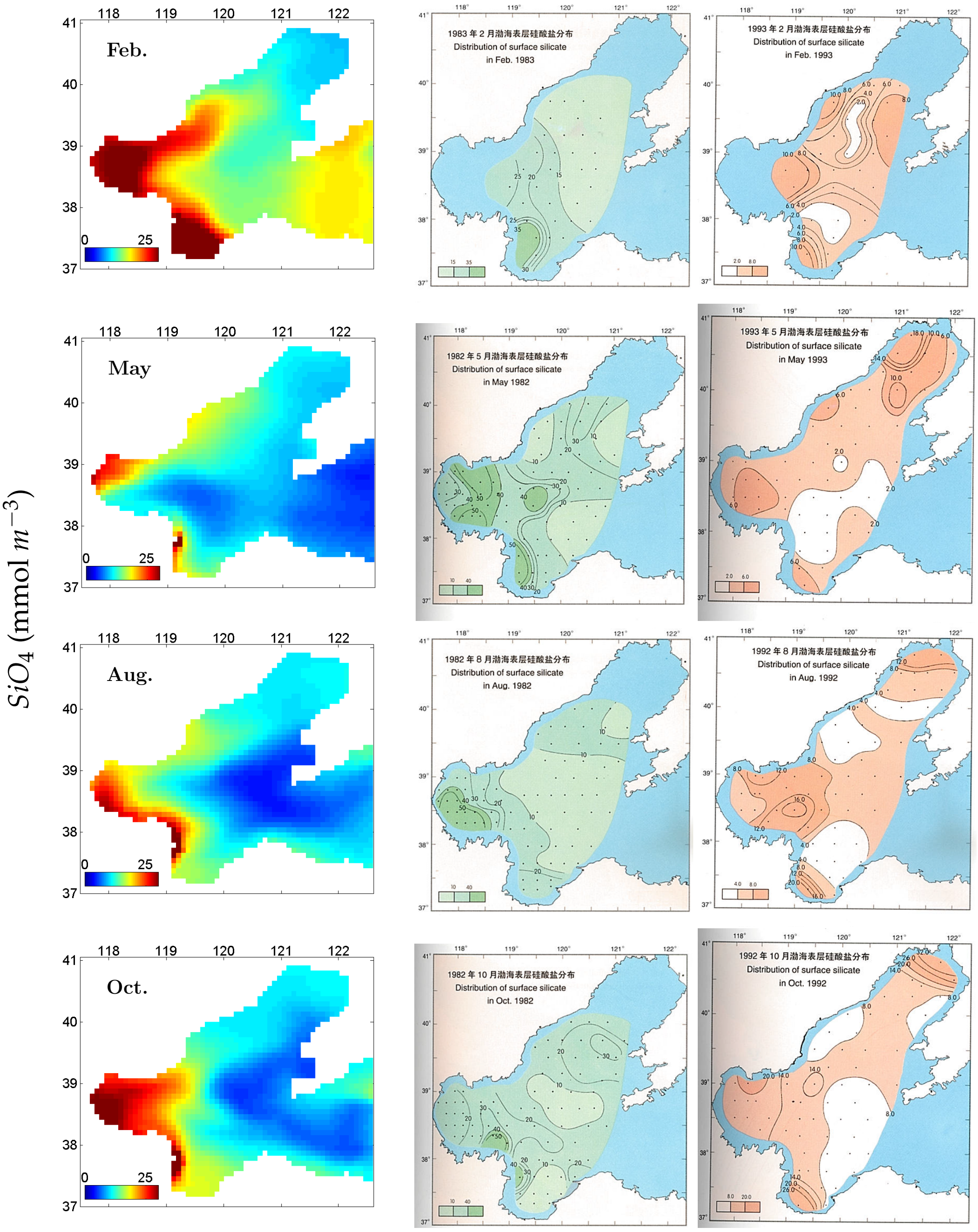

Figure 4.12: Left panel: monthly mean surface silicate concentration derived from model simulation. Middle panel: monthly observed surface silicate concentration in 1982/1983. Right panel: monthly observed surface silicate concentration in 1992/1993. The middle and right panels are taken from Tang and Meng (1997).

4.5 Discussion

4.5.1 Observational data

When observational data are employed for model validation, the properties of the respective data sets have to be discussed because of the potential difficulties arising from the use of observational data (Schrum et al., 2006).

Due to the lack of systematic assessment, several data gaps still exist in the climatological means. This problem has not been yet discussed in the Bohai Sea but has been well mentioned in other coastal areas such as the North Sea (e.g. Radach and Pätsch, 1997). In the Bohai Sea, in terms of the sparse measurements, the observations available by far are inadequate for yielding reliable climatic estimates. The record is deficient in three ways. First, it is highly biased by the unequally distributed measurement numbers in space or in time in coastal waters due to the sparse observation. Second, most measurements are conducted only once at each location during the cruise. The accuracy of these values is unknown given the large temporal and spatial variability within ecosystems. Finally, basin-wide assessments are confounded by measurements that might be not intercomparable because they were made with different methods (Cloern et al., 2014). In the future, a well-established database from field sampling with careful statistical analysis (e.g. ICES database in the North Sea) in the Bohai Sea is necessary (Radach and Pätsch, 1997; Moll, 2000).

Satellite imagery provides a possible data source for ecosystem model validation because the excellent spatial coverage can be used to close the gaps in the field observations (Lacroix et al., 2007; Tiedje et al., 2010). However, the implementation of the satellite data in turbid waters (referred as Case 2 waters) should be very careful, especially in winter time with high concentration of SPM and CDOM in the water column. In the Bohai Sea, the Chl-a concentration in winter is overestimated even though the Case 2 water algorithm is applied (Doerffer and Schiller, 2007). Therefore, in the future, a validation of the satellite images based on a large number of observations in the Bohai Sea should be conducted.

4.5.2 Model assessment

As shown in the comparison of the time series of the model simulation with observations in different regions(Fig. 4.7 and Appendix E), the model reproduces well the Chl-a at the beginning of spring but yields later spring blooms as compared with the in situ data. The discrepancy can be explained by the underwater light availability which is largely depending on the SPM variation. In this study, the SPM is estimated from MERIS data as seasonal climatology which is presented as the monthly climatic concentration. The missing of the tide- and wind-induced high frequency variability of SPM could result in a timing discrepancy of the spring bloom. Similar conditions are also found in the Channel and Southern Bight of the North Sea (Lacroix et al., 2007). This finding further emphasizes the topic of this thesis, the importance of the SPM variation on the phytoplankton dynamics in the Bohai Sea. To successfully simulate the spring bloom in turbid coastal waters (e.g. the Bohai Sea), an accurate expression of the underwater light condition that is directly related to the high SPM variability both in space and time is particularly crucial (Xu et al., 2005; Tian et al., 2009).

General overestimation of Chl-a in summer-autumn time can be seen in each region (Fig. 4.7 and Appendix E) in the Bohai Sea. Similar performance of ECOHAM is also found in the North Sea (Tiedje et al., 2010). One possible interpretation is the arbitrary parameterizations in ECOHAM, concerning some relevant biological processes such as remineralization or biotic functioning. These parameters are very difficult to estimate accurately based on field or laboratory observations and are often adjusted empirically (Lacroix et al., 2007). The dismiss of the spring bloom decay in the simulation is possibly caused by the early increase of the flagellate, which is caused by the overestimated remineralization rate (Fig. 4.8). Another possible issue is due to the less knowledge of the conversion factor from Chl-a to carbon. The common strategy of using a constant conversion ratio when Chl-a is not considered as a model variable, although appropriate for annual averages, introduces a bias when applied to resolve the seasonal cycle (Schrum et al., 2006). In fact, Chl-a to C ratio especially deviates for nutrient and light limiting conditions and is a function of physiology. It might show significant regional variability on small spatial scales and clear seasonal variability (Cloern et al., 1995; Behrenfeld et al., 2005). Tiedje et al. (2010) suggested that a constant value of 75 might be a better choice in the North Sea, given that the model overestimates the Chl-a in summer. However in the Bohai Sea, huge amount of observations are needed to confirm the level as well as its variation.

The deviations in the comparison of the spatial pattern are mostly arising from the omission of the other river inputs other than the Yellow River. Nevertheless, the model simulation exhibits a reasonable reflect to this type of external influence when taking the Yellow River inputs for instance. In this study, we are not aiming to study the influence of river discharge or human activities. The corresponding simplification of the model simulation is therefore acceptable. In the further improvement of the model simulation, the inputs of more rivers around the Bohai Sea should be well considered.

4.5.3 Model improvement in the Bohai Sea

Wei et al. (2004b) has implemented an earlier version of HAMSOM-ECOHAM in the Bohai Sea to study the phytoplankton dynamics. Their efforts act as a basis for our further work with an updated model version. Compared with the earlier application, we conclude: First, ECOHAM develops from a simple NPZD model (ECOHAM1) to a comprehensive ecosystem model that considers more complicated biological processes. For instance, the two phytoplankton species considered in the model allow a better description of the phytoplankton succession (Fig. 4.8), which could result in a better simulation of the nutrient-phytoplankton dynamics. Second, our model establishes a direct linkage of the SPM/phytoplankton with the underwater light climate by calculating the light attenuation coefficient as a combination effect of the various water constituents. Therefore, it is possible to investigate the influence of the SPM variation on the phytoplankton dynamics in the Bohai Sea by using the new model simulation. Our model results also display several improvements. For instance, the spring bloom is better captured in terms of the bloom timing and the Chl-a maximum. In the previous simulation, the phosphorus can not get back to the initial level by the end of the year because the model failed to reproduce the phosphorus recovery after the summer time (Wei et al., 2004b) (Fig.6). The problem has been fitted in our simulation as show in Fig. 4.7.

4.6 Conclusion

Due to the high turbidity, MERIS data can not be used in the winter-spring period to investigate the influence of the SPM variations on the phytoplankton spring bloom in the Bohai Sea. To cover this research gap, a coupled hydrodynamic-ecosystem model simulation is required. In order to reproduce the seasonal dynamics, especially the spring bloom, and the spatial distribution of the phytoplankton and nutrients, the three-dimensional HAMSOM-ECOHAM was implemented in the Bohai Sea for the year 2006. The model results were validated by comparison with available in situ data sets.

Because of the sufficient resolution of trophic dynamics compared with the earlier version implemented in the Bohai Sea (Wei et al., 2004b), ECOHAM in this study allows a clear separation between diatoms and flagellates dominated regimes. The model simulation indicated that the spring bloom was predominated by diatoms while the in summer-autumn period, the phytoplankton biomass is a mixture of the two components.

ECOHAM was capable of reproducing the observed phytoplankton spring bloom development and resolving the spatial differences. The phytoplankton biomass was overestimated in summer time. The discrepancies can be attributed to various reasons (e.g. model parameterization/process describing, variable Chl-a: C ratio). The deviations in the spatial patterns were mainly subject to the ignorance of the river inputs as well as the anthropogenic discharge. To solve these problems, further model improvement is necessary.

Chapter 5

The influence of the SPM variations on the spatial patterns of the spring bloom

As we have discussed in the previous chapters, the effect of the SPM variations on the phytoplankton dynamics is clearly not a trivial question. In Chapter 3, we investigated the influence of the SPM variations on the phytoplankton spring bloom at one station, focusing on the temporal evolution of the bloom. Here we further extended the model analysis to a full three-dimensional simulation, with the focus on the spatial variability of the phytoplankton spring bloom.

In this study, we conducted three experiments simulations. S1 stands for the standard simulation, which was driven by the monthly SPM field. In the second experiment (S2), the annual SPM field was used. In the third experiment (S3), the neap-spring cycle of the SPM was superimposed on the monthly variation following the scenario setting in Fig. 3.4 (b), S3a. The other model configuration was identical with Chapter 4. The phytoplankton spring bloom was quantified with three indices: the bloom onset time, the bloom peak time and the bloom intensity. The definition can be seen in Section 3.3.5.

The spatial pattern of the phytoplankton spring bloom

Fig. 5.1 (a-c) displays the spatial distribution of the phytoplankton spring bloom in terms of the three indices. The results are from the standard run (S1). The spatial distribution of the bloom onset time illustrates the spatial development of the spring bloom (Fig. 5.1 (a)). The bloom is initiated near the coast (mean water depth < 5m), from where the bloom onset spread into offshore regions. The bloom development is slower near the Yellow River mouth than the offshore regions of the northern Central Bohai Sea and the Liaodong Bay. The bloom reaches the peak Chl-a concentration first in the coastal zones and progresses to the Central Bohai Sea (Fig. 5.1 (b)). Patches of late bloom peak appear near the Yellow River mouth, the south part of the Bohai Bay, a small region in the offshore of Qinhuangdao (see Fig. 3.1) and the eastern part of the Liaodong Bay.

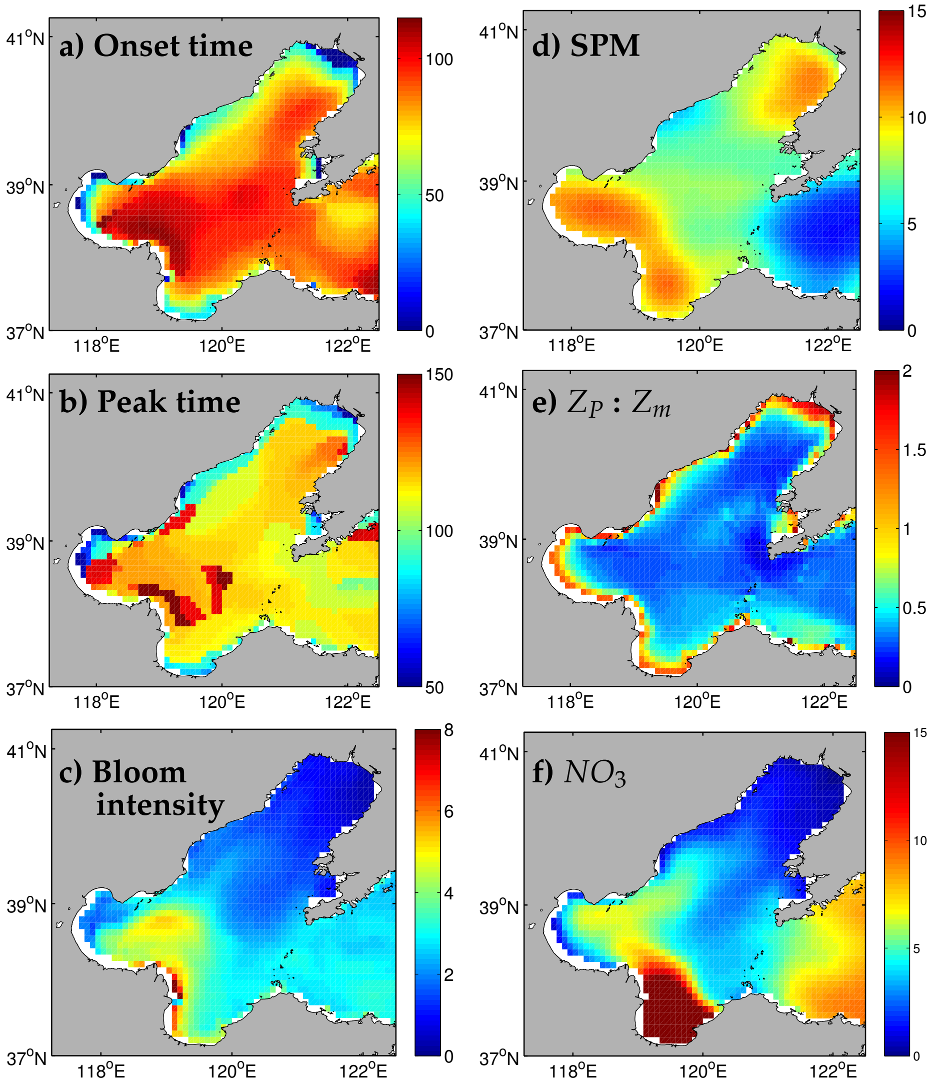

Figure 5.1: Spatial patterns of bloom onset time ((a) *day*), bloom peak time ((b), *day*) and bloom intensity ((c), mg Chl m^{-3}) of the standard run (S1). (d) is the map of SPM concentration averaged over February-April. (e) is the map of the euphotic depth: mixed depth ratio following Cloern (1987). (f) is the spatial distribution of surface nitrate concentration in February calculated in the standard run.

Clearly, the spatial evolution of the spring bloom can not be simply explained by the spatial gradient of the SPM concentration (Fig. 5.1 (d)). Cloern (1987) studied the influence of the water turbidity on estuarine phytoplankton and found that the net productivity was closely linked to the ratio of euphotic depth (Z_p) to mixed depth (Z_m). The euphotic depth is defined as the the depth where the light intensity is 1% of the surface, photosynthesis equals to the phytoplankton respiration (See Fig. 1.1). According to his study, the net productivity was zero when the ratio was less than about 0.2 in San Francisco Bay. Following his method, we calculated the spatial pattern of the Z_p:Z_m ratio averaged over the bloom development period (Fig. 5.1 (e)). Here considering the strong vertical mixing in the Bohai Sea in spring, the water depth was treated as the mixing depth. The high ratios in the marginal areas could, in large part, explain the earlier spring bloom.

Fig. 5.1 (c) shows the horizontal distribution of the bloom intensity. Intensified blooms occur near the Yellow River mouth, while the north part of the Bohai Sea, especially the Liaodong Bay, is characterized by relatively weak bloom intensities. The spatial pattern is in coincidence with the distribution of the surface nutrient concentration (here is nitrate) in February except for the Laizhou Bay. Other physical/biological processes, such as zooplankton grazing, might explain the unexpected low bloom intensity.

Scenario comparisons

The scenario results (Fig. 5.2, middle and low panels) are compared with the standard run (Fig. 5.2, top panels). S2 predicts an earlier bloom onset near the onshore coastal waters. In deep waters, earlier blooms are also observed, such as the South Liaodong Bay. S3 is relatively similar with the standard run. Only blooms in the limited regions of the Central Bohai Sea are characterized with an earlier onset time.

The spatial pattern of the bloom peak time is rather patchy. Due to the absence of the SPM seasonality (S2), the spring bloom peak time is postponed near the Yellow River mouth. On the contrary, bloom development in the northern Central Bohai Sea is stimulated, which is shown by the earlier bloom peak time. When the neap-spring fluctuation of SPM is considered, the model simulation results in a delayed bloom peak time in the Central Bohai Sea.

The three scenarios represent similar patterns of bloom intensity, which is charac-

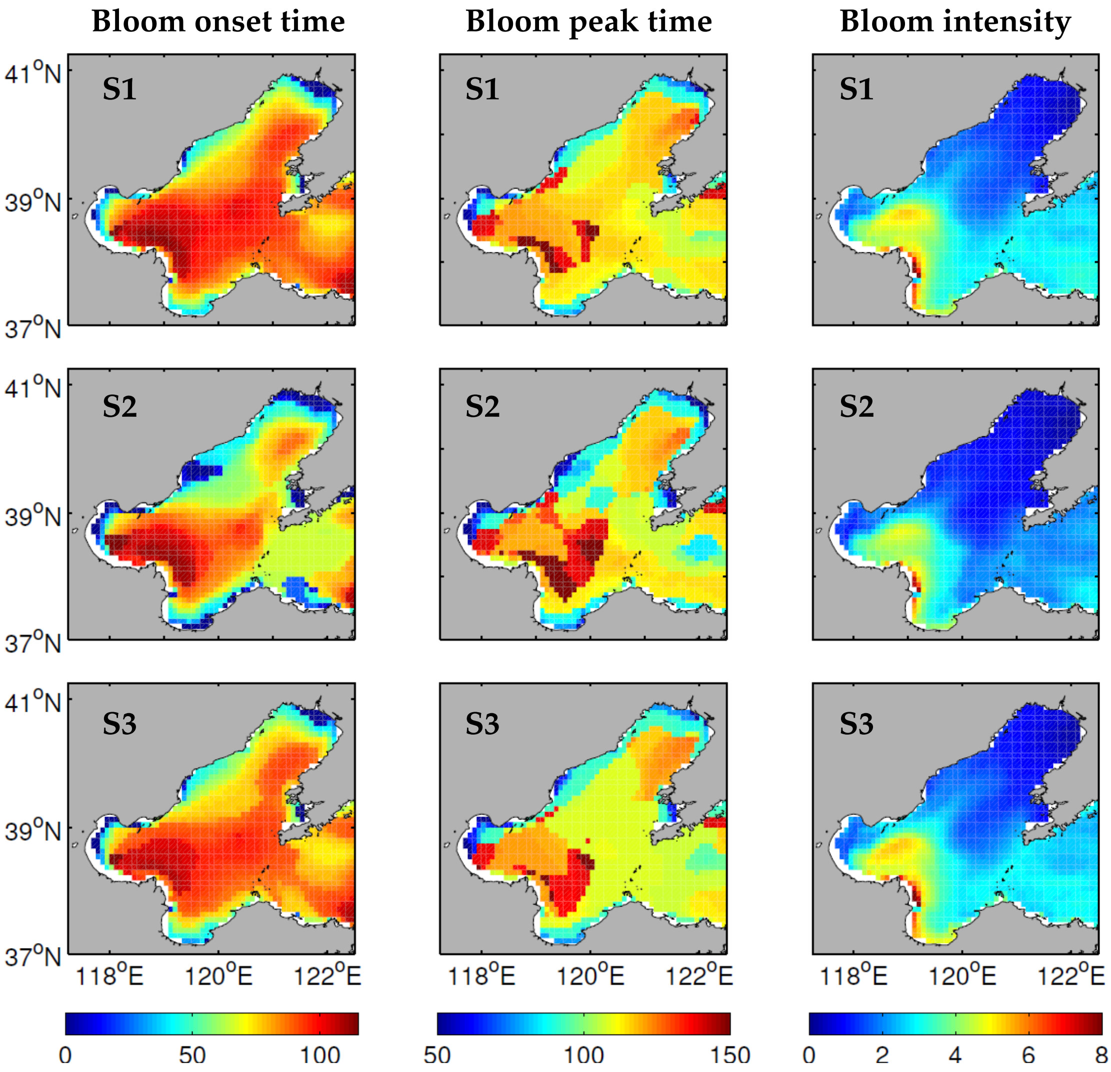

Figure 5.2: Spatial patterns of bloom onset time (left, *day*), bloom peak time (middle, *day*) and bloom intensity (right, mg Chl m^{-3}) for the three experiments. S1: standard run, S2: annual SPM field, S3: neap-spring cycle superimposed on the seasonal cycle of the SPM concentration.

terized with a decreasing tendency from the Yellow River mouth to the Liaodong Bay. Depressions are only found in the Central Bohai Sea and the north of the Yellow River mouth in S2. The relatively robust prediction of the bloom intensity in the Bohai Sea could be linked to the unchanged nutrient condition in the scenario tests.

In this part, I would not give a thorough analysis since the simulation shown in this chapter are the preliminary model results. A three-dimensional investigation needs much more effort to improve. Therefore, further research has to continue step by step into a full three-dimensional analysis concerning the role of the SPM variations on the spatial/temporal variabilities of the phytoplankton.

Chapter 6

Final discussion

6.1 SPM resuspension as a negative factor: light attenuation

In turbid coastal waters, SPM is characterized with high concentrations, such that light is attenuated rapidly in the water column. As a consequence, phytoplankton dynamics are largely controlled by the underwater light availability. This relationship between SPM variations and the phytoplankton dynamics has been identified by both theoretical studies and field investigations (e.g. Cloern, 1987; Desmit et al., 2005; Tian et al., 2009). Many of the studies were focused on nutrient-rich areas, assuming the phytoplankton growth was only regulated by the underwater light (e.g. May et al., 2003; Desmit et al., 2005). This simplification allowed a direct connection between the SPM variation and the phytoplankton growth. However, in summer-autumn time, when nutrient limitation can not be neglected, this relation was not fully specified. We investigated the summer-autumn bloom in the Bohai Sea to identify the influence of the SPM variations on the phytoplankton dynamics. Our analysis revealed negative correlations both spatially and temporally between Chl-a increase rate and the SPM concentration. This finding indicated that in nutrient-limited areas, the phytoplankton dynamics was still influenced by the underwater light availability, which was regulated by the SPM variations.

Resuspension is an important physical process that controls the SPM variations (Jiang et al., 2004). Physical causes of resuspension include strong winds and tidal currents (Su et al., 2015). The different physical processes cause SPM variations on different time scales and thus influence the phytoplankton dynamics in different ways by interfering with other forcing such as the solarly driven physical forcing functions (Lucas et al., 1999; Desmit et al., 2005). May et al. (2003) found that the phytoplankton biomass variability was significantly enhanced when the short-term sediment resuspension caused by wind mixing was involved in the model simulation. Desmit et al. (2005) observed notable errors when the temporal pattern of light penetration was not linked to the tidal cycle of solids settling and resuspension. We systemically investigated the interaction of the SPM resuspension driven by various physical processes with the phytoplankton dynamics. The model analysis recognized that the cutoff time resolution of the SPM concentration is daily in order to accurately reproduce the phytoplankton spring bloom.

6.2 SPM resuspension as a positive factor: nutrient enrichment

SPM resuspension is able to positively influence the phytoplankton dynamics by supplying the water column with nutrients. The record of Klein and Sournia (1987) supported the hypothesis that resuspension events which were associated with spring tides could refuel remineralized nutrients from sediment or the bottom water layer. The nutrient replenishment was found to result in a time lag between resuspension events and phytoplankton growth (Su et al., 2015). In our analysis, the summer-autumn bloom magnitude exhibited a positive response to the interannual variability of the wind mixing (Fig. 2.5). Even though nutrient observations were not available to study the mechanism, this correlation indirectly indicated that enhanced wind mixing tended to supply the surface layer with nutrients to promote a higher bloom intensity. In our model simulation, the impact was not involved because in spring, nutrients are always sufficient for the phytoplankton growth.

6.3 The satellite data-model integration

An important novel aspect of this study is the integration of satellite data with model simulation to study the phytoplankton dynamics. In summer-autumn period, it is difficult to accurately reproduce the repetition of the short-term Chl-a maximum by the model simulation. Satellite Chl-a data have advantages in this period because of the high spatial and temporal coverage. On the seasonal scale, satellite Chl-a data have been used in model validations (Lacroix et al., 2007; Tiedje et al., 2010).

The study of the SPM variations also benefited from the satellite data. In order to examine the impact of the SPM variations, the key issue that must be addressed is how to estimate the SPM concentration in the water column in terms of the spatial and temporal coverage. Ji et al. (2002) used the daily inputs of SPM concentration that were derived from temporally and spatially interpolated satellite imagery in a three-dimensional coupled bio-physical model to study the influences of SPM on the ecosystem in Lake Michigan. Lacroix et al. (2007) employed the seasonal climatology of TSM data that were derived from SeaWiFS to calculate the light attenuation coefficient in their model. In our model, we used the seasonal climatology of SPM concentration from MERIS, which has a better performance in Case 2 waters (Schroeder et al., 2007). Lacroix et al. (2007) discussed that the temporal coarse resolution of TSM concentrations may have contributed in their study to the deviations in the bloom timing and to the underestimation of the simulated Chl-a. Similar model deviations were also found in our study (Chapter 4). Therefore, a higher temporal resolution of the SPM concentration is needed to improve the model performance.

Tian et al. (2009) demonstrated that MERIS derived K_{min} was a more reliable quantity with respect to Chl-a concentration and can be used to constrain the model parameterization for obtaining a more realistic light attenuation coefficient. They also pointed out the possibility to directly use K_{min}, instead of the water constituent-based light attenuation coefficient, to force the biological model. Our calculated K_d exhibited high correlation with the corresponding K_{min} (Fig. 3.5 (c)). Since the overestimated Chl-a concentration in summer would result in biases in the K_d calculation, we can expect an improved formulation of the underwater light by K_{min} in stead.

Chapter 7

Conclusion

In this thesis, the synoptic perspective of the roles of the SPM variations in modulating the phytoplankton dynamics in the Bohai Sea was obtained by satellite data analysis and model simulation.

The summer-autumn bloom was assessed using MERIS-derived Chl-a data. The influence of the SPM variations on the summer-autumn bloom dynamics was discussed by analyzing the simultaneously determined SPM concentration and light attenuation coefficient (K_{min}), as well as the QuikSCAT-derived wind speed. SPM was found to influence the bloom dynamics in two aspects. On one hand, SPM enhancement impeded the phytoplankton bloom development through elevating the light attenuation. The Chl-a increase rate was negatively correlated with the spatial distribution of the SPM concentration and K_{min}. Delayed bloom onset and depressed Chl-a increase rate were found in higher SPM concentration years. Weak wind mixing preceded the bloom onset by 0-10 days. On the other hand, SPM resuspension intensified the blooms by supplying nutrients to the water columns. In strong wind years (e.g. 2003), the bloom magnitude was higher than in the normal years.

The influence of the SPM variations on the phytoplankton spring bloom was investigated by model simulation. By doing scenario simulations, the interaction of the light fluctuation caused by different SPM variations with the phytoplankton growth was identified. The constant SPM concentration led to the highest model deviations, indicating that the seasonal SPM settlement is a primary trigger of the phytoplankton spring bloom. Storm events would induce enhanced phytoplankton growth during the post-storm period when the water column is under calm wind conditions. On average Chl-a returned to pre-storm levels several weeks after the storm passage. The neap-spring tides, when only the effect on light attenuation was concerned, could generate sub-fluctuations of the phytoplankton biomass. Compared with the seasonal variation, the fortnight sub-fluctuations were referred to as a secondary factor of the bloom dynamics. Nevertheless, this small fluctuation could yield earlier bloom developments. The tidally-resolved SPM variation was subject to high uncertainties. It influenced the phytoplankton growth through the interference with the diel solar irradiance cycle. The assumed regular fluctuations of the SPM concentration caused by the diurnal/semi-diurnal tides had no significant effect on the spring bloom. The hourly SPM concentrations that were determined by the current velocity and water depth, though lack of observational support, revealed to some extent the asymmetry of the flood-ebb tide. In order to have a better description of the tidally-resolved SPM variation, a physical model that can generate the hourly SPM field could be an optimal solution.

The influence of the SPM variations can also be found on the spatial patterns of the phytoplankton spring bloom. In this thesis, some preliminary results were presented but a thorough analysis still needs much effort. Further investigation has to continue step by step into a full three-dimensional analysis with more knowledge of the SPM variations.

Appendices

Appendix A

The critical Chl-a concentration for quantifying the bloom frequencies

In this paper, we used the threshold criterion described by Tett (1987) to preliminarily quantify bloom frequencies. However, the critical Chl-a concentration for the bloom definition varies from region to region. Therefore, we applied normalized data to the analysis. We coarsely assume that the time series of Chl-a concentration at a certain grid point obeys a Gaussian distribution. When converted to a standard normal distribution (with $\mu = 0$ and $\sigma = 1$), values higher than 1.5 or less than -1.5 accounted for less than 18 percent of the distribution. Therefore, the period with values higher than 1.5 can be treated as the bloom period.

We also performed a series of experiments to determine the optimal critical value. From Fig. A.1, we can find that the three spatially and temporally averaged biological variables all increased as the critical value increased. Nevertheless, the spatial pattern of the biological variables did not reveal a large difference (not shown). Therefore, we chose the median value (1.5) as the optimal critical value. Although this criterion is not exact, we can reasonably use it to define the first summer-autumn bloom for the further statistical analysis.

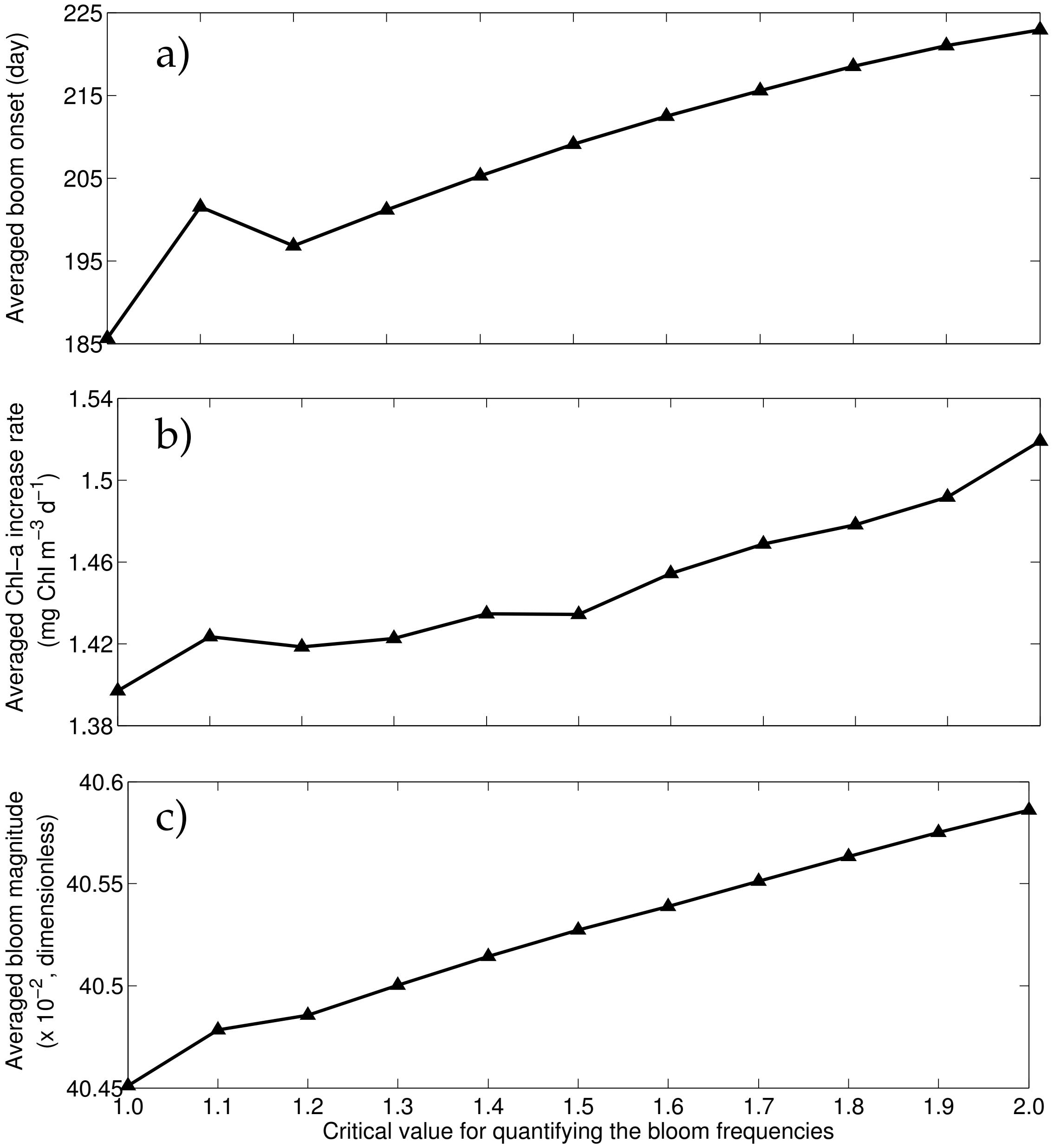

Figure A.1: The spatially and temporally averaged biological variables with different assigned values of the critical Chl-a concentration that was used as the threshold to determine the occurrence of the bloom.

Appendix B

The time interval between two blooms

For a certain grid point, if a second summer-autumn bloom occurred, we performed the analysis based on the first bloom. For these instances, we resampled the time series of Chl-a variance from the very beginning of the study period (1 May) to the day before the initiation of the second bloom and then conducted the further statistical analysis. In Fig. B.1, a second bloom occurred in early September. For case a), we did the curve fitting before the second bloom and successfully captured the first bloom event and obtained reasonable biological variable estimations (e.g., for bloom onset). For case b), we did the curve fitting without excluding the second bloom. The ″S″ curve fitting failed to reproduce the first bloom event and therefore resulted in large deviations for the biological variable estimations.

We assumed that the time interval between two blooms is no less than 15 days so that we could distinguish the second bloom from the first one. With this assumption, we could constrain the time period used for the subsequent logistic curve fitting to dates before the initiation of the second bloom to avoid disturbances to the fitting result caused by second and subsequent blooms.

Because the time interval between two blooms is highly variable, we cannot select a single interval value that works optimally all of the time. To find the best assignment for the time interval, we chose 5 days, 10 days, 15 days, 20 days and 45 days for the experiments and compared the corresponding results. Fig. B.2 presents the spatial distributions of bloom onset, Chl-a increase rate and bloom magnitude. In Fig. B.3 presents the spatial and temporal averages of the three

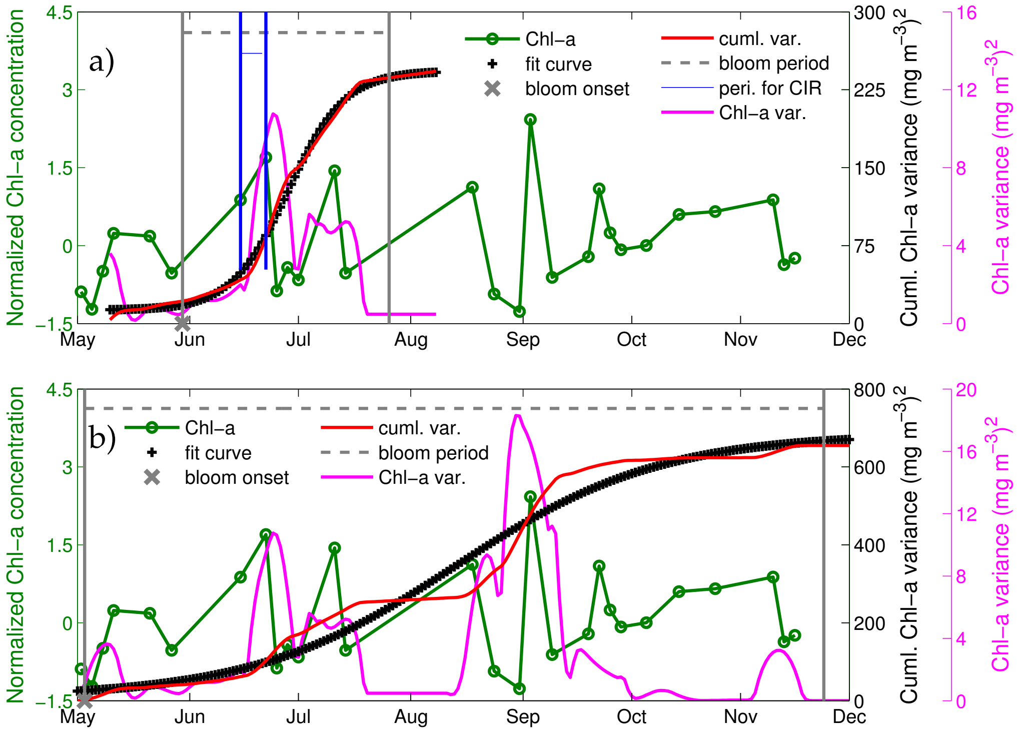

Figure B.1: Illustration of the effect of the disturbance caused by a second bloom on the curve fitting results at a certain point sampled in Fig. 2.2 (a). In a) the second bloom period was excluded, resulting in a reasonable fitting curve and correct estimation of the timing of bloom onset. In b) the estimations of both the bloom onset and the bloom end time for the first bloom show remarkable inaccuracy because the second bloom had a significant influence on the curve fitting.

biological variables. Both of the two statistical results indicate inconspicuous differences among the different assignments. In Fig. B.3 we can see that the experiment with the interval of 15 days exhibited the smallest bias. Hence, we chose 15 days as the optimal time interval.

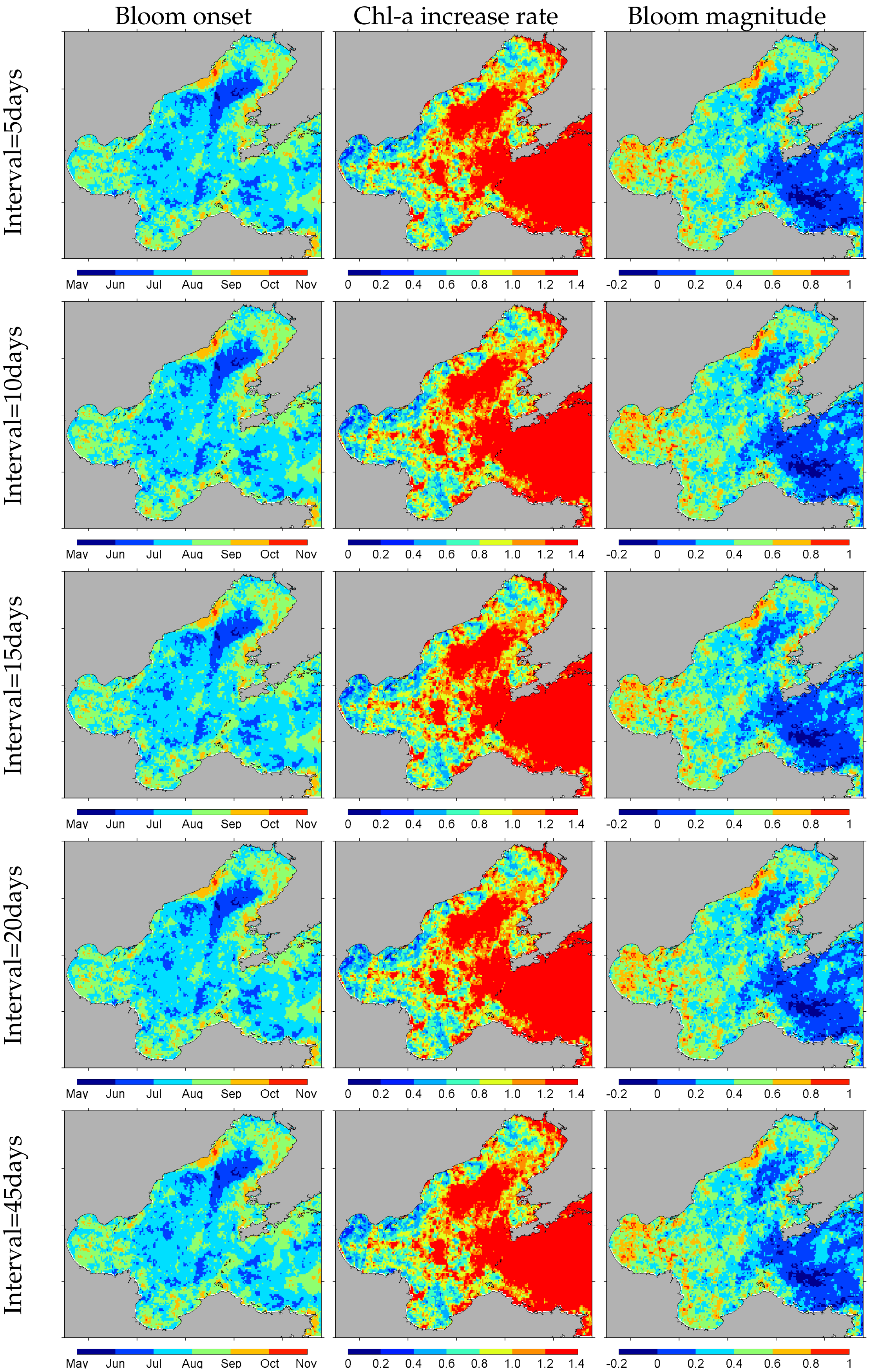

Figure B.2: Spatial distribution of biological variables with different assignments of the time interval between bloom blooms (The same as Fig. 2.3).

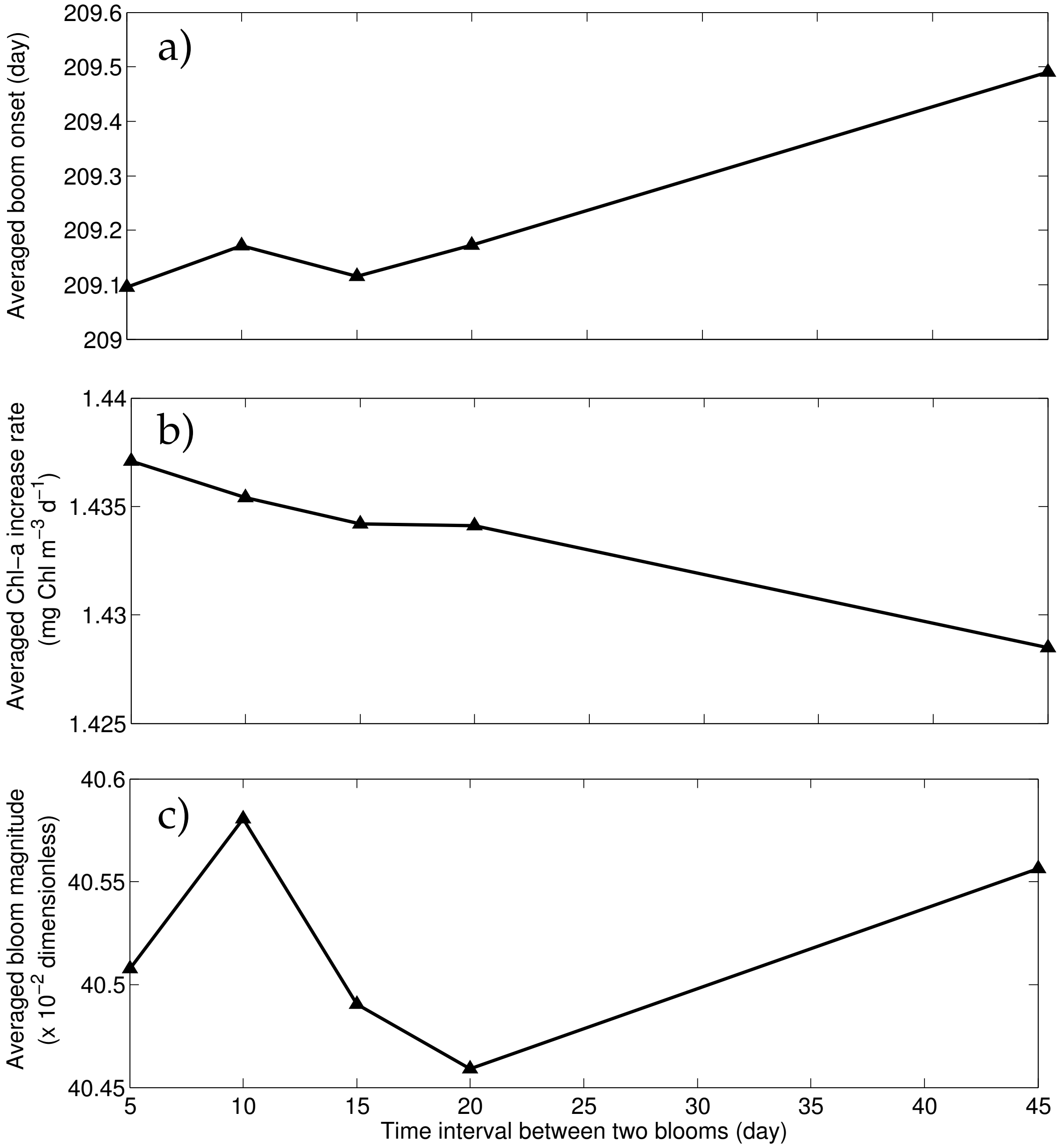

Figure B.3: The spatially and temporally averaged biological variables with different assignments of the time interval between two blooms.

Appendix C

The index of neap-spring tide

We obtained hourly sea surface elevation data from the Finite Volume Coastal Ocean Model (FVCOM) model simulation, which is forced by eight major tidal constituents (M2, S2, N2, K2,K1, O1,P1,Q1) from 2007.12.01 to 2008.12.31. For each grid point, we estimated a time series of sea surface elevation from 1 May, 2008 to 30 November, 2008 (Fig. C.1a, blue line). Next, we calculated the daily maximum sea surface elevation (Fig. C.1a, red line). From there, the 2-day running mean was calculated for the time series of daily maximum sea surface elevation (Fig. C.1b, black dashed line). To create the index of neap-spring tide, we constrained the time series within the range of -1 $\sim$ 1 by the following linear formula:

$$y = \frac{2x}{(a-b)} - \frac{(a+b)}{(a-b)} \tag{C.1}$$

where y is the index of the neap-spring tides, x is the daily maximum sea surface elevation (2d running mean), a is the maximum sea surface elevation during the spring tides (the maximum of the black line in Fig. C.1b) and b is the minimum of the daily maximum sea surface elevation (the minimum of the black line in Fig. C.1b). For a coarse definition, index values less than 0 could represent neap tides, whereas values greater than 0 could represent spring tides. We followed the same procedure for all of the grid points in the Bohai Sea in 2008. Based on the results, we also calculated the spatial correlation between the index of neap-spring tide and the Chl-a increase rate (Fig. C.2). We found the bloom onset was not regulated by the neap-spring tide because the blooms occurred during both the neap tide period (index < 0) and the spring tide period (index > 0). In addition, there is no remarkable correlation between the neap-spring tide and the Chl-a increase rate.

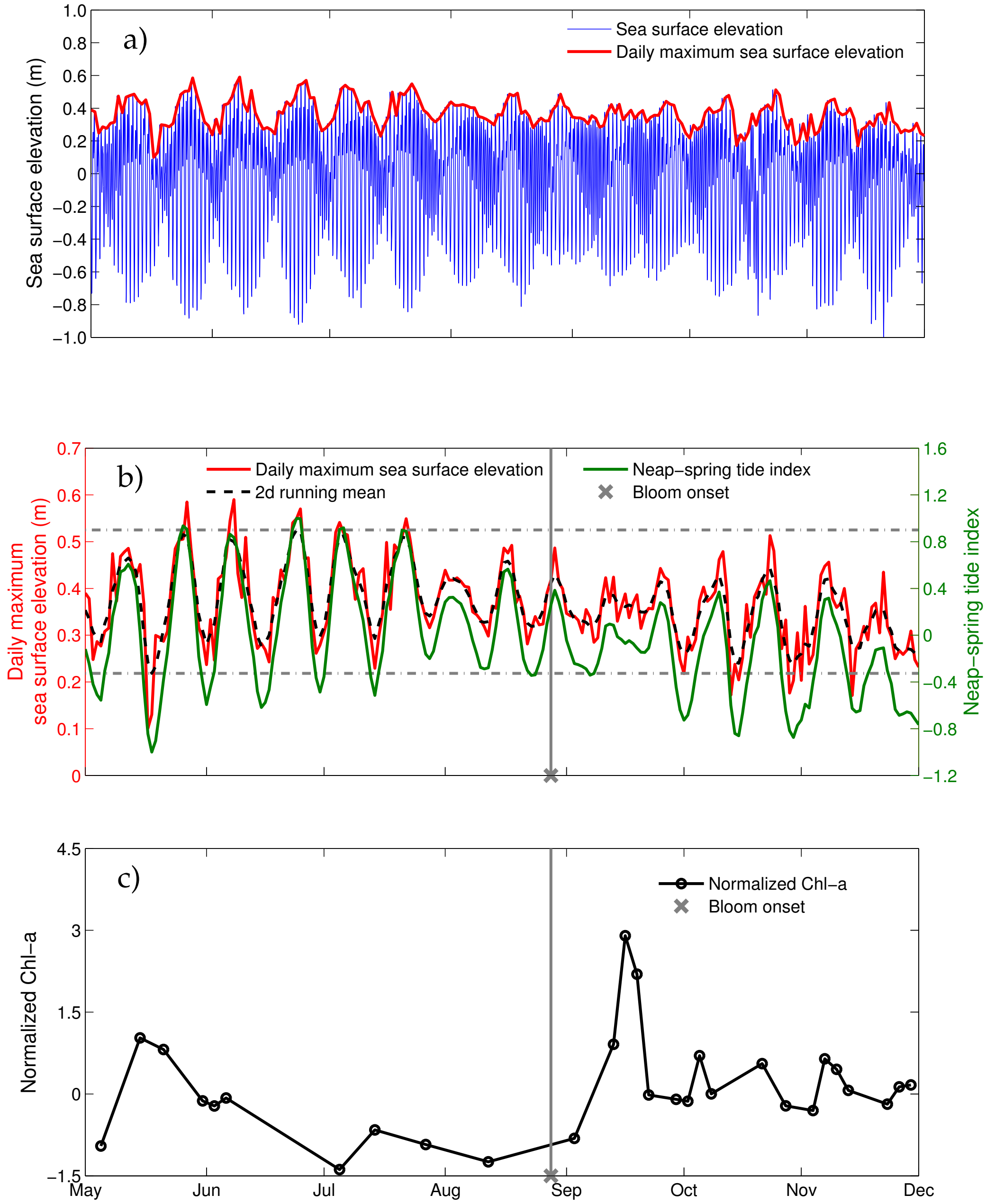

Figure C.1: Example for the procedure calculating the index of neap-spring tides at a certain point sampled in Fig. 3b). a) shows the FVCOM simulated hourly sea surface elevation (blue line) and the daily maximum value (red line). b) shows the 2d running mean (dashed black line) and the dimensionless time series (green line). The dashed-dot lines stand for the maximum and minimum values for the 2d running mean time series, respectively. c) shows the time series of the normalized Chl-a concentration (black line with circle) and bloom onset (vertical line at X) in the sampled point.

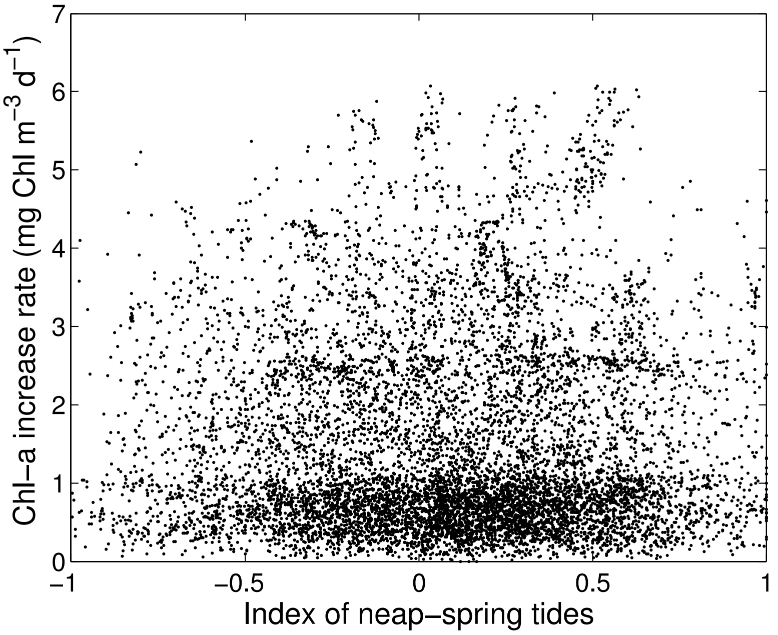

Figure C.2: Index of neap-spring tides on the day of bloom onset versus Chl-a increase rate during the bloom period for each grid point in the Bohai Sea. Blooms occurred during both the neap tide period (index < 0) and the spring tide period (index > 0). There is no good correlation between the spatial distribution of index and the Chl-a increase rate.

Appendix D

The parameters of the ecosystem model

Table D.1: Parameter list of the ecosystem model in the Bohai Sea. Note: All rates are valid for 10 ^oC. Reference in blank means the parameter is the same with Lorkowski (2012). 'Model adjusted' means the parameter is altered from Lorkowski (2012) after the model parameterization described in section 4.3.4. Citation shows the literature where the parameter is referred to.

Symbol	Parameter	Unit	Value	Reference
β	Assimilation coefficient of (micro/meso) zooplankton		0.75	
brc	Remineralisation rate of benthic carbon	d^{-1}	0.028	
brn	Remineralisation rate of benthic nitrogen and phosphate	d^{-1}	0.033	
brs	Remineralisation rate of benthic silicate	d^{-1}	0.033	
δ	DON fraction of losses from (micro/meso) zooplankton		0.4	
ε	Ammonium fraction of losses from (micro/meso) zooplankton		0.4	
φ	ratio of breakdown rates-C to breakdown rate-N	$mol\ C/mol\ N$	0.85	
f_{d2}	Fraction of fast sinking detritus		0.15	
g_1	Maximum ingestion rate of microzooplankton	d^{-1}	0.5	
g_2	maximum ingestion rate of mesozooplankton	d^{-1}	0.4	
γ	Exudation fraction of diatoms/flagellates		0.05	
K_1	Half-saturation constant of nitrate uptake by diatoms/flagellates	$mmol\ N\ m^{-3}$	0.5	

continue

Table D.1 (continue)

Symbol	Parameter	Unit	Value	Reference
K_{21}	Half-saturation constant of ammonium uptake by diatoms	$mmol\ N\ m^{-3}$	0.5	
K_{22}	Half saturation constant of ammonium uptake by flagellates	$mmol\ N\ m^{-3}$	0.05	
K_p	Half-saturation constant of phosphate uptake by diatoms/flagellates	$mmol\ P\ m^{-3}$	0.05	
K_S	Half-saturation constant of silicate uptake by diatoms	$mmol\ Si\ m^{-3}$	0.50	
K_3	Half-saturation constant ingestion by (micro/meso) zooplankton	$mmol\ N\ m^{-3}$	1.00	
K_4	Half-saturation constant uptake by bacteria	$mmol\ N\ m^{-3}$	0.2	Model adjust
K_6	Half-saturation constant loss of (micro/meso) zooplankton-N	$mmol\ N\ m^{-3}$	0.2	
k_c	Extinction coefficient of PAR due to Chl-a	$m^2/(mg\ Chl)$	0.026	Fasham and Platt (1983)
k_s	Extinction coefficient of PAR due to SPM	$m^2\ g^{-1}$	0.06	
k_{par}	Conversion factor for photosynthetically active radiation		0.43	
k_w	Locally varying extinction coefficient of water	m^{-1}	0.13	Model adjust
μ_{11}	Diatom linear mortality rate	d^{-1}	0.035	
μ_{12}	Flagellates linear mortality rate	d^{-1}	0.035	
μ_{21}	Maximum loss rate of microzooplankton	d^{-1}	0.2	

continue

Table D.1 (continue)

Symbol	Parameter	Unit	Value	Reference
μ_{22}	Maximum loss rate of mesozooplankton	d^{-1}	0.2	
μ_3	Excretion rate of bacteria	d^{-1}	0.1	
μ_4	Breakdown rate of slowly sinking detritus-N	d^{-1}	0.12	
μ_5	Breakdown rate of fast sinking detritus-N	d^{-1}	0.10	
μ_6	Phytoplankton quadratic mortality factor (diatoms/flagellates)	$m^3\ mmol\ C^{-1}\ d^{-1}$	0.01	
π_{21}	Grazing preference of microzooplankton for flagellates		0.33	
π_{23}	Grazing preference of microzooplankton for bacteria		0.33	
π_{24}	Grazing preference of microzooplankton for detritus		0.34	
π_{12}	Grazing preference of mesozooplankton for diatoms		0.33	
π_{13}	Grazing preference of mesozooplankton for detritus		0.34	
π_{14}	Grazing preference of mesozooplankton for microzooplankton		0.33	
r_0	Maximum nitrification rate	d^{-1}	0.02	
$rcnb$	C:N ratio of bacteria	$mol\ C/mol\ N$	4.0	
$rcpb$	C:P ratio of bacteria	$mol\ C/mol\ P$	40.0	
$rcnz$	C:N ratio of (micro/meso) zooplankton	$mol\ C/mol\ N$	5.5	
$rcpz$	C:P ratio of (micro/meso) zooplankton	$mol\ C/mol\ P$	110.0	
$rcnp$	C:N ratio of phytoplankton	$mol\ C/mol\ N$	6.625	
$rcpp$	C:P ratio of phytoplankton	$mol\ C/mol\ P$	132.5	
rcs	C:Si ratio of diatoms	$mol\ C/mol\ Si$	5.76	

continue

Table D.1 (continue)

Symbol	Parameter	Unit	Value	Reference
$rpcn$	C:N (Redfield) ratio of phytoplankton (diatoms/flagellates)	$mol\ C/mol\ N$	6.625	
soc	Decay rate of semi-labile dissolved organic carbon	d^{-1}	0.00274	
v_b	Maximum uptake rate of bacteria	d^{-1}	0.5	Model adjust
v_{p1}	Maximum growth rate of diatoms	d^{-1}	1.1	
v_{p2}	Maximum growth rate of flagellates	d^{-1}	0.4	Model adjust
w_{d1}	Velocity of slowly sinking detritus	$m\ d^{-1}$	0.4	
w_{d2}	Velocity of fast sinking detritus	$m\ d^{-1}$	10.0	
I_opt	Optimal light intensity for phytoplankton growth	$W\ m^{-2}$	70	Gao et al. (1998)

Appendix E

Validation of seasonal cycles of Chl-a and nutrients for the other boxes

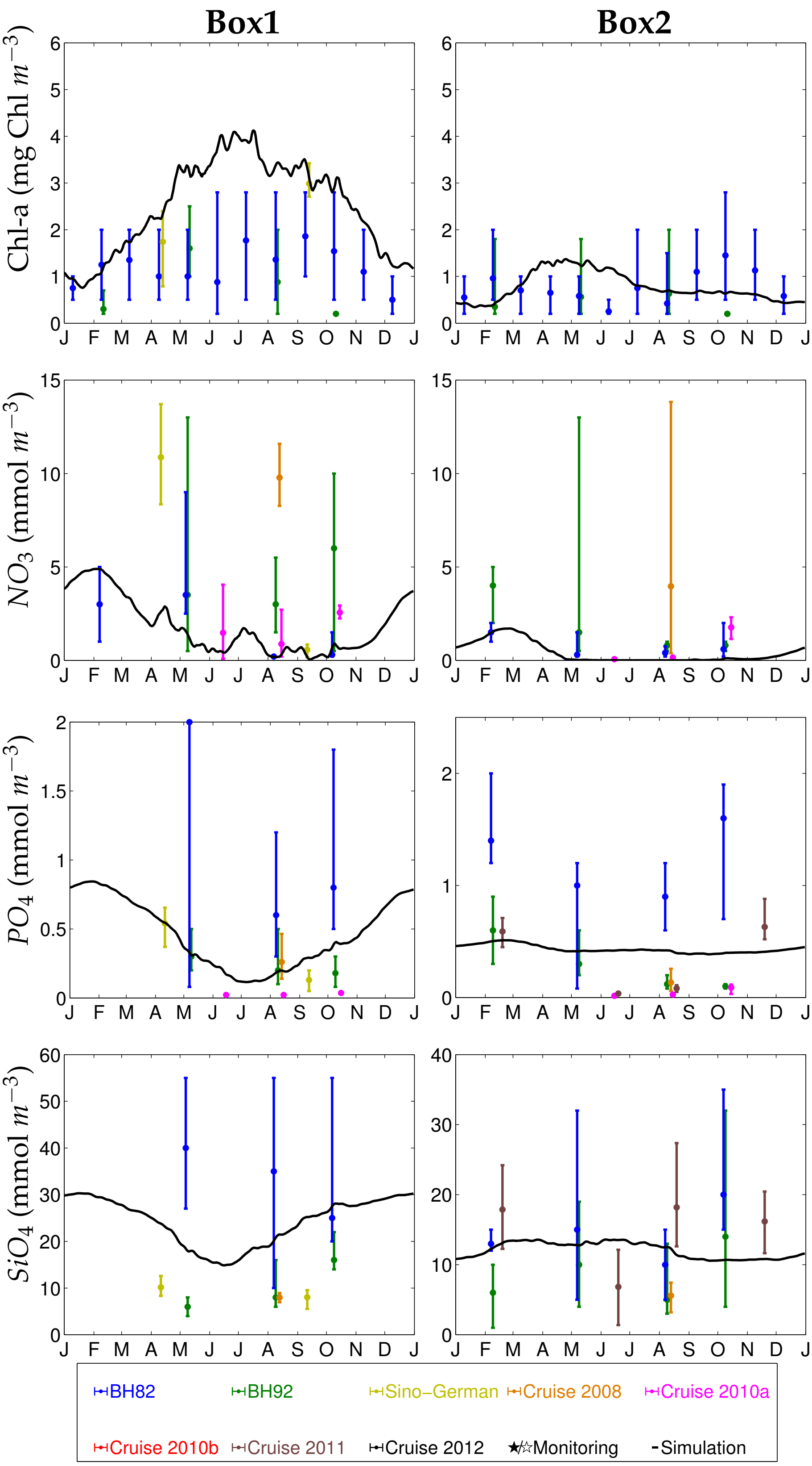

Figure E.1: The same as Fig. 4.7 but for Box1 and Box2. Validation of seasonal cycles of Chl-a and nutrients. Error bars stand for different cruise observations labeled by different colors. Dots of the error bars stand for the spatial average of each cruise. The bars show the maximum and minimum of each cruise. For a clearer view, the monthly means of each data set were shifted by 2 days. Pentagram stands for monitoring measurements at Changdao Station. The filled ones are measurements in 1999 while the others in 1998. Bold black line shows the daily model results averaged over the box.

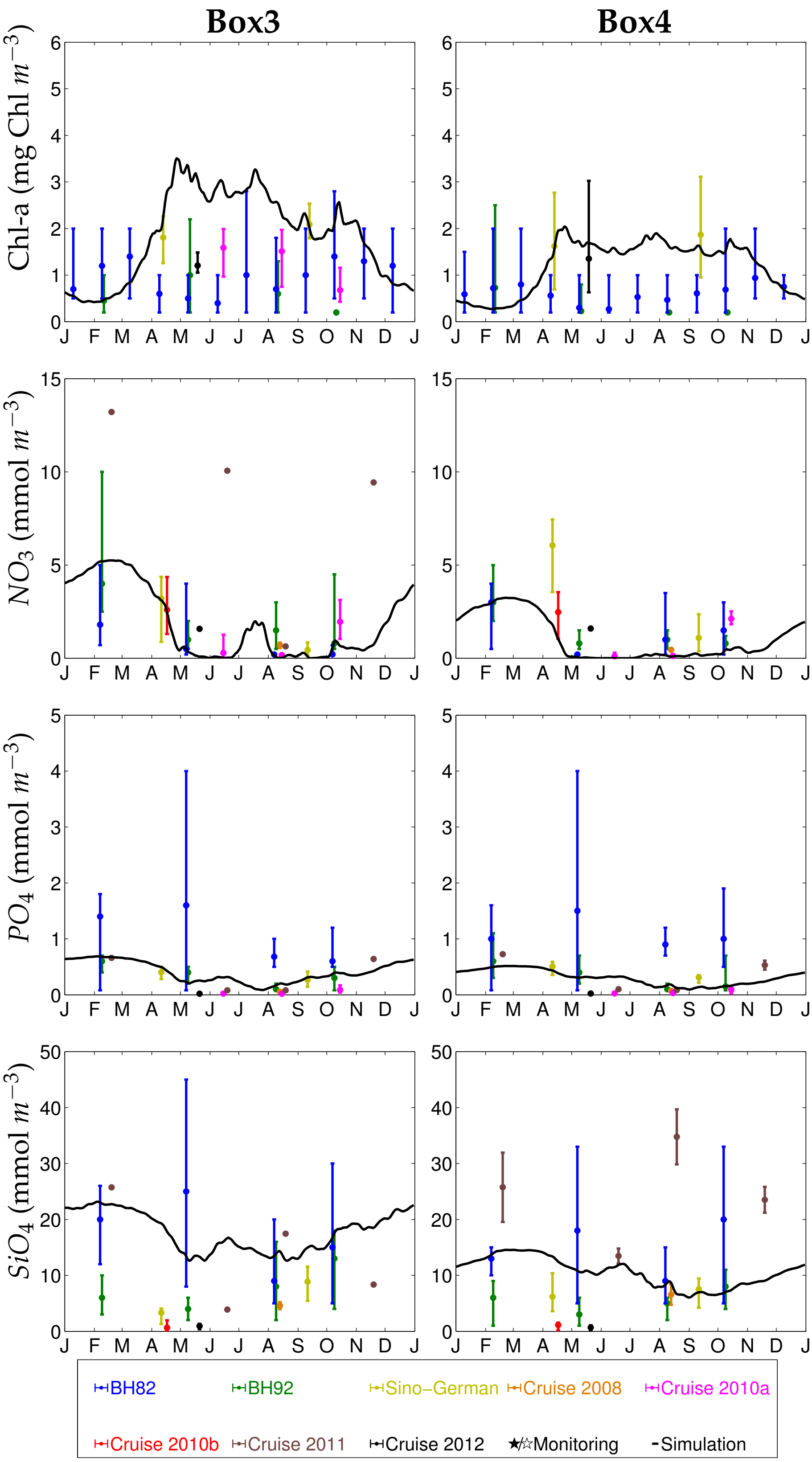

Figure E.2: The same as Fig. 4.7 but for Box3 and Box4

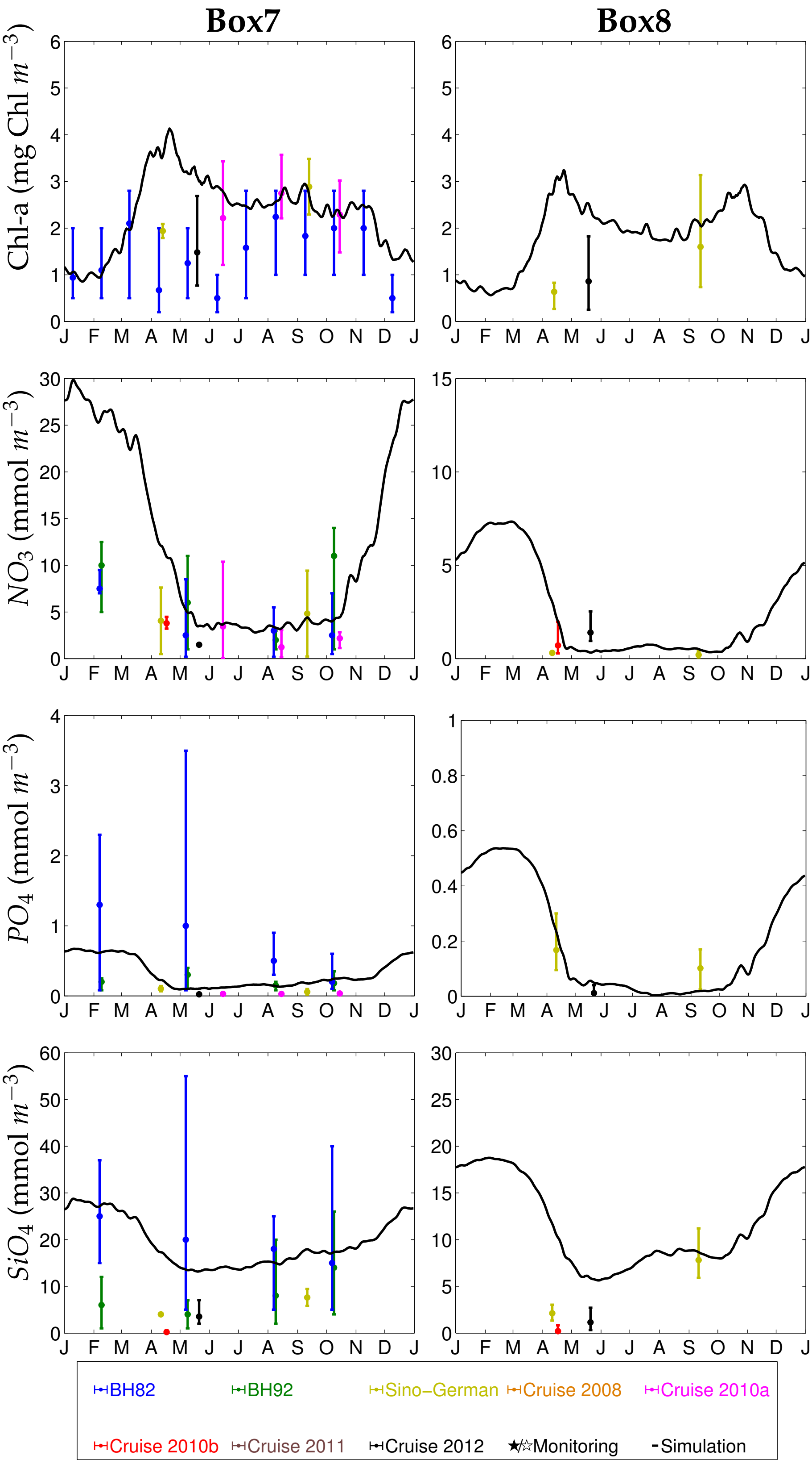

Figure E.3: The same as Fig. 4.7 but for Box7 and Box8

Bibliography

Adolf, J. E., Yeager, C. L., Miller, W. D., Mallonee, M. E., Harding, L. W., 2006. Environmental forcing of phytoplankton floral composition, biomass, and primary productivity in Chesapeake Bay, USA. Estuarine, Coastal and Shelf Science 67 (1), 108–122.

Alaee, M. J., Ivey, G., Pattiaratchi, C., 2004. Secondary circulation induced by flow curvature and Coriolis effects around headlands and islands. Ocean Dynamics 54 (1), 27–38.

Andersen, J. H., Schlüter, L., Ærtebjerg, G., 2006. Coastal eutrophication: recent developments in definitions and implications for monitoring strategies. Journal of Plankton Research 28 (7), 621–628.

Backhaus, J. O., Hainbucher, D., 1987. A finite difference general circulation model for shelf seas and its application to low frequency variability on the North European Shelf. Elsevier Oceanography Series 45, 221–244.

Badewien, T. H., Zimmer, E., Bartholomä, A., Reuter, R., 2009. Towards continuous long-term measurements of suspended particulate matter (SPM) in turbid coastal waters. Ocean Dynamics 59 (2), 227–238.

Behrenfeld, M. J., Boss, E., Siegel, D. A., Shea, D. M., 2005. Carbon-based ocean productivity and phytoplankton physiology from space. Global Biogeochemical Cycles 19 (1).

Bennett, J. P., Woodward, J. W., Shultz, D. J., 1986. Effect of discharge on the chlorophylla distribution in the tidally-influenced Potomac River. Estuaries 9 (4), 250–260.

Beriland, T., 1960. Methods of climatological computation of total incoming solar radiation. Meteorol. Gidrol 6 (9-12), 12.

Branco, A. B., Kremer, J. N., 2005. The relative importance of chlorophyll and colored dissolved organic matter (CDOM) to the prediction of the diffuse attenuation coefficient in shallow estuaries. Estuaries 28 (5), 643–652.

Brickley, P. J., Thomas, A. C., 2004. Satellite-measured seasonal and inter-annual chlorophyll variability in the Northeast Pacific and Coastal Gulf of Alaska. Deep Sea Research Part II: Topical Studies in Oceanography 51 (1), 229–245.

Budyko, M., 1974. Climate and Life. International Geophysical Series, Vol. 18.

Byun, D.-S., Wang, X. H., Zavatarelli, M., Cho, Y.-K., 2007. Effects of resuspended sediments and vertical mixing on phytoplankton spring bloom dynamics in a tidal estuarine embayment. Journal of Marine Systems 67 (1), 102–118.

Carstensen, J., Conley, D. J., 2004. Frequency, composition, and causes of summer phytoplankton blooms in a shallow coastal ecosystem, the Kattegat. Limnology and Oceanography 49 (1), 191–201.

Carstensen, J., Henriksen, P., Heiskanen, A.-S., 2007. Summer algal blooms in shallow estuaries: definition, mechanisms, and link to eutrophication. Limnology and Oceanography 52 (1), 370–384.

Chen, C., Wiesenburg, D. A., Xie, L., 1997. Influences of river discharge on biological production in the inner shelf: A coupled biological and physical model of the Louisiana-Texas Shelf. Journal of Marine Research 55 (2), 293–320.

Chen, C.-T. A., 2009. Chemical and physical fronts in the Bohai, Yellow and East China seas. Journal of Marine Systems 78 (3), 394–410.

Chen, X., Lu, J., Cui, T., Jiang, W., Tian, L., Chen, L., Zhao, W., 2010. Coupling remote sensing retrieval with numerical simulation for SPM studyTaking Bohai Sea in China as a case. International Journal of applied earth observation and geoinformation 12, S203–S211.

Cloern, J. E., 1987. Turbidity as a control on phytoplankton biomass and productivity in estuaries. Continental Shelf Research 7 (11), 1367–1381.

Cloern, J. E., 1991. Tidal stirring and phytoplankton bloom dynamics in an estuary. Journal of Marine Research 49 (1), 203–221.

Cloern, J. E., 1996. Phytoplankton bloom dynamics in coastal ecosystems: a review with some general lessons from sustained investigation of San Francisco Bay, California. Reviews of Geophysics 34 (2), 127–168.

Cloern, J. E., 1999. The relative importance of light and nutrient limitation of phytoplankton growth: a simple index of coastal ecosystem sensitivity to nutrient enrichment. Aquatic Ecology 33 (1), 3–15.

Cloern, J. E., 2001. Our evolving conceptual model of the coastal eutrophication problem. Marine Ecology Progress Series 210 (2001), 223–253.

Cloern, J. E., Foster, S., Kleckner, A., 2014. Phytoplankton primary production in the world's estuarine-coastal ecosystems. Biogeosciences 11 (9), 2477–2501.

Cloern, J. E., Grenz, C., Vidergar-Lucas, L., 1995. An empirical model of the phytoplankton chlorophyll: carbon ratio-the conversion factor between productivity and growth rate. Limnology and Oceanography 40 (7), 1313–1321.

Cloern, J. E., Nichols, F. H., 1985. Time scales and mechanisms of estuarine variability, a synthesis from studies of San Francisco Bay. Hydrobiologia 129 (1), 229–237.

Colijn, F., 1982. Light absorption in the waters of the Ems-Dollard estuary and its consequences for the growth of phytoplankton and microphytobenthos. Netherlands Journal of Sea Research 15 (2), 196–216.

Colijn, F., Cadée, G. C., 2003. Is phytoplankton growth in the Wadden Sea light or nitrogen limited? Journal of Sea Research 49 (2), 83–93.

Cui, T., Zhang, J., Groom, S., Sun, L., Smyth, T., Sathyendranath, S., 2010. Validation of MERIS ocean-color products in the Bohai Sea: A case study for turbid coastal waters. Remote Sensing of Environment 114 (10), 2326–2336.

De Jonge, V., 1994. Wind-driven tidal and annual gross transport of mud and microphytobenthos in the Ems Estuary and its importance for the ecosystem. OLSEN & OLSEN, FREDENSBORG, DENMARK., 29–40.

De Jonge, V. N., 2000. Importance of temporal and spatial scales in applying biological and physical process knowledge in coastal management, an example for the Ems estuary. Continental Shelf Research 20 (12), 1655–1686.

De Jorge, V., Van Beusekom, J., 1995. Wind-and tide-induced resuspension of sediment and microphytobenthos from tidal flats in the Ems estuary. Limnology and Oceanography 40 (4), 776–778.

Dee, D., Uppala, S., Simmons, A., Berrisford, P., Poli, P., Kobayashi, S., Andrae, U., Balmaseda, M., Balsamo, G., Bauer, P., et al., 2011. The ERA-Interim reanalysis: Configuration and performance of the data assimilation system. Quarterly Journal of the Royal Meteorological Society 137 (656), 553–597.

Dekker, A., Vos, R., Peters, S., 2001. Comparison of remote sensing data, model results and in situ data for total suspended matter (TSM) in the southern Frisian lakes. Science of the Total Environment 268 (1), 197–214.

Desmit, X., Vanderborght, J.-P., Regnier, P., Wollast, R., 2005. Control of phytoplankton production by physical forcing in a strongly tidal, well-mixed estuary. Biogeosciences 2 (2), 205–218.

Devlin, M., Barry, J., Mills, D., Gowen, R., Foden, J., Sivyer, D., Tett, P., 2008. Relationships between suspended particulate material, light attenuation and Secchi depth in UK marine waters. Estuarine, Coastal and Shelf Science 79 (3), 429–439.

Doerffer, R., Schiller, H., 2007. The MERIS Case 2 water algorithm. International Journal of Remote Sensing 28 (3-4), 517–535.

Doerffer, R., Sorensen, K., Aiken, J., 1999. MERIS potential for coastal zone applications. International Journal of Remote Sensing 20 (9), 1809–1818.

Domingues, R. B., Anselmo, T. P., Barbosa, A. B., Sommer, U., Galvão, H. M., 2011. Light as a driver of phytoplankton growth and production in the freshwater tidal zone of a turbid estuary. Estuarine, Coastal and Shelf Science 91 (4), 526–535.

Dore, J. E., Brum, J. R., Tupas, L. M., Karl, D. M., 2002. Seasonal and interannual variability in sources of nitrogen supporting export in the oligotrophic subtropical North Pacific Ocean. Limnology and Oceanography 47 (6), 1595–1607.

Edwards, M., Richardson, A. J., 2004. Impact of climate change on marine pelagic phenology and trophic mismatch. Nature 430 (7002), 881–884.

Falkowski, P. G., Raven, J. A., 2013. Aquatic photosynthesis. Princeton University Press.

Fan, H., Liu, Y., Huang, H., 2009. Long term trend and change point analysis on runoff and sediment fluxes into the sea from the Yellow River during the period of 1950 - 2007. Journal of Sediment Research 5, 9–16 (in Chinese with English Abstract).

Fasham, M., Ducklow, H., McKelvie, S., 1990. A nitrogen-based model of plankton dynamics in the oceanic mixed layer. Journal of Marine Research 48 (3), 591–639.

Fasham, M., Platt, T., 1983. Photosynthetic response of phytoplankton to light: a physiological model. Proceedings of the Royal Society of London B: Biological Sciences 219 (1217), 355–370.

Fei, Z., 1986. Study on the water colour and transparency in the Bohai Sea. Journal of Oceangraphy of Huanghai and Bohai Seas 4, 33–40 (in Chinese with English Abstract).

Fei, Z., 1991. The study of primary productivity in the Bohai Sea: chlorophyll a, primary productivity and potential fisheries resources. Mar. Fish. Res. 12, 55–69.

Fettweis, M., Francken, F., Van den Eynde, D., Verwaest, T., Janssens, J., Van Lancker, V., 2010. Storm influence on SPM concentrations in a coastal turbidity maximum area with high anthropogenic impact (southern North Sea). Continental Shelf Research 30 (13), 1417–1427.

Fettweis, M., Sas, M., Monbaliu, J., 1998. Seasonal, neap-spring and tidal variation of cohesive sediment concentration in the Scheldt Estuary, Belgium. Estuarine, Coastal and Shelf Science 47 (1), 21–36.

Findlay, H. S., Yool, A., Nodale, M., Pitchford, J. W., 2006. Modelling of autumn plankton bloom dynamics. Journal of plankton research 28 (2), 209–220.

Fisher, T., Carlson, P., Barber, R., 1982. Carbon and nitrogen primary productivity in three North Carolina estuaries. Estuarine, Coastal and Shelf Science 15 (6), 621–644.

Fox, D., Teague, W., Barron, C., Carnes, M., Lee, C., 2002. The Modular Ocean Data Assimilation System (MODAS)*. Journal of Atmospheric and Oceanic Technology 19 (2), 240–252.

Fuentes-Yaco, C., Koeller, P., Sathyendranath, S., Platt, T., 2007. Shrimp (Pandalus borealis) growth and timing of the spring phytoplankton bloom on the Newfoundland–Labrador Shelf. Fisheries oceanography 16 (2), 116–129.

Gao, H., Feng, S., Guan, Y., 1998. Modelling annual cycles of primary production in different regions of the Bohai Sea. Fisheries Oceanography 7 (3-4), 258–264.

Gao, H., Yang, H., Zhang, Y., Lu, J., 2001. A preliminary study on factors affecting the primary production in the Bohai Sea. Journal-Ocean University of Qingdao 31 (004), 487–497.

Gohin, F., Bryere, P., Griffiths, J., 2015. The exceptional surface turbidity of the North-West European shelf seas during the stormy 2013–2014 winter: Consequences for the initiation of the phytoplankton blooms? Journal of Marine Systems 148, 70–85.

Gohin, F., Loyer, S., Lunven, M., Labry, C., Froidefond, J., Delmas, D., Huret, M., Herbland, A., 2005. Satellite-derived parameters for biological modelling in coastal waters: Illustration over the eastern continental shelf of the Bay of Biscay. rse 95, 29–46.

Gomes, H., Goes, J., Saino, T., 2000. Influence of physical processes and freshwater discharge on the seasonality of phytoplankton regime in the Bay of Bengal. Continental Shelf Research 20, 313–330.

Grabemann, I., Krause, G., 2001. On different time scales of suspended matter dynamics in the Weser estuary. Estuaries 24 (5), 688–698.

Guinder, V. A., Popovich, C. A., Perillo, G. M., 2009. Particulate suspended matter concentrations in the Bahía Blanca Estuary, Argentina: implication for the development of phytoplankton blooms. Estuarine, Coastal and Shelf Science 85 (1), 157–165.

Guo, Y., 1994. Primary productivity and phytoplankton in China Seas. Oceanology of China Seas 1, 227–242.

Hainbucher, D., Hao, W., Pohlmann, T., Sündermann, J., Feng, S., 2004. Variability of the Bohai Sea circulation based on model calculations. Journal of Marine Systems 44 (3), 153–174.

Hatcher, B. G., 2006. Dynamics of marine ecosystems biological-physical interactions in the oceans. Botanica Marina 49 (3), 272–273.

Henson, S. A., Robinson, I., Allen, J. T., Waniek, J. J., 2006. Effect of meteorological conditions on interannual variability in timing and magnitude of the spring bloom in the Irminger Basin, North Atlantic. Deep Sea Research Part I: Oceanographic Research Papers 53 (10), 1601–1615.

Howarth, R. W., Marino, R., 2006. Nitrogen as the limiting nutrient for eutrophication in coastal marine ecosystems: evolving views over three decades. Limnology and Oceanography 51 (1part2), 364–376.

Huang, D., Su, J., Backhaus, J., 1999. Modelling the seasonal thermal stratification and baroclinic circulation in the Bohai Sea. Continental Shelf Research 19, 1485–1505.

Iida, T., Saitoh, S., 2007. Temporal and spatial variability of chlorophyll concentrations in the Bering Sea using empirical orthogonal function (EOF) analysis of remote sensing data. Deep Sea Research Part II: Topical Studies in Oceanography 54, 2657–2671.

Irigoien, X., Castel, J., 1997. Light limitation and distribution of chlorophyll pigments in a highly turbid estuary: the Gironde (SW France). Estuarine, Coastal and Shelf Science 44 (4), 507–517.

Ji, R., Chen, C., Budd, J. W., Schwab, D. J., Beletsky, D., Fahnenstiel, G. L., Johengen, T. H., Vanderploeg, H., Eadie, B., Cotner, J., et al., 2002. Influences of suspended sediments on the ecosystem in Lake Michigan: a 3-D coupled biophysical modeling experiment. Ecological Modelling 152 (2), 169–190.

Jiang, W., Pohlmann, T., Sun, J., Starke, A., 2004. SPM transport in the Bohai Sea: field experiments and numerical modelling. Journal of Marine Systems 44, 175–188.

Jiang, W., Pohlmann, T., Sündermann, J., Feng, S., 2000. A modelling study of SPM transport in the Bohai Sea. Journal of Marine Systems 24 (3), 175–200.

Jo, C. O., Lee, J.-Y., Park, K., Kim, Y. H., Kim, K.-R., 2007. Asian dust initiated early spring bloom in the northern East/Japan Sea. Geophysical Research Letters 34 (5).

Kashino, Y., España, N., Syamsudin, F., Richards, K. J., Jensen, T., Dutrieux, P., Ishida, A., 2009. Observations of the North Equatorial Current, Mindanao Current, and Kuroshio Current System during the 2006/07 El Niño and 2007/08 La Niña. Journal of Oceanography 65, 325–333.

Kim, H., Yoo, S., Oh, I., 2007. Relationship between phytoplankton bloom and wind stress in the sub-polar frontal area of the Japan/East Sea. Journal of Marine Systems 67, 205–216.

Klein, B., Sournia, A., 1987. A daily study of the diatom spring bloom at Roscoff. Marine Ecology-Progress Series 37, 265–275.

Kocum, E., Underwood, G. J., Nedwell, D. B., 2002. Simultaneous measurement of phytoplanktonic primary production, nutrient and light availability along a turbid, eutrophic UK east coast estuary (the Colne Estuary). Marine ecology. Progress series 231, 1–12.

Lacroix, G., Ruddick, K., Park, Y., Gypens, N., Lancelot, C., 2007. Validation of the 3D biogeochemical model MIRO&CO with field nutrient and phytoplankton data and MERIS-derived surface chlorophyll a images. Journal of Marine Systems 64 (1), 66–88.

Lancelot, C., Billen, G., 1984. Activity of heterotrophic bacteria and its coupling to primary production during the spring phytoplankton bloom in the southern bight of the North Sea. Limnology and Oceanography 29 (4), 721–730.

Large, W., Yeager, S., 2009. The global climatology of an interannually varying air–sea flux data set. Climate Dynamics 33 (2-3), 341–364.

Lewandowska, A. M., Striebel, M., Feudel, U., Hillebrand, H., Sommer, U., 2015. The importance of phytoplankton trait variability in spring bloom formation. ICES Journal of Marine Science, fsv059.

Lin, S., Zou, T., Gao, H., Guo, X., 2009. The vertical attenuation of irradiance as a function of turbidity: a case of the Huanghai (Yellow) Sea in spring. Acta Oceanologica Sinica 28 (5), 66–75.

Liu, D., Shen, X., Di, B., Shi, Y., Keesing, J. K., Wang, Y., Wang, Y., 2013. Palaeoecological analysis of phytoplankton regime shifts in response to coastal eutrophication. Marine ecology. Progress series 475, 1–14.

Liu, F., Su, J., Moll, A., Krasemann, H., Chen, X., Pohlmann, T., Wirtz, K., 2014. Assessment of the summer–autumn bloom in the Bohai Sea using satellite images to identify the roles of wind mixing and light conditions. Journal of Marine Systems 129, 303–317.

Liu, H., Yin, B., 2006. Model study on Bohai ecosystem: 1. model description and primary productivity. Acta Oceanologica Sinica-English Edition 25 (4), 77.

Liu, H., Yin, B., 2007a. Annual cycle of carbon, nitrogen and phosphorus in the Bohai Sea: A model study. Continental Shelf Research 27 (10-11), 1399–1407.

Liu, H., Yin, B., 2007b. Model study on Bohai ecosystem 2. Annual cycle of nutrient-phytoplankton dynamics. Acta Oceanologica Sinica, 04.

Liu, H., Yin, B., 2010. Numerical investigation of nutrient limitations in the Bohai Sea. Marine Environmental Research 70 (3-4), 308–317.

Liu, S., Wei Li, L., Zhang, Z., 2011. Inventory of nutrients in the Bohai. Continental Shelf Research 31, 1790–1797.

Logan, J. A., Megretskaia, I., Nassar, R., Murray, L. T., Zhang, L., Bowman, K. W., Worden, H. M., Luo, M., 2008. Effects of the 2006 El Nino on tropospheric composition as revealed by data from the Tropospheric Emission Spectrometer (TES). Geophysical Research Letters 35, L03816.

Lorenzen, C. J., 1972. Extinction of light in the ocean by phytoplankton. Journal du Conseil 34 (2), 262–267.

Lorkowski, I., 2012. The Carbon Pump of the Northwest-European Shelf-Variability due to Phytoplankton Dynamics and Climate Change. Ph.D. thesis, Universität Hamburg Hamburg.

Lorkowski, I., Pätsch, J., Moll, A., Kühn, W., 2012. Interannual variability of carbon fluxes in the North Sea from 1970 to 2006–Competing effects of abiotic and biotic drivers on the gas-exchange of CO2. Estuarine, Coastal and Shelf Science 100, 38–57.

Lucas, L. V., Koseff, J. R., Monismith, S. G., Cloern, J. E., Thompson, J. K., 1999. Processes governing phytoplankton blooms in estuaries. II: The role of horizontal transport. Marine ecology. Progress series 187, 17–30.

Lunau, M., Lemke, A., Dellwig, O., Simon, M., 2006. Physical and biogeochemical controls of microaggregate dynamics in a tidally affected coastal ecosystem. Limnology and Oceanography 51 (2), 847–859.

Martinez-Vicente, V., Tilstone, G. H., Blondeau-Patissier, D., Menezes, A., 2004. Validation of MERIS geophysical products in open ocean and coastal waters in the Southern North Sea. In: Proceeding MERIS val. Workshop 2003. Frascati, Spain.

May, C. L., Koseff, J. R., Lucas, L. V., Cloern, J. E., Schoellhamer, D. H., et al., 2003. Effects of spatial and temporal variability of turbidity on phytoplankton blooms. Marine Ecology Progress Series 254, 111–128.

McPhaden, M., 2008. Evolution of the 2006–2007 El Niño: the role of intraseasonal to interannual time scale dynamics. Advances in Geosciences 14, 219–230.

Meyer, E. M., Pohlmann, T., Weisse, R., 2011. Thermodynamic variability and change in the North Sea (1948–2007) derived from a multidecadal hindcast. Journal of Marine Systems 86 (3), 35–44.

Moll, A., 1998. Regional distribution of primary production in the North Sea simulated by a three-dimensional model. Journal of Marine Systems 16 (1), 151–170.

Moll, A., 2000. Assessment of three-dimensional physical-biological ECOHAM1 simulations by quantified validation for the North Sea with ICES and ERSEM data. ICES Journal of Marine Science 57 (4), 1060–1068.

Moll, A., Radach, G., 1991. Application of Dobson and Smith's solar radiation model to German Bight data. Quarterly Journal of the Royal Meteorological Society 117 (500), 845–851.

Moll, A., Stegert, C., 2007. Modelling Pseudocalanus elongatus stage-structured population dynamics embedded in a water column ecosystem model for the northern North Sea. Journal of Marine Systems 64 (1), 35–46.

Moore, G., Aiken, J., Lavender, S., 1999. The atmospheric correction of water colour and the quantitative retrieval of suspended particulate matter in Case II waters: application to MERIS. International Journal of Remote Sensing 20 (9), 1713–1733.

Moran, S., Moore, R., 1988. Temporal variations in dissolved and particulate aluminum during a spring bloom. Estuarine, Coastal and Shelf Science 27 (2), 205–215.

Navarro, G., Ruiz, J., 2006. Spatial and temporal variability of phytoplankton in the Gulf of Cádiz through remote sensing images. dsrb 53, 1241–1260.

Nechad, B., Ruddick, K., Park, Y., 2010. Calibration and validation of a generic multisensor algorithm for mapping of total suspended matter in turbid waters. Remote Sensing of Environment 114 (4), 854–866.

Neukermans, G., Ruddick, K., Greenwood, N., 2012. Diurnal variability of turbidity and light attenuation in the southern North Sea from the SEVIRI geostationary sensor. Remote Sensing of Environment 124, 564–580.

Ouillon, S., Douillet, P., Petrenko, A., Neveux, J., Dupouy, C., Froidefond, J.-M., Andréfouët, S., Muñoz-Caravaca, A., 2008. Optical algorithms at satellite wavelengths for total suspended matter in tropical coastal waters. Sensors 8 (7), 4165–4185.

Pätsch, J., Kühn, W., 2008. Nitrogen and carbon cycling in the North Sea and exchange with the North Atlantica model study. Part I. Nitrogen budget and fluxes. Continental Shelf Research 28 (6), 767–787.

Peeters, F., Straile, D., Lorke, A., Livingstone, D. M., 2007. Earlier onset of the spring phytoplankton bloom in lakes of the temperate zone in a warmer climate. Global Change Biology 13 (9), 1898–1909.

Peng, S., Qin, X., Shi, H., Zhou, R., Dai, M., Ding, D., 2012. Distribution and controlling factors of phytoplankton assemblages in a semi-enclosed bay during spring and summer. Marine Pollution Bulletin 64, 941–948.

Peng, Z., Wensheng, J., 2011. A numerical study of the effects of coastal geometry in the Bohai Sea on storm surges induced by cold-air outbreaks. Journal of Ocean University of China 10 (1).

Pennock, J. R., 1985. Chlorophyll distributions in the Delaware estuary: regulation by light-limitation. Estuarine, Coastal and Shelf Science 21 (5), 711–725.

Peterson, D. H., Smith, R. E., Hager, S. W., Harmon, D. D., Herndon, R. E., Schemel, L. E., 1985. Interannual variability in dissolved inorganic nutrients in Northern San Francisco Bay Estuary. In: Temporal Dynamics of an Estuary: San Francisco Bay. Springer, pp. 37–58.

Platt, T., Bird, D. F., Sathyendranath, S., 1991. Critical depth and marine primary production. Proceedings of the Royal Society of London B: Biological Sciences 246 (1317), 205–217.

Platt, T., Fuentes-Yaco, C., Frank, K. T., 2003. Marine ecology: spring algal bloom and larval fish survival. Nature 423 (6938), 398–399.

Pohlmann, T., 1996. Predicting the thermocline in a circulation model of the North SeaPart I: model description, calibration and verification. Continental Shelf Research 16 (2), 131–146.

Pohlmann, T., 2006. A meso-scale model of the central and southern North Sea: consequences of an improved resolution. Continental Shelf Research 26 (19), 2367–2385.

Pörtner, H.-O., Peck, M., 2010. Climate change effects on fishes and fisheries: towards a cause-and-effect understanding. Journal of Fish Biology 77 (8), 1745–1779.

Postma, H., 1967. Sediment transport and sedimentation in the estuarine environment.

Radach, G., Pätsch, J., 1997. Climatological annual cycles of nutrients and chlorophyll in the North Sea. Journal of Sea Research 38 (3), 231–248.

Rast, M., Bezy, J., Bruzzi, S., 1999. The ESA Medium Resolution Imaging Spectrometer MERIS a review of the instrument and its mission. International Journal of Remote Sensing 20 (9), 1681–1702.

Rey, F., Skjoldal, H. R., Slagstad, D., 1987. Primary production in relation to climatic changes in the Barents Sea.

Richardson, K., 1997. Harmful or exceptional phytoplankton blooms in the marine ecosystem. Advances in Marine Biology 31, 301–385.

Roden, C., 1994. Chlorophyll blooms and the spring/neap tidal cycle: observations at two stations on the coast of Connemara, Ireland. Marine Biology 118 (2), 209–213.

Roegner, G., Hickey, B., Newton, J., Shanks, A., Armstrong, D., 2002. Wind-induced plume and bloom intrusions into Willapa Bay, Washington. Limnology and Oceanography 47, 1033–1042.

Rousseaux, C., Lowe, R., Feng, M., Waite, A., Thompson, P., 2012. The role of the Leeuwin Current and mixed layer depth on the autumn phytoplankton bloom off Ningaloo Reef, Western Australia. Continental Shelf Research 32, 22–35.

Ruddick, K., Park, Y., Astoreca, R., Neukermans, G., Van Mol, B., 2008. Validation of MERIS water products in the Southern North Sea. In: Proceedings of the 2nd MERIS -(A)ATSR workshop. Frascati, Spain.

Sackmann, B., Mack, L., Logsdon, M., Perry, M., 2004. Seasonal and inter-annual variability of SeaWiFS-derived chlorophyll a concentrations in waters off the Washington and Vancouver Island coasts, 1998–2002. Deep Sea Research Part II: Topical Studies in Oceanography 51, 945–965.

Saito, Y., Yang, Z., Hori, K., 2001. The Huanghe (Yellow River) and Changjiang (Yangtze River) deltas: a review on their characteristics, evolution and sediment discharge during the Holocene. Geomorphology 41, 219–231.

Schroeder, T., Behnert, I., Schaale, M., Fischer, J., Doerffer, R., 2007. Atmospheric correction algorithm for MERIS above case-2 waters. International Journal of Remote Sensing 28 (7), 1469–1486.

Schrum, C., Alekseeva, I., John, M. S., 2006. Development of a coupled physical–biological ecosystem model ECOSMO: part I: model description and validation for the North Sea. Journal of Marine Systems 61 (1), 79–99.

Sharples, J., 2008. Potential impacts of the spring-neap tidal cycle on shelf sea primary production. Journal of Plankton Research 30 (2), 183–197.

Shi, W., Wang, M., Jiang, L., 2011. Spring-neap tidal effects on satellite ocean color observations in the Bohai Sea, Yellow Sea, and East China Sea. Journal of Geophysical Research: Oceans (1978–2012) 116 (C12).

Simpson, J., Sharples, J., Rippeth, T., 1991. A prescriptive model of stratification induced by freshwater runoff. Estuarine, Coastal and Shelf Science 33 (1), 23–35.

Skogen, M. D., Moll, A., 2005. Importance of ocean circulation in ecological modeling: An example from the North Sea. Journal of Marine Systems 57 (3), 289–300.

Smetacek, V., Bathmann, U., Nöthig, E., Scharek, R., 1991. Coastal eutrophication: Causes and consequences. RFC Mantoura, J.-M. Martin, R. Wollast (eds.) Ocean margin processes in global change. John Wiley, Chichester.

Son, S., Campbell, J., Dowell, M., Yoo, S., Noh, J., 2005. Primary production in the Yellow Sea determined by ocean color remote sensing. Marine Ecology Progress Series 303, 91–103.

Stegert, C., Moll, A., Kreus, M., 2009. Validation of the three-dimensional ECOHAM model in the German Bight for 2004 including population dynamics of Pseudocalanus elongatus. Journal of Sea Research 62 (1), 1–15.

Su, J., Tian, T., Krasemann, H., Schartau, M., Wirtz, K., 2015. Response patterns of phytoplankton growth to variations in resuspension in the German Bight revealed by daily MERIS data in 2003 and 2004. Oceanologia 57 (4), 328–341.

Sun, J., Liu, D., Yang, S., Guo, J., Qian, S., 2002. The preliminary study on phytoplankton community structure in the central Bohai Sea and the Bohai Strait and its adjacent area. Oceanologia Et Limnologia Sinica 33, 461–471 (in Chinses with English Abstract).

Sündermann, J., Feng, S., 2004. Analysis and modelling of the Bohai sea ecosystem–a joint German-Chinese study. Journal of Marine Systems 44 (3-4), 127–140.

Sverdrup, H., 1953. On conditions for the vernal blooming of phytoplankton. Journal du Conseil 18, 287–295.

Tang, D., Kester, D., Ni, I., Qi, Y., Kawamura, H., et al., 2003a. In situ and satellite observations of a harmful algal bloom and water condition at the Pearl River estuary in late autumn 1998. Harmful Algae 2, 89–99.

Tang, Q., Jin, X., Wang, J., Zhuang, Z., Cui, Y., Meng, T., 2003b. Decadal-scale variations of ecosystem productivity and control mechanisms in the Bohai Sea. Fisheries Oceanography 12, 223–233.

Tang, Q., Meng, T., 1997. Atlas of the Ecological Environment and Living Resources in the Bohai Sea. Qingdao Press (In Chinese).

Tett, P., 1987. The ecophysiology of exceptional blooms. Rapp. PV Reun. Cons. Int. Explor. Mer 187, 47–60.

Tian, T., Merico, A., Su, J., Staneva, J., Wiltshire, K., Wirtz, K., 2009. Importance of resuspended sediment dynamics for the phytoplankton spring bloom in a coastal marine ecosystem. Journal of Sea Research 62, 214–228.

Tian, T., Su, J., Floser, G., Wiltshire, K., Wirtz, K., 2011. Factors controlling the onset of spring blooms in the German Bight 2002-2005: Light, wind and stratification. Continental Shelf Research 31, 1140–1148.

Tiedje, B., Moll, A., Kaleschke, L., 2010. Comparison of temporal and spatial structures of chlorophyll derived from MODIS satellite data and ECOHAM3 model data in the North Sea. Journal of Sea Research 64 (3), 250–259.

Ueyama, R., Monger, B., 2005. Wind-induced modulation of seasonal phytoplankton blooms in the North Atlantic derived from satellite observations. Limnology and Oceanography 50, 1820–1829.

Van Der Woerd, H., Pasterkamp, R., 2008. HYDROPT: A fast and flexible method to retrieve chlorophyll-a from multispectral satellite observations of optically complex coastal waters. Remote Sensing of Environment 112, 1795–1807.

Velegrakis, A., Gao, S., Lafite, R., Dupont, J., Huault, M., Nash, L., Collins, M., 1997. Resuspension and advection processes affecting suspended particulate matter concentrations in the central English Channel. Journal of Sea Research 38 (1), 17–34.

Verspecht, F., Pattiaratchi, C., 2010. On the significance of wind event frequency for particulate resuspension and light attenuation in coastal waters. Continental Shelf Research 30 (18), 1971–1982.

Walsh, J., 1988. On the nature of continental shelves. Academic Press New York.

Wang, H., Yang, Z., Saito, Y., Liu, J., Sun, X., 2006. Interannual and seasonal variation of the Huanghe (Yellow River) water discharge over the past 50 years: Connections to impacts from ENSO events and dams. Global Planet Change 50, 212–225.

Wang, X., Cui, Z., Guo, Q., Han, X., Wang, J., 2009. Distribution of nutrients and eutrophication assessment in the Bohai Sea of China. Chinese Journal of Oceanology and Limnology 27, 177–183.

Wei, H., Hainbucher, D., Pohlmann, T., Feng, S., Suendermann, J., 2004a. Tidal-induced Lagrangian and Eulerian mean circulation in the Bohai Sea. Journal of Marine Systems 44 (3), 141–151.

Wei, H., Sun, J., Moll, A., Zhao, L., 2004b. Phytoplankton dynamics in the Bohai Sea–observations and modelling. Journal of Marine Systems 44, 233–251.

Wilkerson, F., Lassiter, A., Dugdale, R., Marchi, A., Hogue, V., 2006. The phytoplankton bloom response to wind events and upwelled nutrients during the CoOP WEST study. Deep Sea Research Part II: Topical Studies in Oceanography 53, 3023–3048.

Wiltshire, K. H., Malzahn, A. M., Wirtz, K., Greve, W., Janisch, S., Mangelsdorf, P., Manly, B. F., Boersma, M., 2008. Resilience of North Sea phytoplankton spring bloom dynamics: An analysis of long-term data at Helgoland Roads. Limnology and Oceanography 53, 1294–1302.

Winter, D. F., Banse, K., Anderson, G. C., 1975. The dynamics of phytoplankton blooms in puget sound a fjord in the northwestern united states. Marine Biology 29 (2), 139–176.

Wu, Y., Peterson, I. K., Tang, C. C., Platt, T., Sathyendranath, S., Fuentes-Yaco, C., 2007. The impact of sea ice on the initiation of the spring bloom on the Newfoundland and Labrador Shelves. Journal of Plankton Research 29 (6), 509–514.

Xu, J., Hood, R. R., Chao, S.-Y., 2005. A simple empirical optical model for simulating light attenuation variability in a partially mixed estuary. Estuaries 28 (4), 572–580.

Yellow River Conservancy Commission of MWR, 2009. Yellow River Sediment Bulletin.

Yin, K., Goldblatt, R., Harrison, P., St John, M., Clifford, P., Beamish, R., 1997. Importance of wind and river discharge in influencing nutrient dynamics and phytoplankton production in summer in the central Strait of Georgia. Marine Ecology-Progress Series 161, 173–183.

Yoder, J., McClain, C., Feldman, G., Esaias, W., 1993. Annual cycles of phytoplankton chlorophyll concentrations in the global ocean: a satellite view. Global Biogeochemical Cycles 7, 181–193.

Zhang, J., Ning, X., Jiang, J., et al., 1991. Marine Atlas of Bohai Sea, Yellow Sea and East China Sea (Biology).

Zhang, J., Yu, Z., Raabe, T., Liu, S., Starke, A., Zou, L., Gao, H., Brockmann, U., 2004. Dynamics of inorganic nutrient species in the Bohai seawaters. Journal of Marine Systems 44 (3), 189–212.

Zhao, J., Shi, M., 1993. Numerical modelling of three-dimension characteristics of wind-driven current in the Bohai Sea. Chinese Journal of Oceanology and Limnology 11, 70–79.

Zhao, L., Wei, H., 2005. The influence of physical factors on the variation of phytoplankton and nutrients in the Bohai Sea. Journal of Oceanography 61 (2), 335–342.

Zhao, L., Wei, H., Feng, S., 2002. Annual cycle and budgets of nutrients in the Bohai Sea. Journal of Ocean University of Qingdao 1 (1), 29–37.

Acknowledgements

During the work on my thesis project, I learned a lot from several people on a scientific level as well as related to soft skills and I want to say thank you here.

I am grateful for the advise and support by PD Dr. Thomas Pohlmann. He taught me a lot about how to do research and I thank him for sharing his knowledge and experience with me and for having an open ear for all kinds of questions. I am grateful for his financial support during the last 6 six months of my PhD study.

I would like to show my deep gratitude to Dr. Andreas Moll. During my PhD period, we met bi-weekly to talk about my process. He provided me guidance in every stage and helped me with all kinds of issues. He is responsible and patient. I am grateful for his detailed comments and editing for my thesis writing.

I would also like to thank Dr. Jian Su for his guidance and helpful recommendations during the whole thesis process, especially with the satellite data and HAMSOM.

I would like to thank Dr. Johannes Pätsch and Markus Kreus for sharing their knowledge and experience for the ECOHAM setup and help me to improve the model simulation.

Thanks Prof. Dongyan Liu, Prof. Sumei Liu, Prof. Jun Sun and Donglin Guo to provide me observation data sets.

Special thanks go to Prof. Xueen Chen, who was the first to introduce me to mathematical modeling, specially ecosystem modeling and who fascinated me with his enthusiasm.

Thanks to Daniel Mukiibi and Fabian Grosse, you were great office mates, sources of inspiration and helpful discussion partners.

Last but not the least, I would like to thank the China Scholarship Council (CSC) for giving me the change to have my PhD study abroad with financially support in the last 4 years.

Eidesstattliche Versicherung/Declaration

Hiermit erkläre ich an Eides statt, dass ich die vorliegende Dissertationsschrift selbst verfasst und keine anderen als die angegebenen Quellen und Hilfsmittel benutz habe.

I hereby declare, on oath, that I have written the present dissertation by my own and have not used other than the acknowledged resources and aids.

August 2, 2016
. . . .
Hamburg, den   Unterschrift